PROPAGATION AND RETENTION OF VISCOELASTIC SURFACTANTS IN CARBONATE CORES

A Dissertation

by

MENG YU

Submitted to the Office of Graduate Studies of
Texas A&M University
in partial fulfillment of the requirements for the degree of

DOCTOR OF PHILOSOPHY

May 2011

Major Subject: Petroleum Engineering

Propagation and Retention of Viscoelastic Surfactants in Carbonate Cores

PROPAGATION AND RETENTION OF VISCOELASTIC SURFACTANTS IN CARBONATE CORES

A Dissertation

by

MENG YU

Submitted to the Office of Graduate Studies of
Texas A&M University
in partial fulfillment of the requirements for the degree of

DOCTOR OF PHILOSOPHY

Approved by:

Chair of Committee,	Hisham A. Nasr-El-Din
Committee Members,	Stephen A. Holditch
	A. Daniel Hill
	Mahmoud El-Halwagi
Head of Department,	Stephen A. Holditch

May 2011

Major Subject: Petroleum Engineering

ABSTRACT

Propagation and Retention of Viscoelastic Surfactants in Carbonate Cores. (May 2011)

Meng Yu, B.S., Sichuan University; M.S., Texas A&M University

Chair of Advisory Committee: Dr. Hisham A. Nasr-El-Din

Viscoelastic surfactants have found numerous applications in oil fields as fracturing and matrix acidizing fluid additives in recent years. They have the ability to form long, worm-like micelles with increasing pH and calcium concentration, which results in increasing the viscosity and elasticity of partially spent acids.

On the one hand, the concentration of surfactant in the fluids has profound effects on their performance downhole. Additionally, there is continuous debate in the industry on whether the gel generated by these surfactants causes formation damage, especially in dry gas wells. Therefore, being able to analyze the concentration of these surfactants in both live and spent acids is of great importance for production engineers who apply surfactant-based fluids in the oil fields. In the present work, a two-phase titration method was optimized for quantitative analysis of a carboxybetaine viscoelastic surfactant, and surfactant retention in calcite cores was quantitatively determined by a two phase titration method and the benefits of using mutual solvents to break the surfactant gel formed inside the cores were assessed.

On the other hand, high temperatures and low pH are usually involved in surfactant applications. Surfactants are subjected to hydrolysis under such conditions due

to the existence of a peptide bond (-CO-NH-) in their molecules, leading to changes in the rheological properties of the acid. The impact of hydrolysis at high temperatures on the apparent viscosity of carboxybetaine viscoelastic surfactant-based acids was evaluated in the present study, and the mechanism of viscosity changes was determined by molecular dynamics (MD) simulations.

Our results indicate that, first, a significant amount of surfactant has been retained in the carbonate matrix after acidizing treatment and there is a need to use internal breakers when surfactant-based acids are used in dry gas wells or water injectors. Second, hydrolysis at high temperatures has great impact on surfactant-acid rheological properties. Short time viscosity build-up and effective gel break-down can be achieved if surfactant-acid treatments are carefully designed; otherwise, unexpected viscosity reduction and phase separation may occur, which will affect the outcome of acid treatments.

DEDICATION

To my parents

ACKNOWLEDGEMENTS

I am most thankful to my advisor, Dr. Hisham Nasr-El-Din, for the enormous support he provided during my entire Ph.D. program. He was always willing to provide insightful comments and suggestions on my research work, and gave me freedom to pursue the ideas I found most interesting. His kindness, patience and encouragement have gone a long way in improving this research.

I would also like to extend my most sincere thanks to the members of my advisory committee, Dr. Stephen Holditch, Dr. Daniel Hill and Dr. Mahmoud El-Halwagi, for their guidance and support throughout the course of my research.

The accomplishment of the present research work is unimaginable without the constant assistance of many individuals, who made my time at Texas A&M University an unforgettable experience. I am extremely grateful to my coauthors, Mahmoud Mohammed and Dr. Yan Mu. Without their effort and generous support, it would not have been possible for me to overcome many difficulties I encountered. I also appreciate many helpful discussions and comments from all my group members.

Most importantly, I would like to thank my family, from my grandparents to my younger cousins, for their love and support. Particularly, I thank my parents for their selfless contribution toward my education and the completion of my Ph.D. program.

Finally, I thank the Crisman Institute for Petroleum Research and the Texas Engineering Experiment Station at Texas A&M University for providing financial support.

NOMENCLATURE

$\frac{\partial c_A}{\partial Y}$	concentration gradient;
A	cross-sectional area of the core;
a	contact area of acid solution and the rock;
b	equilibrium bond length;
b_0	actual bond length;
D_A	molecular diffusion coefficient
E	total potential energy of the atom;
f	force acting on the atom;
H_b	bond stretching force constant;
H_θ	bond bending force constant;
H_φ	torsional force constant;
H_χ	bending constant;
J	undamaged formation productivity;
J_s	productivity of the damaged well;
k	permeability of the undamaged zone;
k_c	core permeability;
k_m	mass transfer coefficient;
k_s	reduced permeability of the damaged zone ;
L	characteristic length (given by $L = 0.05\ k^{0.5}$);

m	weight of sample used to prepare the sample solution;
m_a	atomic mass;
N	number of atoms;
q	flow rate;
q_i and q_j	point charge;
r	distance between two particles;
r^*	distance at which the potential reaches its minimum;
r_a	reaction rate;
r_e	drainage radius;
r_{ij}	separation distance;
r_s	radius of the damaged zone;
r_w	wellbore radius;
$\ddot{r}$	acceleration of the atom;
S	phase factor (1 or –1 based on the dihedral angle);
u	Darcy velocity (given by $u = q/A$);
$u_{A,Y}$	flux of component A;
θ	equilibrium bond angle;
θ_0	actual bond angle;
χ	bending angle;
ε	strength of the vdW potential;
ϕ	core porosity;
ϕ_a	torsional angle.

TABLE OF CONTENTS

Page

LIST OF FIGURES

FIGURE Page

FIGURE Page

FIGURE Page

FIGURE Page

LIST OF TABLES

TABLE Page

1. INTRODUCTION

Matrix acidizing is an effective method of removing formation damage caused by drilling-mud invasion, clay migration, clay swelling and inorganic scaling. The aim of matrix acidizing is to reduce skin and improve production by creating new pathways within several inches to one foot or two around the wellbore. This is accomplished by pumping treatment fluid below the fracturing rate and pressure. Compared to high-pressure fracturing treatment, matrix acidizing is a low-volume, low-budget operation.

1.1. Carbonate Matrix Acidizing

1.1.1. History

Carbonate matrix acidizing can be dated back to the early days of oil well drilling. The earliest application of limestone acidizing treatment with hydrochloric acid (HCl) was done by the Ohio Oil Company in 1895. This technique was first recorded in 1896 (Williams et al. 1979). Although the production of oil wells increased by three times, the well casing was severely corroded by the strong acid. Thus the popularity of this technique declined, and little application was reported in the following 30 years.

In 1931, arsenic was discovered to have corrosion inhibition capability of HCl on metal by Dr. John Grebe of the Dow Chemical Company. One year later, 500 gallons of HCl was pumped down to a dead well in a limestone formation by the Michigan-based Pure Oil Company, using arsenic provided by the Dow Chemical Company as the

---

This dissertation follows the style of *SPE Production & Operations*.

corrosion inhibitor (Williams et al. 1979). The oil production of the well increased from zero to 16 bbl/day. Followed by the success, commercial acidizing services were established by different companies in several years. Carbonate acidizing has been dependent on the use of a wide range of acid additives to enhance the effectiveness of the treatments since the mid 1930's (Chilingarian et al. 1989), including surfactants, corrosion inhibitors, pH buffers, fluid loss additives, friction reducers and so on.

1.1.2. Theoretical Productivity Enhancement

Matrix acid treatments are conducted primarily in wells with near-wellbore flow restriction, which are often called damaged wells. **Fig. 1.1** illustrates a radial fluid production system, in which a damaged zone of reduced permeability, k_s, extends from the wellbore radius, r_w, to a damaged radius, r_s. The carbonate formation has a constant permeability, k, from r_s to the drainage radius, r_e.

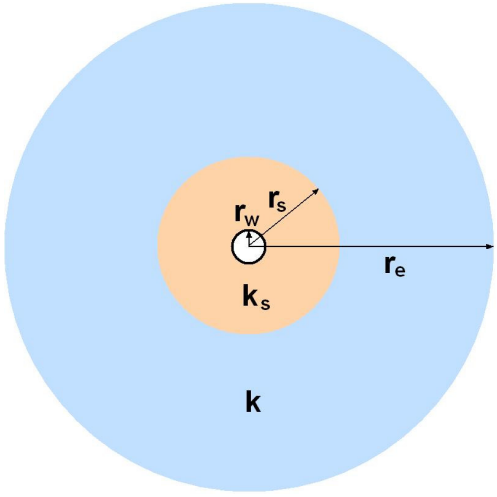

Fig. 1.1: Schematic of the damaged zone of a radial production system.

In this system, the fluid production compared to that of an undamaged system of uniform permeability k is given by **Eq. 1.1** (Muskat 1949):

$$\frac{J_s}{J} = \frac{(k_s/k)\log(r_e/r_w)}{\log(r_s/r_w)+(k_s/k)\log(r_e/r_s)} \tag{1.1}$$

where J is the undamaged formation productivity, and J_s is the productivity of the damaged well. **Fig. 1.2** gives the enhancement in productivity by increasing the permeability of damaged zone after matrix acidizing treatment. In this case, it is assumed that the wellbore radius r_w = 0.33 ft, and the drainage radius r_e = 1000 ft.

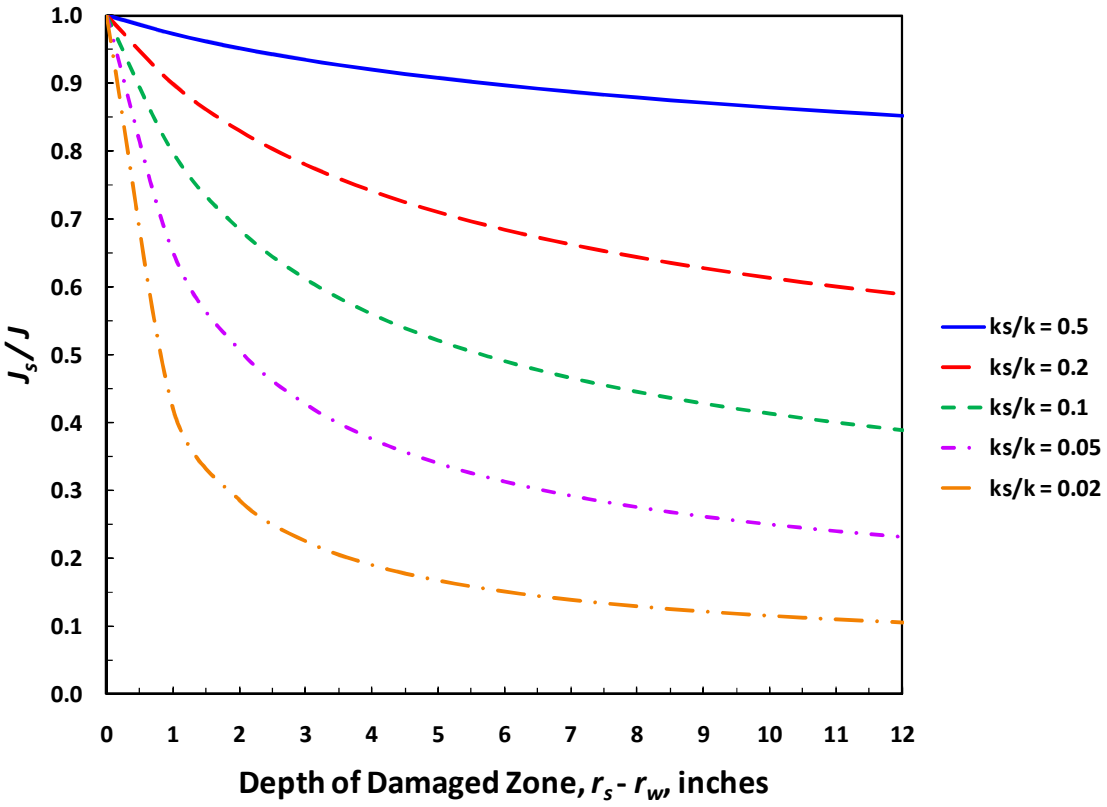

Fig. 1.2: Production enhancement by increasing damaged permeability.

As an example, if the depth of the damaged zone ($r_s - r_w$) is 10 in. beyond the wellbore and the permeability ratio k_s/k is 0.05, the productivity of the damaged well would be 0.25 of that of an undamaged well. After a matrix acidizing treatment that removes the damage around the wellbore, a 4-fold enhancement in production rate can be obtained.

1.1.3. Chemistry of Carbonate Matrix Acidizing

Acid-Carbonate Reaction Stoichiometry

Carbonate rocks are formed in water environments by precipitation and/or grain transportation from chemical or biochemical processes. Originally formed sedimentary carbonate rocks may be nearly pure calcite ($CaCO_3$) or dolomite ($CaMg(CO_3)_2$). However, the calcium in the calcite rock could be partially replaced by magnesium over time, and the rock thereby formed is a dolomitic limestone. Dolomite and calcite rocks may be interbedded in the reservoir (Wayne 2008).

Carbonate acidizing is generally conducted with hydrochloric acid. In some cases where temperatures are very high and corrosion is an issue, less corrosive organic acids like acetic or formic acids are used.

When stimulating a carbonate reservoir, carbonate rocks, comprising predominantly limestone and dolomite, rapidly dissolve in HCl by the following reactions (**Eqs. 1.2 and 1.3**):

$$CaCO_3 + 2\ HCl \rightarrow CaCl_2 + CO_2 + H_2O \quad (1.2)$$

$$CaMg(CO_3)_2 + 4\ HCl \rightarrow CaCl_2 + MgCl_2 + 2\ CO_2 + 2\ H_2O \quad (1.3)$$

For calcite, the rate of dissolution is limited mainly by the speed with which acid can be delivered to the rock surface. This results in rapid generation of irregularly shaped channels, called wormholes. The acid increases production by creating bypasses around the damage rather than directly removing it (Economides et al. 1994).

Acid Types

Hydrochloric acid, HCl, is by far the overwhelmingly employed acid in most acid treatments of carbonate formations. Usually, 15 wt% HCl solution in water is used, which is often called regular acid. With improved inhibitors, higher concentrations have become practical. The wide application of hydrochloric acid is a result of its cost-effectiveness and soluble reaction products with carbonate rocks (calcium chloride, $CaCl_2$, and magnesium chloride, $MgCl_2$). However, hydrochloric acid is relatively corrosive on wellbore tubular and pumps, especially at temperatures above 250°F.

Organic acids, including formic acid (CH_3COOH) and acetic acid (CH_3CH_2COOH), are employed in carbonate matrix acidizing treatments because of their lower corrosivity and easier inhibition at elevated temperatures. Acetic acid is commonly available as a 10 wt% solution in water. The reaction products of 10 wt% acetic acid and carbonate rocks (calcium acetates, $Ca(COOCH_2CH_3)_2$, and magnesium acetates, $Mg(COOCH_2CH_3)_2$) are generally soluble in the spent acid. Acetic acid is often used as a perforating fluid or as a fluid of low corrosivity. However, it is more expensive than either hydrochloric acid or formic acid based on the cost per unit of dissolving power. Formic acid offers a cheaper option, although it is more corrosive than acetic

acid and more difficult to control in the presence of acid-sensitive metals such as aluminum or chromium. However, effective inhibitors are available for formic acid at temperatures as high as 400°F (Williams et al. 1979).

Recently, dicarboxylic acids have found to be useful in acidizing subterranean formations, particularly at elevated temperatures up to 400°F (Huang et al. 2004; Crews and Huang 2007a). These acids or their mixtures are referred to as high temperature organic acids (HTO acids). Suitable dicarboxylic acids include, but not limited to, oxalic acid, malonic acid, pimelic acid, succinic acid, glutaric acid, adipic acid, and mixtures thereof. HTO acids can effectively generate wormholes in carbonate formations and remove carbonate scale at high temperatures, and cause very low corrosion to the tubing, casing and down hole equipment.

Retarded Acid Systems

This reduction in acid-rock reaction rate often can increase the depth of acid penetration and therefore enhance the effectiveness of carbonate acidizing treatments. Theoretically, the heterogeneous reaction between calcite and aqueous solutions of hydrochloric acid involves three main steps (Mumallah 1991):

1. Transportation of acid molecules from the bulk fluid to the fluid-solid interface at the rock surface (a mass transfer step);

2. Chemical reaction of the acid with the calcite at the surface (chemical reaction);

3. Transport of the reaction products (CO_2 and $CaCl_2$) from the solid-liquid interface to the bulk fluid (a mass transfer step).

It is well known that during an acid fracturing operation, the overall reaction rate of hydrochloric acid with carbonate is mass transfer limited (Economides et al. 1991). Reducing the mass transfer rate of the reaction of HCl and carbonate can effectively reduce the overall reaction rate. According to Fick's law (**Eq. 1.4**),

$$u_{A,Y} = -D_A \frac{\partial c_A}{\partial Y} \tag{1.4}$$

where $u_{A,Y}$ is the flux of component A, $\frac{\partial c_A}{\partial Y}$ is the concentration gradient, and D_A is the molecular diffusion coefficient, which is proportional to the squared velocity of the diffusing particles (which depends on the temperature), the viscosity of the fluid, and the size of the particles according to the Stokes-Einstein relation. If the viscosity of the solution is increased, the mass transfer rate will be decreased, and thus the reaction rate will be retarded.

Viscosifying the fracturing fluid has been prevalently used to retard the acid-carbonate reaction rate. Polymers or cross-linked polymers have been applied to increase the solution viscosity. Viscoelastic surfactant (VES) has also proved to be successful to retard HCl-carbonate reaction rate (Nasr-El-Din et al. 2006b).

Besides viscosifying the fluid, according to reaction rate expression (**Eq. 1.5**):

$$r_a = K_m a \Delta c \tag{1.5}$$

where r_a is the reaction rate, a is the contact area of acid solution and the rock, K_m is the mass transfer coefficient, and Δc is the concentration difference, the reaction rate of HCl

and carbonate can also be retarded by decreasing the contacting area of the rock to the solution. This can be accomplished by applying chemicals that can form a layer of coating on the rock surface.

Another method of retarding acid-carbonate reaction rate is using emulsified acids. Emulsified acids may contain the acid as either the internal or the external phase. The reaction rate, in this case, is governed by the Brownian motion of the acid in the micro-drops in the emulsion instead of the molecular diffusion of HCl molecules. This makes the reaction rate between the emulsified HCl and carbonate about one order of magnitude lower than that of the regular acid and carbonate (Williams et al. 1979).

1.1.4. Diversion

After injection, acid preferably enters the region with the highest permeability, leaving the damage zone untreated. Thus proper diversion is needed to direct the acidizing fluid into the damage zone to achieve maximum benefit of the matrix acidizing treatment.

A variety of diversion techniques exist in oil field applications. By using drillpipes or coiled-tubing tools with mechanical packers, treatment fluid can be directed exclusively toward a low-permeability zone. Fluid flow into high permeability zone can also be blocked by injected ball sealers that seat at perforations with higher flow rates. In carbonates, filter cake can be created inside wormholes by bridging agents, such as benzoic acid particles or salts, so that acid can be directed elsewhere.

Stringent requirements exist on the selection of diverting agent. First, it must effectively divert acid. Second, it is supposed to have limited solubility in the carrying fluid or formation fluids. Finally, it must have high cleaned-up efficiency, leaving minimum damage to the near wellbore region after the treatment. Among available diversion techniques, however, ball sealers are lost by either dropping into the rathole or floating to the surface. Benzoic acid particles and oil-soluble resins could be consumed by contacting hydrocarbons.

In practice, acid and diverting agents could be pumped continuously or in alternating stages. The number of stages depends on the length of zone being treated.

1.2. Oil Field Applications of Viscoelastic Surfactant

The rate of acid spending decreases as the viscosity of the acid increases; as a result, deeper acid penetration can be achieved (Deysarkar et al. 1984). Thus to achieve acid diversion and to reduce leakoff rate during acid injection into the fracture in many applications, high-viscosity fluids are needed during matrix acidizing and acid-fracturing treatments.

Different chemicals have been developed as additives of the acid treatment fluid to enhance the viscosity of the injected acid, including polymers and viscoelastic surfactants. Acid-soluble polymers (Pabley et al. 1982; Crowe et al. 1989) or crosslinked polymers (Metcalf et al. 2000) have been used to increase the viscosity and to improve the performance of HCl, in which the latter were introduced in the mid 70's and proven to be more effective than uncross-linked polymers (Yeager and Shuchart 1997).

The *in-situ* gelled acids, which consist of a polymer, a crosslinker, a buffer, a breaker, and other acid additives, have been reported to be able to forms a gel within a narrow pH range (Yeager and Shuchart 1997; Taylor and Nasr-El-Din 2003). Acid diversion can be achieved as a result of *in-situ* gel formation.

The outcome of *in-situ* gelled acids was generally positive; however, certain drawbacks were noted for these acids. These concerns include but not limited to: polymer retention and loss of permeability in tight carbonate cores (Taylor and Nasr-El-Din 2002; 2003); precipitation of the crosslinker (Fe(III)) in tight carbonate cores at high temperatures (Lynn and Nasr-El-Din 2001); precipitation of the crosslinker (Fe(III)) in sour environments (Nasr-El-Din et al. 2002); and consumption of hydrogen sulfide (H_2S) scavengers (aldehydes) by reacting with the polymer (Nasr-El-Din and Al-Humaidan 2001).

Surfactant-based acids were introduced during the last decade to overcome potential problems associated with polymer-based acids. Typical surfactant-based acids consisted of hydrochloric acid (HCl), a viscoelastic surfactant, and other acid additives as necessary. Commonly used viscoelastic surfactants include amineoxide surfactants and carboxybetaine surfactants (Fu and Chang 2005). During matrix acidizing treatment, as the acid spending process proceeds, the pH rises and the concentrations of calcium and magnesium ions increase (Eqs. 1.1 and 1.2). The presence of salts and the increase in pH will cause the surfactant molecules to form long worm-like micelles. These micelles further entangle and result in a 3D structure, which greatly increase the apparent viscosity of the solution (Chang et al. 1998; Card et al. 1999; Nasr-El-Din et al.

2003) (**Fig. 1.3**). The gelled acid could be broken down by converting the surfactant worm-like micelles to spherical micelles, which can be accomplished by reducing the concentration of salts and/or surfactant by the injection water in water injectors, or by mixing the spent acid with the native oil or condensate in oil and gas wells. Alternatively, by using a preflush that contains a mutual solvent (e.g., ethylenegylcol monobutyl ether), the surfactant gel can be broken in any well. Internal breakers can also be used to break the surfactant gel, if necessary.

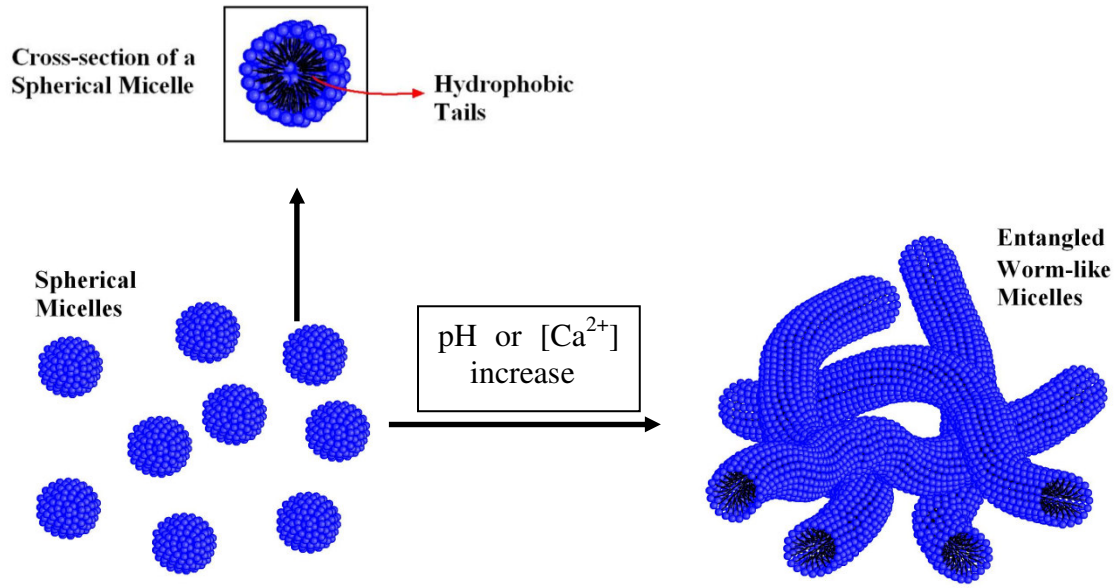

Fig. 1.3: A schematic illustration of entangled wormlike micelles network (Yu et al. 2009).

1.2.1. Diversion in High Water-Cut Oil Wells

The ability of viscoelastic surfactants to form viscous gels in aqueous solutions makes them suitable for applications in matrix acidizing treatments. Chang et al. (1998) and Card et al. (1999) first introduced this concept, which was later applied to stimulate high-water-cut oil wells. When injected into the formation, the viscoelastic surfactant gel that is formed in high oil saturation zones breaks, and the fluid that enters water-producing zones would maintain its viscosity. This in turn ensures minimum subsequent fluid flow into the water-producing zone. As a result, any injected acid following the diverting stage would be directed into high oil saturation zones and away from water-producing zones (Chang et al. 1998; Chang et al. 2001a). Positive field data was obtained showing enhanced oil production and decreased water-cut.

1.2.2. Diversion in Matrix Stimulation

When mixed with acid, some viscoelastic surfactants are capable of enhancing the viscosity of the acid when the acid is spent by carbonate (Chang et al. 1999; 2001a and Samuel 2001). An amphoteric-type viscoelastic surfactant was investigated by Al-Ghamdi et al. (2004). In live acids, this surfactant is cationic (carries positive charges), while it becomes zwitterionic (i.e., carries both positive and negative charges) once the acid is spent by carbonate rocks and the pH increases to values higher than 2. Since both pH and divalent cation (Ca^{2+} and Mg^{2+}) concentration are increased, the viscosity of surfactant-based acid can be greatly enhanced. Unlike spent polymer-based acids, spent surfactant-based acid can remain viscous even at high pH values (high than 4).

The first successful field application using surfactant-based acid was reported in Kuwait (Al-Mutawa et al. 2005). Similar successful applications were reported in Bahrain (Samuel 2003) and Egypt (Samuel and Sandhu 2004).

1.2.3. Leak-Off Control in Acid Fracturing

Since temperature accelerates the reaction rate between HCl and carbonate rocks, most acid would be completely consumed near the wellbore and thus would not result in deep penetration into the formation. This in turn adversely affects the outcome of the acid treatment. Conventionally, uncross-linked or cross-linked polymers were used to reduce the acid-carbonate reaction rate. However, severe polymer retention in the wormhole could result; in some cases, crosslinkers (especially Fe(III)) are precipitated in sour environment.

Viscoelastic surfactant-based acids were used as retarded acids to acid fracture water injectors and deep gas wells in Saudi Arabia (Nasr-El-Din and Samuel 2007). The results obtained from treating more than 250 wells were positive, and significant improvements in oil and gas production were observed.

1.2.4. Pad Fluid in Acid Fracturing

For both hydraulic and acid-fracturing treatments, high-pH borate gels are conventionally used as a pad. High-pH borate gels provide viscosity at pH values greater than 9, and this high pH value must be maintained in order to keep the fluid crosslinked. The fluid viscosity and its leakoff characteristics can be significantly affected even with

a slight decrease in the pH value. In a typical acid-fracturing treatment, the pad stage is followed by a regular or emulsified acid, which can decrease the pH and adversely affect the effect of borate gel pad.

Viscoelastic surfactant-based gel can be used to substitute the high-pH borate gel. Surfactant-based acid performs well at lower-to-neutral pH range, and thus is stable when the gel contacts acids. As a result, the volume of the pad can be effectively reduced with enhanced fluid efficiency.

1.3. Statement of the Problem

1.3.1. Viscoelastic Surfactant Retention in Carbonate Reservoirs

One of the amphoteric surfactants, carboxybetaine, has been used for matrix acidizing treatments (Nasr-El-Din et al. 2006a; Nasr-El-Din and Samuel 2007). Lab and field studies showed that the concentration of surfactant-based fluids can greatly influence the characteristics of these fluids, and the outcome of matrix acid of the treatment fluids (Nasr-El-Din et al. 2008). In field treatments, surfactant-based fluids are injected into formations, and they are flowed back after the fracturing and/or acidizing job is done. The difference in the concentration of surfactant in live and spent acids corresponds to the amount of surfactant retained or trapped in the formation, and/or partition into the hydrocarbon phase (oil or condensate). As a result, being able to analyze the concentration of surfactant is of great importance for production engineers who use these surfactants as fracturing or acidizing fluids. However, to the best of the

author's knowledge, no previous studies reported the quantitative analysis of viscoelastic surfactants in acidizing fluids.

Successful acid treatments using viscoelastic surfactants have been reported by several authors (McCarthy et al. 2002; Mohammed et al. 2005; Arangath et al. 2008), and were considered as "non-damaging" by Al-Mutawa et al. 2005 and Kristopher (2009). Lungwitz et al. (2007) demonstrated that cleanup of retained surfactant in carbonate cores by 2 wt% KCl brine or 10 vol% mutual solvent could result in high permeability regain. A few treatments, however, produced results below expectations (Nasr-El-Din et al. 2006b). This was explained in terms of retention of surfactant gel in the formation and the inability of the cleaning fluids to remove the surfactant gel. Hence, based on field results, it is very important to understand retention of viscoelastic surfactants used for diversion in carbonate rocks. However, to the best of our knowledge, no systematic work has been reported about determining surfactant concentration in live and spent acids, or about viscoelastic surfactant retention in carbonate cores and its impact in field applications.

1.3.2. Hydrolysis of Viscoelastic Surfactant at High Temperatures

Worm-like micelles can be formed by individual surfactants with certain molecular structures (Yang 2002). One kind of amphoteric surfactants, amido-carboxybetaine, has been used for matrix acidizing treatments (Nasr-El-Din et al. 2006a,c; Nasr-El-Din and Samuel 2007). However, Fu and Chang (2005) observed that this type of surfactant-acid fluid experienced viscosity reduction when subjected to high

temperatures. For 4 wt% of surfactant-acid fluid incubated at 88°C for 90 min, viscosity was significantly decreased. Phase separation occurred in those samples with longer incubation time. These observations indicate that, on one hand, high temperatures may cause fluid viscosity reduction for surfactant-acids, and cause fluid phase separation. On the other hand, it helps breaking down the gel. In this case, no additional breaker is needed.

Although the phenomenon of viscosity change of amido-carboxybetaine surfactant has been observed, to the best of our knowledge, no systematic study on the impact of hydrolysis at high temperatures on the viscosity changes of amido-carboxybetaine surfactant fluid was reported.

1.4. Research Objectives

1.4.1. Viscoelastic Surfactant Retention in Carbonate Reservoirs

The objectives regarding to the research about viscoelastic surfactant retention in carbonate reservoirs are to:

1. Develop a quantitative analysis method for surfactant concentration, and evaluate the method as a means for measuring the concentration of carboxybetaine surfactant that is used in matrix acidizing treatments;

2. Assess the effect of acid additives, reaction products, and contaminants (mainly Fe^{2+} and Fe^{3+}) on the accuracy of this method;

3. Conduct core flood experiments using calcite and dolomite cores using surfactant-based acids;

4. Study the effect of flow rate on amount of surfactant retained inside the core, and

5. Assess the effectiveness of mutual solvent in removing surfactant gel from the treated cores.

1.4.2. Hydrolysis of Viscoelastic Surfactant at High Temperatures

The objectives of this section are to:

1. Experimentally determine the viscosity changes of amido-carboxybetaine acid fluids by high temperatures, and

2. Determine the mechanism for viscosity changes on molecular level by carrying out molecular dynamics (MD) simulations.

2. CHEMISTRY OF VISCOELASTIC SURFACTANT

2.1. Introduction

Viscoelastic surfactants have been successfully applied in the oilfield as fracturing fluids (Al-Muhareb et al. 2003, Artola et al. 2004; Bustos et al. 2007; Fontana et al. 2007; Bulat et al. 2008), fluid loss pill (Samuel et al. 2003) and matrix acidizing fluids (Nasr-El-Din et al. 2003; 2006b,c; Al-Mutawa et al. 2005; Zeiler et al. 2006; Liu et al. 2009; Nasr-El-Din et al. 2009a,b). As the pH increases above 2, surfactant molecules form wormlike micelles, which exhibit viscoelastic behavior (Samuel et al. 1997) (Fig. 1.1).

Wormlike micelles can be formed by individual surfactants with certain molecular structures (Yang 2002). A series of surfactants with various hydrophobic chain lengths and asymmetry, which can be either amphoteric, cationic, or nonionic surfactants, have been shown to form wormlike micelles. These micelles result in rapid viscosity buildup during acid spending process by entangling to form a very viscous gel. The highly viscous fluid significantly slows down the reaction of HCl acid with carbonate rocks (Nasr-El-Din et al. 2009a) and reduces acid loss into wormholes. After the treatment, highly viscous gel is broken down by contacting either the formation hydrocarbons or pre/post flush fluids (Chang et al. 2001b; Taylor and Nasr-El-Din 2003).

2.2. Carboxybetaines: Amphoteric Viscoelastic Surfactants

Surfactants which include or have the potential to form both positive and negative functional groups under particular conditions belong to the family of amphoteric surfactants. Betaine is a naturally occurring material, which was first identified in the nineteenth century and has the chemical structure of trimethyl aminoacetate (Domingo 1996) (**Fig. 2.1**). This compound is an internal salt that has most of the characteristics of a totally un-ionized material in its natural form.

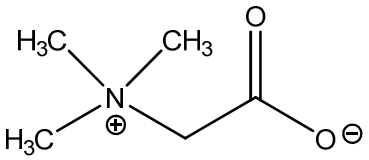

Fig. 2.1: Molecular formula of trimethyl aminoacetate at a high pH value such that the carboxyl group is deprotonated.

Betaine surfactants generally refer to the materials with one or more methyl groups replaced by a long alkyl chain, such as a fatty acid residue. Alkyl dimethyl betaines ((**Fig. 2.2a**) and alkyl amidopropyl betaines (**Fig. 2.2b**) are the most produced class of amphoteric in the 1990's (Lomax 1996).

Betaines show the characteristics of amphoteric surfactants in many ways, such as their solubility and electrical nature in alkaline solution. Betaines do not acquire any significant anionic character even at high pH, and maintain good water solubility even at

the isoelectric pH (the pH at which the surfactant molecule carries zero net electrical charge). Moreover, they are compatible with anionic surfactant at all pH's without problems of complex formation. It has been found that the carboxyl-containing betaines can form external salts in very strong acids (e.g, hydrochlorides in HCl). In general, this kind of surfactants usually performs well in hard water due to their insensitivity to the presence of electrolytes. The followings are the general properties of betaines (Porter 1994):

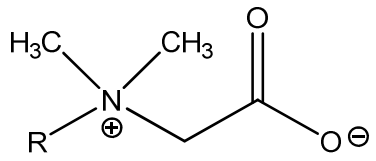

(a)

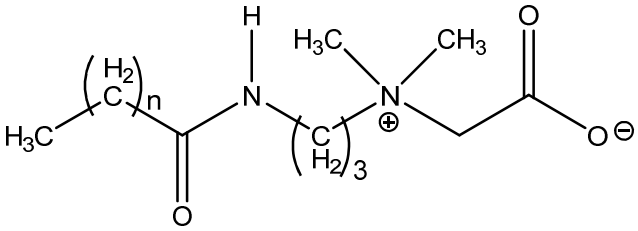

(b)

Fig. 2.2: Molecular formulae of: (a) alkyl dimethyl betaine and (b) alkyl amidopropyl betaine, where n = 6-16. pH value is high enough such that the carboxyl group is deprotonated.

Betaines are actually not amphoterics because they cannot donate H^+ in alkaline solution and are never anionic. They are internal salts of quaternary ammonium compounds at pH at and above their isoelectric point (neutral and alkaline pH), but they behave like zwitterionic surfactant in this pH region.

Betaines are soluble in water and insoluble in mineral oil and aromatic solvents. Different from other surfactant species, betaines show good solubility even near the isoelectric pH. Additionally, they are compatible with alkaline earth metals (Mg^{2+}, Ca^{2+} etc.) and other metallic ions (Al^{3+}, Cr^{3+}, Cu^{2+}, Ni^{2+} and Zn^{2+}) in acidic and neutral aqueous solutions. They also show excellent compatibility with all surfactant species, except with anionic surfactants at low pH. In this case, precipitation of betaines/anionic appears because betaines act like cationic surfactants in acidic environments. The addition of salts, especially divalent cations, thickens betaines/anionics mixture.

Chemically, betaine shows excellent stability in the presence of oxidization agents. Non-amido-type betaines, namely the betaines that have no peptide bond (-CO-NH), are resistant to hydrolysis at high and low pH values.

The Critical Micelle Concentration (CMC) of betaines is generally much lower than that of nonionic surfactant. The CMC values decrease with the increase in the length of the hydrophobic tail. For example, CMC of the C10 dimethyl betaine = 2.4 mM, while that of the C16 dimethyl betaine = 0.02 mM.

Betaines are good foaming agents. Compared to alkyl sulphates or ether sulphates, they are not as good in foaming ability but they show better solubility at alkaline pH and better compatibility with many metallic ions.

2.3. Hydrolysis of Amido Viscoelastic Surfactant at High Temperatures

It is well known that in aqueous solutions, peptide bond (-CO-NH-) can be easily broken in acidic environments at high temperatures, which is referred to as acidic hydrolysis reaction (Long and Truscott 1968; Qian et al. 1993). Because of the existence of peptide bonds in amido-carboxybetaine surfactants, acid hydrolysis reaction occurs for this type of surfactant at high temperatures. Original betaine surfactant molecules are cleaved at the peptide bond by hydrolysis reaction at high temperatures, resulting in reduction of amido-carboxybetaine surfactant concentration. At the same time, another type of surfactant, fatty acid soap, is generated by hydrolysis reaction, and its concentration keeps increasing with time.

Fatty acid has not been found to exhibit viscoelastic properties at ambient or typical field application conditions (Kaibara et al. 1997), and has much lower solubility in aqueous solutions compared to amido-carboxybetaine surfactants (Pohle 1941; Graham and Sackman 1983). Thus, viscosity alteration and phase separation of amido-carboxybetaine surfactants at high temperatures may be due to acid hydrolysis reaction. Crews et al. (2007) observed the effect of fatty acid soaps on enhancing or reducing the viscosity of viscoelastic surfactant gels.

The hydrolysis reaction of amido-surfactants has the following mechanism (**Fig. 2.3**):

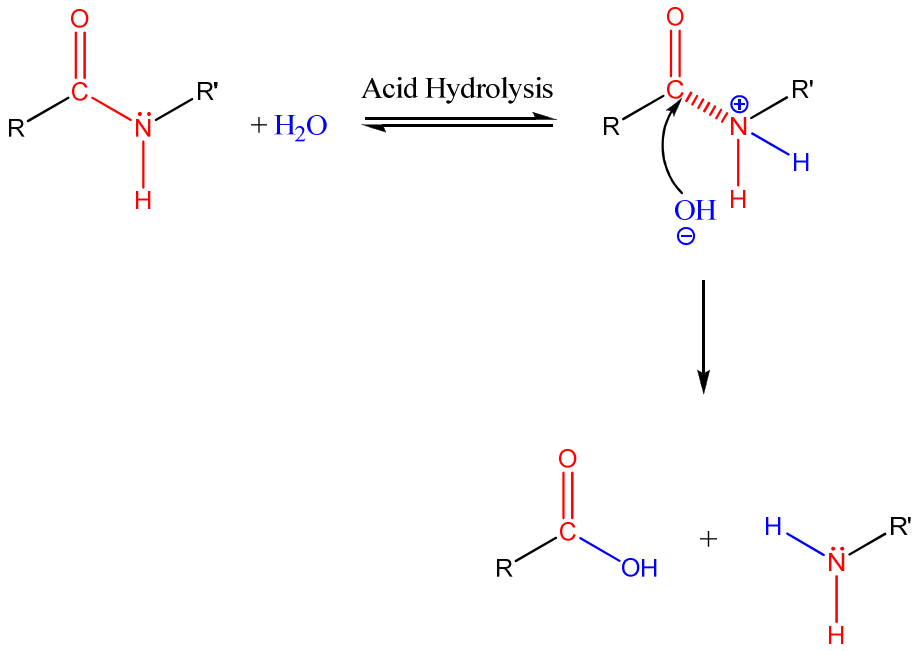

Fig. 2.3: Mechanism of acid-hydrolysis reaction of amido-surfactants.

3. QUANTITATIVE ANALYSIS METHODS FOR AQUEOUS CONCENTRATION OF AMPHOTERIC VISCOELASTIC SURFACTANTS

3.1. Introduction

Different methods were developed to measure concentration of amphoteric surfactants. Chromatographical methods have been used for the determination of amphoteric surfactants. Betaine surfactant analysis by direct high performance liquid chromatography (HPLC) is difficult, and typically the refractive index detector (Parris 1978) and UV detector (Kondoh and Takano 1986) are suitable. The latter requires pre-relabeling of carboxyl group with a UV-absorbing compound such as 4-bromomethyl-7-methoxycoumarin. Some amphoterics containing carboxylic groups, including N-alkylaminopropylglyscines, can be readily analyzed by gas chromatography after the formation of methyl ester (Campeau et al. 1987). Additionally, proton NMR methods have been proposed to the assay of betaines (Gerhards 1996), with a betaine-specific signal at 3.3 ppm versus trimethylsilylpropionate internal standard.

Amphoteric surfactants containing carboxylate groups can be successfully titrated at low pH with tetraphenylborate using a membrane electrode (Oei et al. 1991; Buschmann and Schulz 1992) or a coated-wire electrode (Vytras et al. 1985) for end-point detection. Plantinga et al. (1993) claimed that the potentiometric titration method can be used to determine alkyldimethylbetaine and free amine. In addition, Gerhards et al. (1996) presented in their work that tetraphenylborate titration can be used to

determine carboxybetaines of alkyl chain length of C8 at concentrations higher than 0.2 wt%.

3.2. Chromatographic Methods

3.2.1. High Performance Liquid Chromatography

Theoretically, amphoteric surfactants can be well separated from each other and from other surfactant species by High Performance Liquid Chromatography (HPLC) columns; but because of difficulties encountered in the surfactant detection, only a few applications have been reported by direct HPLC analysis of amphoteric surfactants. Because they are internal salts, amphoteric surfactants cannot be easily labeled with UV-absorbing ion-paring reagents to improve their detectability. In some cases, the refractive index detector (Parris 1978) and the low wavelength (~200 nm) UV detector (Kondoh and Takano 1986; Tegeler et al. 1995) are applicable. For reverse phase HPLC, evaporative light scattering detector (ELSD) can be used (Im et al. 2008).

The detection difficulties can be overcome for specific types of carboxybetaines, such as 4-bromomethyl-7-methoxycoumarin, if the carboxyl group is labeled with a UV-absorbing compound (Kondoh and Takano 1986).

A rapid analysis for mixtures of amphoteric surfactants and soaps with the aid of reverse phase high performance liquid chromatography (HPLC) has been developed by Parris et al. (1978). An HPLC method with diode-array detection at 210 nm is described for the routine determination of various betaine amphoteric surfactants in cosmetic cleansing products by Tegeler et al. (1995). A simple and simultaneous analysis method

for four (anionic, amphoteric, nonionic, and cationic) classes of surfactants in shampoo and hair conditioner was recently developed by Im et al. (2008). Analysis of the surfactants was performed using a reversed-phase HPLC (RPLC) combined with ELSD without any pre-treatment. **Table 3.1** lists the details of some HPLC analysis methods available for betaine surfactants.

Table 3.1. HPLC analysis methods of amphoteric surfactants (Parris et al. 1978; Tegeler et al. 1995; Im et al. 2008).

Compound separated	Column	Mobile phase	Detector
Amphoteric surfactants and soaps	μ-Bondapak-C 18 (guard column containing Co:Pell ODS)	Methanol-water (85:15, v/v) with 0.2 vol% acetic acid (pH 4)	Differential refractometer (Waters Assoc. Model R-401)
Betaine surfactants, various	Cation-exchange column, Nucleosil 100-5 SA (5 μm, 250 × 4 mm I.D.)	Acetonitrile-(0.05 M lithium hydroxide in water) (70:30, v/v) with phosphoric acid (pH 1.6)	Diodearray detector (wave length 210 nm)
Mixture of nonionic and ionic surfactants	Reverse phase column, YMC-J'sphere ODS-H80 (150mm×4.6mm, 4 mm)	Mixture of acetonitrile (ACN), trifluoroacetic acid (TFA) containing water and tetrahydrofuran (THF)	Evaporative light scattering detector (ELSD) (Alltech 500)

3.2.2. Gas Chromatography

Because of the lack of volatility of the amphoteric surfactants, directly analysis of amphoteric surfactants by Gas Chromatography (GC) has not been reported extensively. Quaternary ammoniums with low molecular weights can be analyzed by several GC methods using different stationary phases; however, these analytes lack the hydrophobic tails and are too light to be surfactants. Thus, if they are chemically decomposed into lighter and more volatile compounds, quaternary ammonium amphoteric surfactants with higher molecular weight can be analyzed by direct GC.

However, Campeau et al. (1987) showed that some amphoteric surfactants containing carboxyl functional groups can be readily analyzed by GC. In their work, a group of carboxy-quaternary ammonium surfactants, N-alkylaminopropylglyscines, was separated and respectively quantified by GC after the formation of methyl ester.

3.2.3. Thin-Layer Chromatography

Thin-layer chromatography (TLC) methods are most extensively applied in the qualitative and quantitative analysis of phosphatides. Some published methods for the analysis of amphoteric surfactants by TLC are listed in **Table 3.2**.

Table 3.2. TLC analysis of amphoteric surfactants (Koenig 1970, Read 1985).

Compound separated	Stationary phase	Developer
Amphoteric surfactants, various	Silica gel G containing 10% $(NH_4)_2SO_4$	80:19:1 chloroform/methanol/ (0.05 M sulfuric acid)
Amphoteric surfactants, various	Silica gel GF-254	10:10:5:2 *n*propanol/chloroform/methanlo/ (10 M ammonia)
Betaine; separation of reaction mixture	Iatroscan Chromarod SI and SII	2:1 chloroform/ethanol

3.3. Spectroscopic Methods

3.3.1. Mass Spectrometry

The application of mass Spectrometry (MS) on the routine analysis of amphoteric surfactants has not been successful. As an example, shown by Myers (1988), conventional GC-MS or direct electron impact MS is not suitable for direct analysis of the quaternary ammonium salts due to their low volatility.

Amphoteric surfactant molecules are often cleaved before MS detection by either Electron Impact Ionization (EI) or Chemical Ionization (CI), so that only fragments and rearrangement products can be obtained after ionization by EI or CI. For instance, quaternary ammonium surfactants are normally decomposed into tertiary amines, which can be ionized or protonated for MS detection. In addition, MS method is especially difficult for surfactant samples with unknown composition and impurities.

3.4. Titration Methods

3.4.1. Titration with Anionic and Cationic Surfactants

Potentiometric Titration with Anionic and Cationic Surfactants

Carboxyl groups are protonated at low pH and carry zero net charge, while quaternary amine groups are always cationic. Thus betaine surfactants are cationic at low pH values. As a result, many betaines can be titrated with sodium dodecyl sulfate (SDS) in an acidic medium. However, only a poor and approximate end point can be obtained using indicators (for instance methylene blue), and potentiometrical titrations are therefore preferable.

By using a surfactant ion-selective electrode to detect the end point, betaines can be titrated potentiometrically with SDS. In this case, the pH of the solution should be lower than 1 because most amphoterics can be titrated with sodium dodecyl sulfate in an acidic medium.

Alternatively, benzethonium chloride can be used as the titrant. Weakly basic amphoterics can be readily titrated in an alkaline medium, with an exception of betaines which are zwitterionic in alkaline media. Success of these measurements depends on the surfactants being sufficiently hydrophobic to form complexes with the titrant and/or the indicators (Lomax 1996).

Two-Phase Titration of Mixtures of Anionics and Amphoterics

Mixtures of anionics and some amphoterics can be analyzed by titration with benzethonium chloride at high and low pH by two-phase titration method. The lower and

upper phases of the two-phase system are chloroform and aqueous solution, respectively. Bromophenol blue, which is cationic, is used as the indicator. Titration is continued until the upper phase is colorless. The indicator blank is determined and subtracted from the measurements.

At low pH, the amphoteric, being cationic in acidic environment, titrates part of the anionic. At high pH, it is converted to an anionic. Therefore the two titrations give the sum and the difference for both species (Lomax 1996). However, since betaines are zwitterionic at high pH, this method does not apply to surfactant mixtures containing betaines.

3.4.2. Other Titration Methods

Determination of Amphoterics by Acid-Base Titration

The principles of acid/base titrations can be applied in the determination of amphoteric surfactant concentrations as well. The reason is that the amphoterics are able to absorb/lose a hydrogen atom (H^+) or a hydroxide group (OH^-) under different circumstances. Specifically, when the pH value of the solution changes, strong basic amphoterics such as betaines absorb/lose hydrogen atoms with a molar ratio of 1:1.

In practice, ethanol or isopropanol is used to suppress hydrolysis reaction for amido-type amphoteric surfactants in high and low pH solutions. However, even with alcohol, the end point may not be sharp for this type of surfactant (Lomax 1996).

Surfactant sample solutions are prepared in alcohol with an excess amount of HCl or NaOH added. Bromophenol blue is used as indicator if the titrant is base, and

phenolphthalein is used as indicator is the titrant is acid. Similar to regular acid/base titration, the end point appears at pH =3 for bromophenol blue and pH = 10 for phenolphthalein during the surfactant acid/base titration. The amount of amphoteric surfactant in the sample can be calculated by subtracting total amount of titrant by the excess amount of HCl/NaOH. Such titration can be accomplished without prior separation of surfactant species, as long as no other acids/bases are present (Plantinga et al. 1993).

Titration with Sodium Tetraphenylborate

Sodium tetraphenylborate titration can be used to measure the concentration of both betaines and amphoterics with weakly basic nitrogen, provided that there is no other basic component in the sample. This method takes advantage of the fact that these amphoterics act like cationics in acidic solutions.

When the pH of the solution is lower than 1, surfactant with basic nitrogen can form insoluble salt with the titrant (sodium tetraphenylborate) and precipitate. The end point can be detected potentiometrically (Vytras et al. 1985), or the two-phase titration method can be used (Cross 1998).

3.5. Other Methods

3.5.1. Gravimetric Methods

Compared with other methods, gravimetric techniques are generally more labor-intensive. However, this kind of methods has two significant merits: cost-effectiveness

and high reproducibility. A number of ions have been used to precipitate quaternary ammonium. Quantitative determination can be done by weighing the precipitate, titrating the residual reagent, or titrating the isolated precipitate. Divalent and multivalent anions generally have lower solubility products with quaternaries than do monovalent ions (Koenig 1970).

3.5.2. Alternative Analysis Method for Amidobetaines

For amido-type amphoteric surfactants including amido-betaines, an alternative analysis method can be used. This method takes advantage of acid hydrolysis reaction of amido-surfactants in acidic conditions. A surfactant sample is weighted then mixed with acid, preferably hydrochloric acid (HCl), and heated in water bath above 90°C under reflux for more than 3 hours. The produced fatty acid can be extracted by petroleum ether, during which process the emulsion formed can be broken by adding ethanol. Fatty acid residue is dried by evaporating off the petroleum ether, and is weighted to calculate the number of moles of surfactant (Lomax 1996).

The requirements for surfactant samples for this method are:

1. Only a single type of amido-surfactant with a defined molecular structure is presented in the solution;

2. The amido-surfactant being analyzed and the produced fatty acid have known molecular structure/molecular weight;

3. The sample does not contain other sources of fatty acid or fatty alcohol.

The disadvantage of this method is that stable emulsions are easily formed for surfactant samples with relatively high concentrations, and adding alcohol as demulsifier makes the evaporation process difficult.

4. QUANTITATIVE ANALYSIS OF CARBOXYBETAINE VISCOELASTIC SURFACTANT IN ACIDIZING FLUIDS AND COREFLOOD EFFLUENT BY TWO PHASE TITRATION METHOD

Surfactant concentration is a necessary parameter in carrying out material balance calculations to obtain surfactant retention in carbonate rocks after matrix acidizing treatments. As a result, the first research objective was to develop a quantitative analysis method for amphoteric surfactant concentration, and evaluate the method as a means for measuring the concentration of carboxybetaine surfactant that is used in matrix acidizing treatments.

In this section, we further developed a two-phase titration quantitative analysis method for amphoteric surfactant concentration in typical matrix acidizing treatment fluids that was originally reported by Reid et al. (1967; 1968) and Rosen et al. (1987). The two-phase titration method was proven to be accurate and reliable, and was not interfered by typical impurities, such as acid additives, reaction products, and contaminants (mainly Fe^{2+} and Fe^{3+}) (Yu et al. 2009).

4.1. Two-Phase Titration Method

The two-phase titration method developed for anionic surfactants (Reid et al. 1967; 1968) has been extended to the analysis of betaine surfactants (Rosen et al. 1987). This method involves using an acid-mixed indicator solution, along with an anionic surfactant to titrate the betaine surfactant in a two-phase system (organic and aqueous

phases). According to Rosen et al. (1987), the mixed-indicator solution composed of disulphine blue V (also called acid blue, whose molecular formula is shown in **Fig. 4.1**) and dimidium bromide (molecular formula shown in **Fig. 4.2a**). In the present study, a cost effective substitute for dimidium bromide, ethidium bromide (**Fig. 4.2b**), was used (Buschmann 1995; Cross 1998). The mechanism of this method is given in **Eqs. 4.1 to 4.3**:

Aqueous phase:

$[\text{Betaine}]^{+-} + H^+ + [\text{Disulphine Blue V}]^- \rightarrow [\text{Betaine}\cdot H]^+\cdot[\text{Disulphine Blue V}]^-$ (Blue, to the organic phase) (4.1)

Organic phase:

$[\text{Betaine}\cdot H]^+\cdot[\text{Disulphine Blue V}]^-$ + [Dodecanesulfonate]$^-$ (from the aqueous phase) $\rightarrow$ $[\text{Betaine}\cdot H]^+\cdot[\text{Dodecanesulfonate}]^-$ (colorless) + $[\text{Disulphine Blue V}]^-$ (to the aqueous phase) (4.2)

At the end point:

[Ethidium Bromide] (Aqueous phase) + [Dodecanesulfonate]$^-$ (aqueous phase) $\rightarrow$ [Ethidium Dodecanesulfonate]$^-$ (light purple, to the organic phase) + Br^- (4.3)

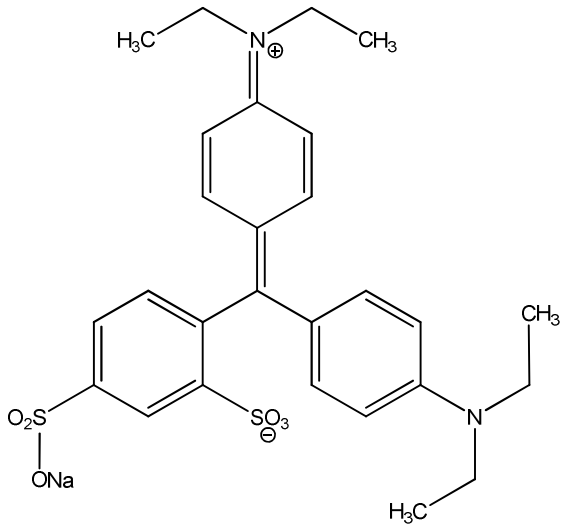

Fig. 4.1: Molecular formula of disulphine blue V (acid blue).

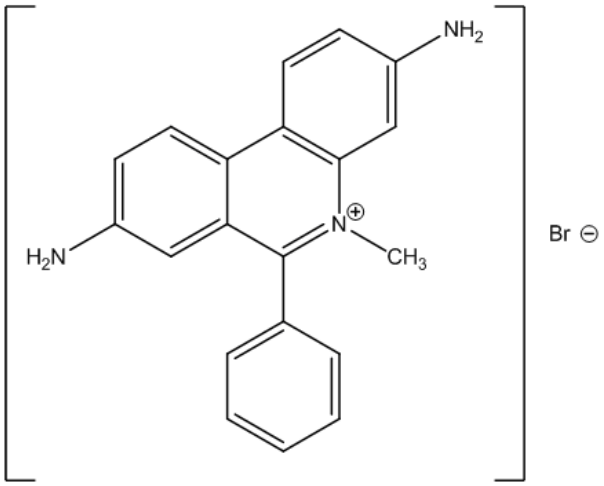

(a)

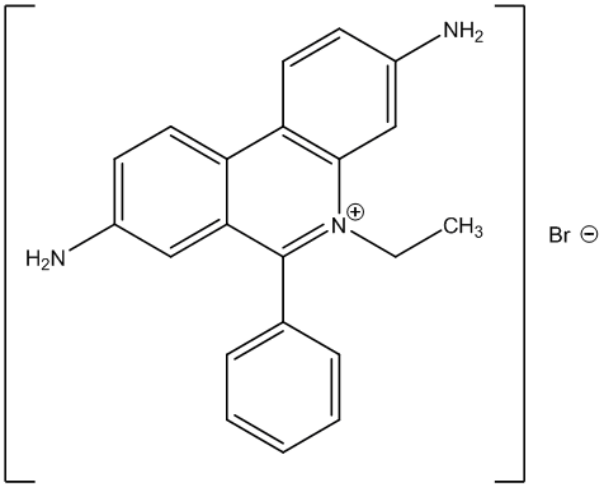

(b)

Fig. 4.2: Molecular formulae of: (a) dimidium bromide and (b) ethidium bromide.

In a two-phase system of an organic phase (chloroform, $CHCl_3$) and an aqueous phase, betaine surfactant complexes with disulphine blue V in the aqueous phase and displaces into the organic phase, which shows a blue color in the organic phase. After the addition of the titrant (sodium dodecanesulfonate, **Fig. 4.3**) to this two-phase system, titrant replaces disulphine blue V and forms complex with betaine, so that disulphine blue V returns to aqueous phase and the blue color of the organic phase starts to fade. When the end point is reached, titrant complexes with ethidium bromide in the aqueous phase and the produced complex partitions into the organic phase, and therefore the color of the organic phase becomes purple.

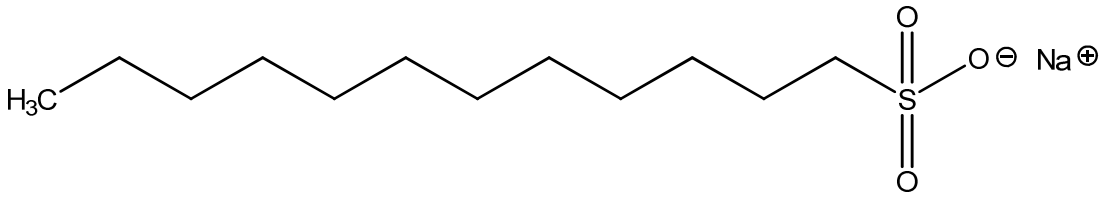

Fig. 4.3: Molecular formula of sodium dodecanesulfonate.

Emulsions can form during titrations, and ethanol was used to prevent it. However, Rosen et al. (1987) noted that the end point of titration depends on ethanol concentration. If end point is advanced, amount of ethanol should be increased. Conversely, ethanol concentration must be decreased if end point is delayed. The addition of ethanol to the two-phase system increases polarity of organic phase, and

therefore increases the solubility of betaine and $[Betaine{\cdot}H]^{+}{\cdot}[Disulphine\ Blue\ V]^{-}$ complex in it. As a result, the increase of ethanol in the system increases the percent assay of the measurements. However, once the optimal amount of ethanol is determined, this method is accurate to ±1%.

The advantages of this method are:

1. It is established for the analysis of betaine surfactants.
2. It does not require expensive instruments or especial electrodes.
3. It has a small error of ±1%.

These advantages make this method amenable in the determination of betaine surfactants in lab and field samples. The main disadvantage of this method is that the amount of ethanol has some influence on the end point detection and therefore, calibration of ethanol volume is needed for each new surfactant. In addition, this method uses a small volume of chloroform; therefore, all measurements should be conducted in a fume hood or a well ventilated place.

4.2. Experimental Studies

4.2.1. Materials

The original sample, whose active ingredient is carboxybetaine surfactant, was supplied by Rhodia Inc. Winder, Georgia. It contained nearly 37.5 wt% active ingredient. **Fig. 4.4** shows the general molecular formula of this carboxybetaine surfactant. The titrant (sodium dodecanesulfonate, > 99%) and two main components of indicator solution (ethidium bromide, 95% HPLC and acid blue, Patent Blue V C.I.)

were obtained from Sigma-Aldrich Inc. Other materials included ethanol (CH_3CH_2OH, ACS/USP grade, obtained from Pharmco Products Inc.), concentrated sulfuric acid (H_2SO_4, 98 wt%, Sigma Aldrich Inc.), 1 mol/l sulfuric acid (Fisher Chemical Inc.) and chloroform ($CHCl_3$, 100 wt%, Mallinckrodt Baker Inc.).

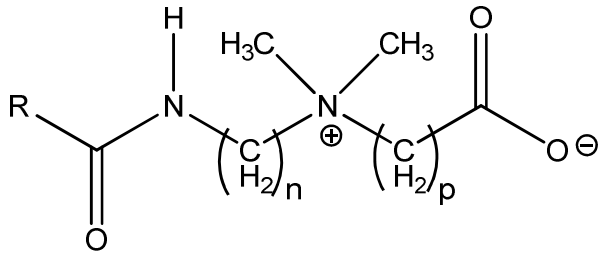

Fig. 4.4: General formula of carboxybetaine surfactant, in which R may contain 14 to 26 carbon atoms, and may be straight chain or branched alkyl, aromatic, aliphatic or olefinic groups. n is from 2 to 4 and p is from 1 to 5. pH value is high enough such that the carboxyl group is deprotonated.

Interferences of acids, common metal ions in spent acids and common additives on surfactant concentration measurements were studied, including hydrochloric acid (HCl, 36.8 wt%, Mallinckrodt Backer Inc.), 10 wt% HTO acid (organic acid mixture, services company), corrosion inhibitor (services company), calcium chloride ($CaCl_2.2H_2O$, ACS reagent grade, > 99.0%, Sigma Aldrich Inc.), magnesium chloride ($MgCl_2$, anhydrous, 99.99%, Sigma Aldrich Inc.), iron (II) chloride ($FeCl_2$, anhydrous, 99.99%, Sigma Aldrich Inc.), iron (III) chloride ($FeCl_3$, anhydrous, 99.99%, Sigma

Aldrich Inc.), methanol (CH_3OH, GR ACS grade, > 99.8%, EMD Chemicals Inc.) and 10 vol% mutual solvent (ethylene glycol monobutyl ether, obtained from a services company). To the best of our knowledge, HTO acid is the only organic acid system that has been used in diverting fluids for acid treatments (Huang and Crews 2008). All solutions were prepared using de-ionized water with a resistivity of 18.2 mΩ-cm at 25ºC.

4.2.2. Procedure

Acid-mixed indicator solution was prepared by the following procedure: Weigh 0.050 g dimidium bromide into a 50 ml beaker and dissolve it in 10 ml hot 1:9 EtOH/H_2O solution. Weigh 0.050 g disulphine blue V into a second 50 ml beaker and dissolve it in 10 ml 1:9 EtOH/H_2O solution. Add the contents of the second beaker to that of the first one and then add another 5 ml hot 1:9 EtOH/H_2O solution. Stir the solution and transfer it to a brown bottle; add 100 ml deionized water, 25 ml 1 mol/l H_2SO_4 solution and then 100 ml de-ionized water to the bottle.

An aqueous sample solution, approximately 1×10^{-3} mol/l, was prepared by dissolving *m* g of surfactant sample with 10.00 ml ethanol and diluting to 50.00 ml with deionized water. Next, 10.00 ml sample solution was pipetted to an Erlenmeyer flask, followed by 10 ml acid-mixed indicator solution, 0.235 ml concentrated H_2SO_4, 15 ml chloroform and 2.40 ml ethanol. The mixture was titrated with 1.003×10^{-3} mol/l titrant solution. Note that the two-phase mixture was shaken vigorously after each addition of titrant. At the end point, the color of the organic phase turned from blue to light purple. **Fig. 4.5** shows the color of the organic phase during titration.

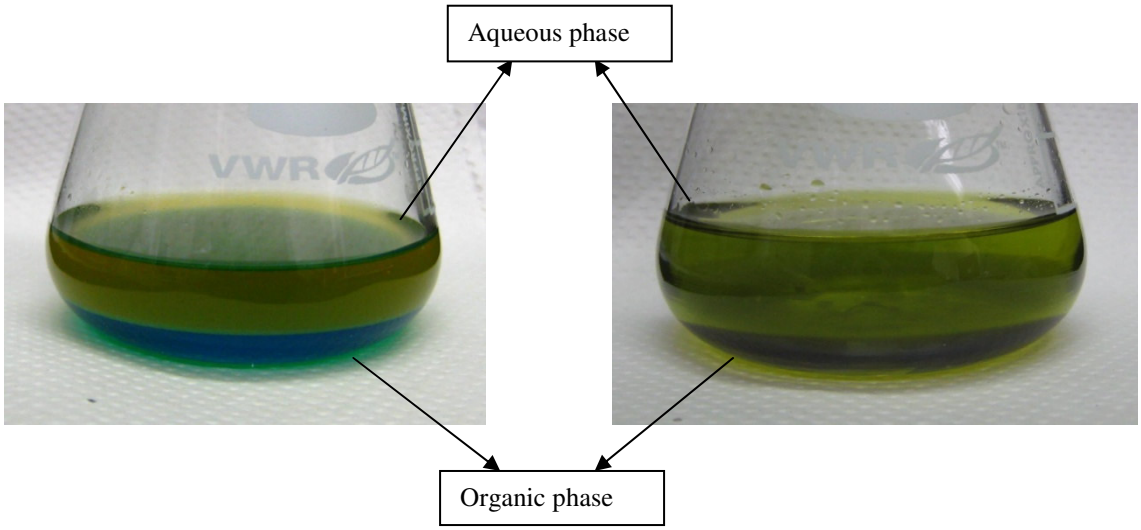

(a) During titration (b) At the end point

Fig. 4.5: The color of the organic phase changes during the titration. (a) blue before the end point and (b) purple at the end point. The organic phase is the lower phase and the aqueous phase is the upper phase.

The concentration (wt%) of surfactant sample was calculated using **Eq. 4.4**.

$$\text{Surfactant Concentration (wt\%)} = \frac{(\text{molarity of titrant}) \times (\text{volume of titrant}) \times (\text{molecular weight of surfactant})}{m \times \frac{10.00\ \text{ml}}{50.00\ \text{ml}} \times 0.375} \times 100\% \quad (4.4)$$

where m = weight of sample used to prepare the sample solution, g. The molarity of titrant is in mol/l, the volume of titrant is in liters and the molecular weight of surfactant is in g/mol.

4.3. Results and Discussion

4.3.1. Measurement of Surfactant Concentration in Aqueous Solutions

Preliminary studies were conducted to determine the amount of ethanol required for titration. Ethanol is needed to prevent the formation of emulsions during mixing the two phases, as shown in **Fig. 4.6.** The beaker on the left shows emulsion in the system without ethanol, while the beaker on the right shows the system with ethanol, in which no emulsion is noted. The picture was taken after the same amount of titrant was added (6.0 ml) to both samples, and setting them still for 2 minutes after vigorous mixing.

For the measurement on 10.00 ml sample solution as described previously, different volumes of ethanol, from 2.00 to 2.50 ml with an increment of 0.10 ml, were used to determine the effect of ethanol on the end point. The results are listed in **Table 4.1**. Percent assay increased as the volume of ethanol was increased, and 100% percent assay was obtained when the ethanol volume was 2.40 ml.

In addition, methanol was tested as a substitute for ethanol for the two-phase system. It was found that methanol functions in a way similar to ethanol. However, the color change at the end point with methanol was not as sharp as that with ethanol. Moreover, methanol is toxic and thus is more difficult to handle. Therefore, ethanol was used as demulsifier in the present study.

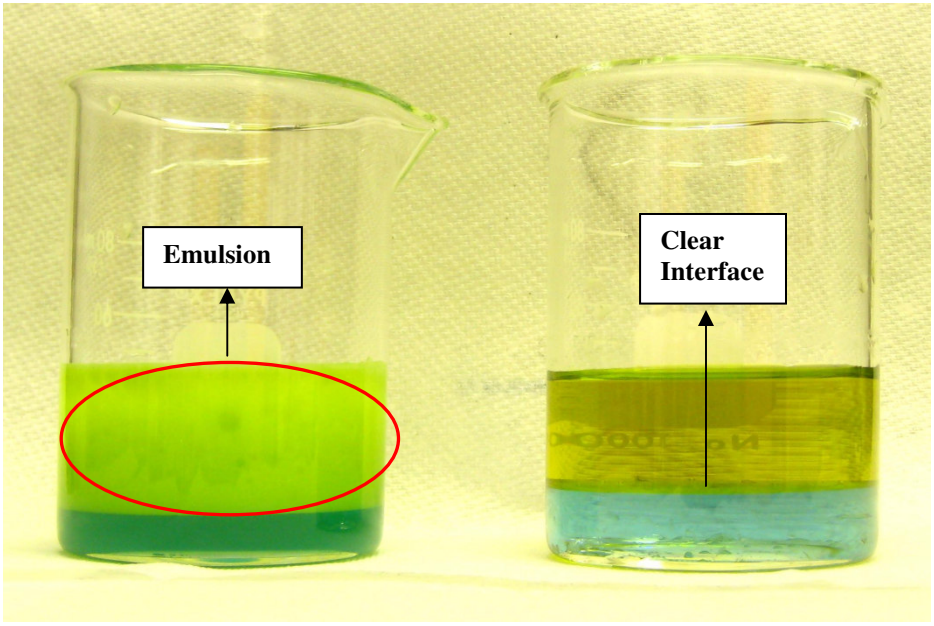

(a) (b)

Fig. 4.6: The two-phase systems (a) with no ethanol added, in which emulsion was noted and (b) with 2.4 ml ethanol added and no emulsion was present. Both systems contained 6.0 ml titrant, and were set still for 2 minutes after vigorous mixing.

Table 4.1. Effect of ethanol on surfactant concentration measurements. [a]

Volume of Ethanol, ml	Measured Value/Actual Value, %
2.50	101.37
2.40	100.21
2.30	98.46
2.20	97.97
2.10	97.02
2.00	95.80

a. Volume of ethanol is based on 10 ml surfactant sample solution.

In the subsequent experiments, stock solutions containing 2, 4, 6, 8, and 10 wt% surfactant were prepared from the as received surfactant solution using deionized water. Diluted solutions with surfactant concentration of approximately 1×10^{-3} mol/l were prepared from these stock solutions, which were titrated with 1.003×10^{-3} mol/l sodium dodecanesulfonate. For each stock solution, three diluted solutions were made, and each diluted solution was titrated three times. Surfactant concentration was calculated by averaging the results of these measurements (**Table 4.2**).

Fig. 4.7 shows the measured surfactant concentration as a function of actual surfactant concentration for all stock solutions, and the errors are listed in **Table 4.3**. All surfactant solutions were titrated with errors within ±1.1%. This error range is slightly higher than that obtained by Rosen et al. (1987). This may be due to the fact that the analyte in the present study, carboxybetaine, is not a single betaine, whereas a relatively better-defined betaine (Monateric LMAB, $RCONH\text{-}C_3H_6N^+(CH_3)_2CH_2COO^-$, where RCO = "cocoyl") was used by Rosen et al. (1987).

Table 4.2. Example of surfactant concentration calculation for one sample.

Stock Solution	m[a], g	Trial	$V_{titrant}$, L	Average $V_{titrant}$, L	Measured Surfactant Concentration, wt%	Average Measured Concentration, wt%	Actual Surfactant Concentration, wt%	Error, %
1	1.0024	1	0.00952	0.00953	6.11	6.11	6.05	0.99
		2	0.0095					
		3	0.00956					
2	1.0315	1	0.00979	0.00979	6.1			
		2	0.00977					
		3	0.0098					
3	0.9956	1	0.00949	0.00947	6.12			
		2	0.00947					
		3	0.00946					

a. m = weight of sample used to prepare the solution, g.

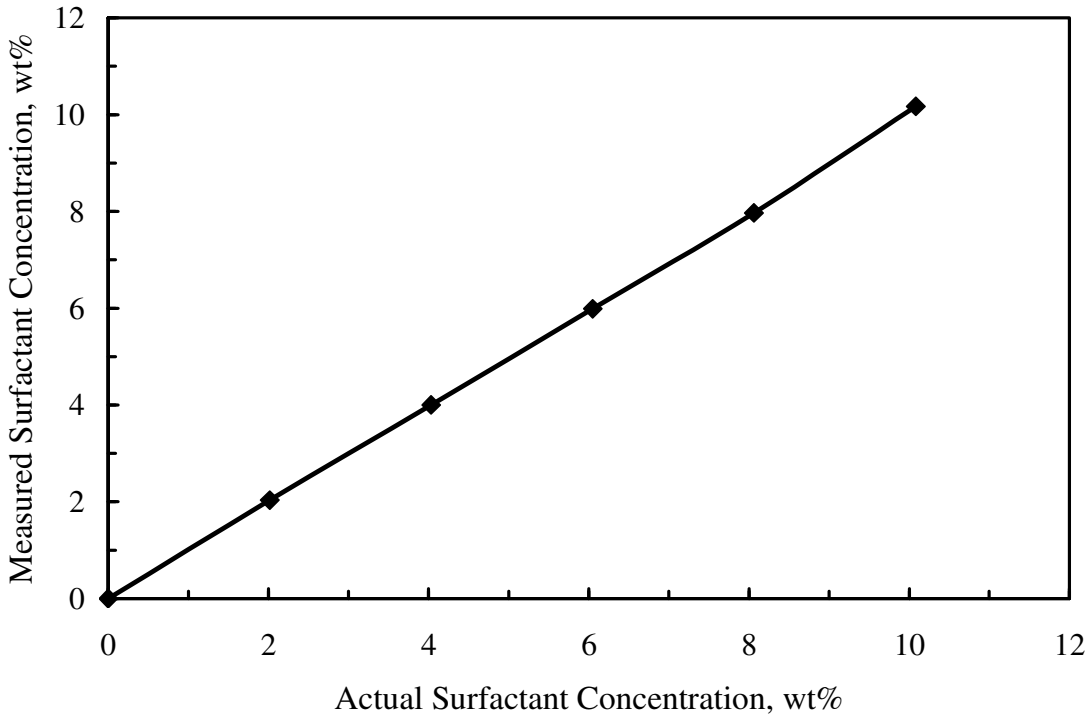

Fig. 4.7: Measured versus actual surfactant concentration.

Table 4.3. Measurement of surfactant concentration in various aqueous solutions.

Number	Actual Surfactant, wt%	Measured Surfactant, wt%	Error, %
1	2.02	2.04	+ 0.99
2	4.03	4.01	- 0.69
3	6.05	5.99	- 0.99
4	8.06	7.97	- 1.11
5	10.08	10.17	+ 0.89

4.3.2. Impact of Acid Additives on Surfactant Measurements

During acidizing treatments, surfactant solutions are pumped into the well with acids and various additives. Live acid can be contaminated by Fe^{3+} that is dissolved from rust by live acids. Chloride salts will be present in the spent acids. Therefore, it is important to examine the effect of these components on the accuracy of the two-phase titration method.

In the present work, effect of various additives on the analysis of aqueous solutions that contained 6 wt% surfactant was determined, including HCl, HTO acid, $CaCl_2$, $MgCl_2$, $FeCl_2$, $FeCl_3$, corrosion inhibitor, methanol, and mutual solvent. The components and their composition in different stock solutions are listed in **Table 4.4**. All of the stock solutions were prepared such that the final concentration of the surfactant was 6 wt%. Three diluted solutions were made from each stock solution and each of them was titrated in triplicates. The results are listed in Table 4.4.

Similar to the results obtained for surfactant solutions prepared in de-ionized water, the titration errors were within ±1.33%. This is good indication that the effects of these additives on the analysis of surfactant were not significant. As a result, acid-mixed indicator two-phase titration method can be used to measure carboxybetaine concentration in typical acid treatment fluids in both live and spent acids.

Table 4.4. Impact of typical acid additives, reaction products and contaminants on the accuracy of the two-phase titration method. All solutions contained 6 wt% surfactant.

Solution	Actual Surfactant, wt%	Measured Surfactant, wt%	Error, %
20 wt% HCl,	6.00	6.07	1.14
20 wt% HCl, 1 wt% Corrosion Inhibitor	6.03	6.11	1.33
15 wt% $CaCl_2$	6.02	6.04	0.27
7.5 wt% $CaCl_2$, 6.4 wt% $MgCl_2$	6.01	6.06	0.83
5 wt% $FeCl_2$	5.97	6.02	–0.84
5 wt% $FeCl_3$	6.10	6.05	0.82
10 wt% HTO acid	6.04	5.94	–1.16
10 wt% Methanol	6.05	6.04	–0.23
10 wt% Mutual Solvent	6.05	5.97	–1.32
5 wt% Mutual Solvent	6.06	6.10	0.59

4.4. Summary

The two-phase titration method for amphoteric surfactant that was first reported by Rosen et al. (1987) is further developed in this research to analyze the concentration of carboxybetaine viscoelastic surfactant in typical acidizing fluids. The optimized two-phase titration method was used to measure surfactant concentration, and the impact of acid additives, reaction products, and contaminants was examined on these measurements.

Based on results obtained, surfactant concentration in both live and spent acid with various acid additives can be measured by the two-phase titration method. The accuracy of this method was ±1.33%. The interference of typical impurities, including acid additives, reaction products, contaminants and HCl and HTO acid did not interfere with the measurements.

5. PROPAGATION AND RETENTION OF VISCOELASTIC SURFACTANTS FOLLOWING MATRIX ACIDIZING TREATMENTS IN CARBONATE CORES

Carboxybetaine surfactants were extensively examined in various labs, and applied in several carbonate fields. To the best of our knowledge, the concentration of these surfactants in live or spent acids was never measured. By conducting core flood experiments on both calcite and dolomite cores, we report the first complete set of measurements where the concentration of carboxybetaine surfactant was analyzed in both live acid with various additives, and in spent acids with high levels of calcium, magnesium, iron(II) and iron(III) ions. These extensive measurements allowed us to perform material balance calculation to determine the amount of surfactant retained inside the core (Yu et al. 2010)

5.1. Experimental Studies

5.1.1. Materials

The original surfactant sample, whose active ingredient is carboxybetaine surfactant, was supplied by Rhodia Inc., Georgia. As received, it contained nearly 37.5 wt% active ingredient. Fig. 4.4 shows the general molecular formula of this carboxybetaine surfactant. The titrant (sodium dodecanesulfonate, > 99%) and two main components of the indicator solution (ethidium bromide, 95% HPLC; and acid blue, Patent Blue V C.I.) were obtained from Sigma-Aldrich Inc. Other materials included ethanol (CH_3CH_2OH, ACS/USP grade, obtained from Pharmco Products Inc.),

concentrated sulfuric acid (H_2SO_4, 98 wt%, Sigma Aldrich Inc.), 1 mol/l sulfuric acid (Fisher Chemical Inc.), chloroform ($CHCl_3$, 100 wt%, Mallinckrodt Baker Inc.) and mutual solvent (ethylene glycol monobutyl ether, obtained from a services company). All solutions were prepared using de-ionized water with a resistivity 18.2 mΩ-cm at 25ºC. All cores used in the present study were cut from large blocks of Pink Desert limestone.

The preparation of acid mixed indicator solution of the two-phase titration experiment and details of the procedure used to measure the surfactant concentration in live and spent acids were given in Section 4.

5.1.2. Core Flood Experiment

Core flood tests were performed using Pink Desert cores with 1.5 in. diameter and 20 in. length. Core flood apparatus is shown schematically in **Fig. 5.1**. Cores were saturated with fresh water (total dissolved solids, TDS, of 500 ppm), and their initial permeability was measured by injecting fresh water at a constant rate of 15 cm^3/min. Core flood data are listed in **Table 5.1**. After measuring core permeability, a surfactant-based acid, which contained 15 wt% HCl, 7 vol% surfactant and 0.3 vol% corrosion inhibitor, was injected at a constant flow rate (1.5 to 40 cm^3/min). The formula used to prepare the surfactant-based acid is given in **Table 5.2**.

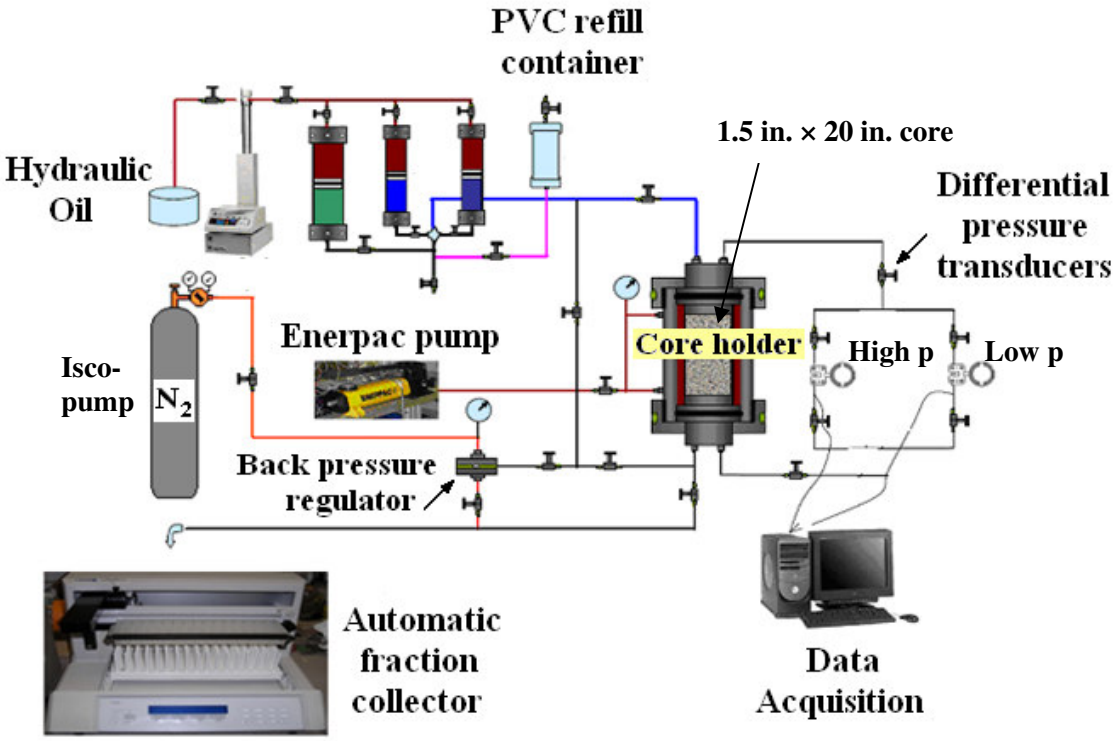

Fig. 5.1: Core flood set-up.

Table 5.1. Core flood data for calcite.

Experiment	Pore volume, cm^3	Porosity, volume fraction	Permeability, md	Injection flow rate, cm^3/min	Shear rate, s^{-1}
1	106.9	0.195	75.0	3	533
2	101.1	0.185	73.5	5	921
3	130.0	0.220	130.0	10	1,165
4	148.2	0.256	85.5	15	2,258
5	121.0	0.214	90.0	20	2,879
6	97.8	0.167	70.0	15	3,082
7	124.5	0.227	90.0	40	5,429
8 [a]	130.0	0.237	54.0	1.5	251

a. In experiment #8, 10 vol% mutual solvent solution was injected after acid breakthrough noted at 1.80 PV.

Table 5.2. Composition of surfactant-based acid.[a]

Component	Concentration, vol%
De-ionized water	51.7
31.5 wt% HCl	41.0
Surfactant	7.0
Corrosion inhibitor	0.3

a. Acid concentration was 14.7 wt%, and surfactant concentration was 6.44 wt%.

Viscoelastic surfactant-based acids are non-Newtonian fluids (Nasr-El-Din et al. 2008). The apparent viscosity of partially spent acid (pH 4.5) was measured using a HP/HT rheometer and the results are shown in **Fig. 5.2.** The viscosity decreased with increasing shear rate highlighting the shear thinning behavior of these fluids.

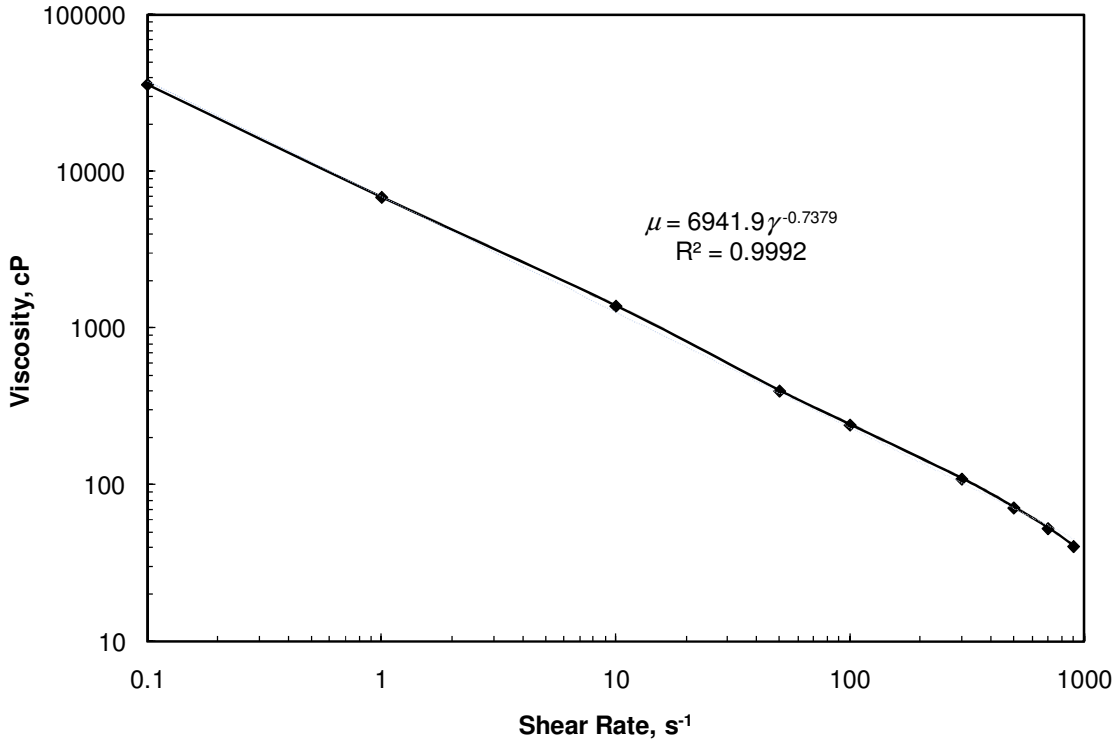

Fig. 5.2: Viscosity of partially spent (pH 4.5) surfactant-based acid as a function of shear rate. The composition of surfactant based acid is given in Table 6.2, and the viscosity measurement was conducted at ambient conditions.

In all core flood tests, fresh water was injected immediately after acid breakthrough. Surfactant concentration was analyzed quantitatively in the injected acid and core effluent using the two-phase titration method.

5.2. Results and Discussion

5.2.1. Propagation of Surfactant-Based Acids in Calcite Cores

Photos of the inlet and outlet faces of the core after acid injection for Test #1 of calcite core flood experiment are shown in **Fig. 5.3**, and those of the coreflood effluent samples are shown in **Fig. 5.4**. Similar sets of photos were obtained with other calcite core flood tests.

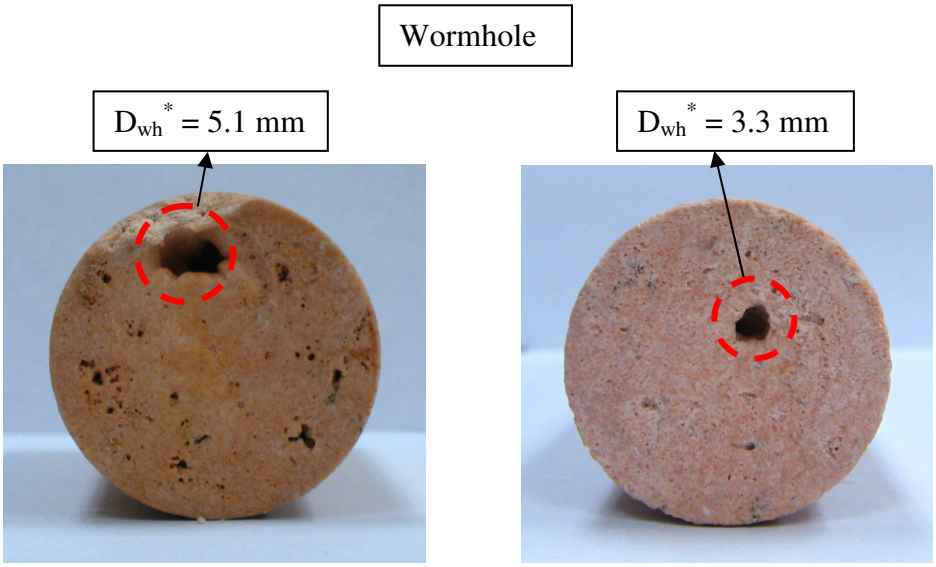

* D_{wh} denotes wormhole diameter.

Fig. 5.3: Core inlet (a) and outlet (b) after acid injection for calcite core flood test #1. Test was conducted at 15 cm^3/min and room temperature.

(a) (b) (c) (d)

Fig. 5.4: (a) Surfactant-based acid used (b) coreflood effluent before acid breakthrough; (c) coreflood effluent after acid breakthrough and, (d) coreflood effluent after the injection of fresh water.

Figs. 5.5 and 5.6 illustrate the pressure drop across the core as a function of the cumulative injected volume at flow rates of 10 and 40 cm^3/min, respectively. At 10 cm^3/min, Fig. 5.5, the pressure drop across the core initially increased from 75 to 95 psi, then decreased linearly with the cumulative volume injected until acid breakthrough where the presser drop was almost zero. The initial increase in pressure drop is partially due to the release of CO_2 (Shaughnessy and Kunze, 1981) and partially due to the formation of surfactant gel. At 40 cm^3/min, Fig. 5.6, the pressure drop decreased almost 50 psi after the injection of 0.5 PV of acid, and then significantly decreased until acid breakthrough after the injection of 1.45 PV.

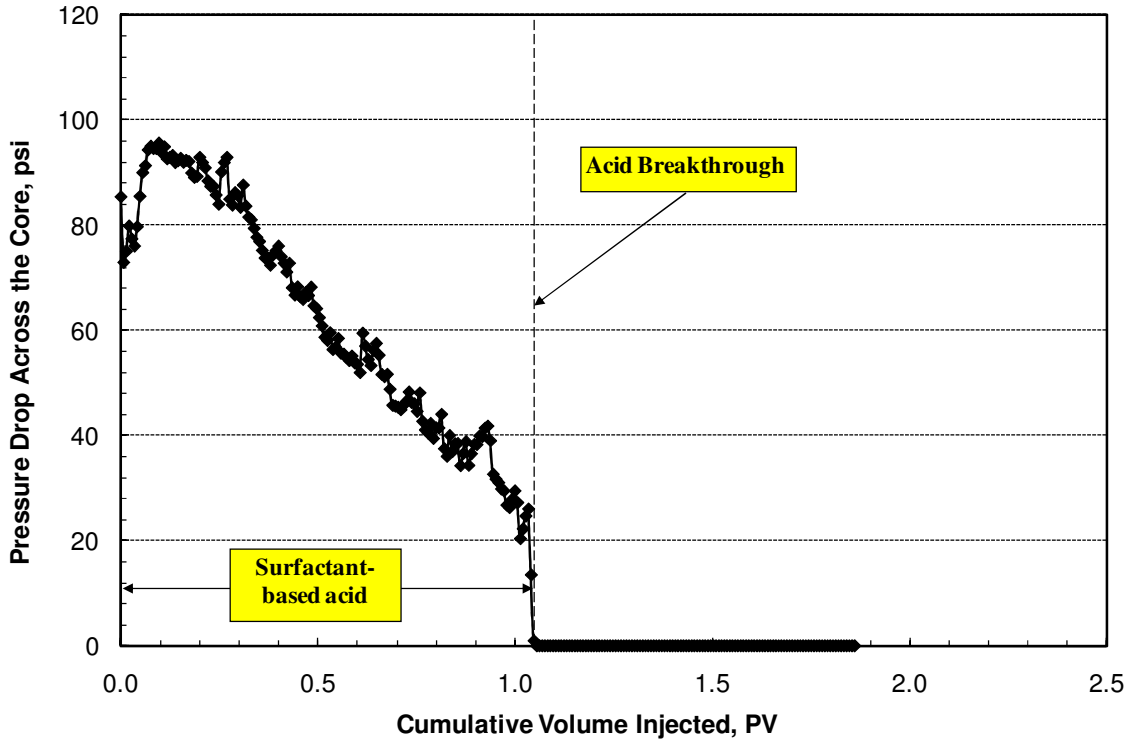

Fig. 5.5: Pressure drop across the core. Flow rate = 10 cm^3/min.

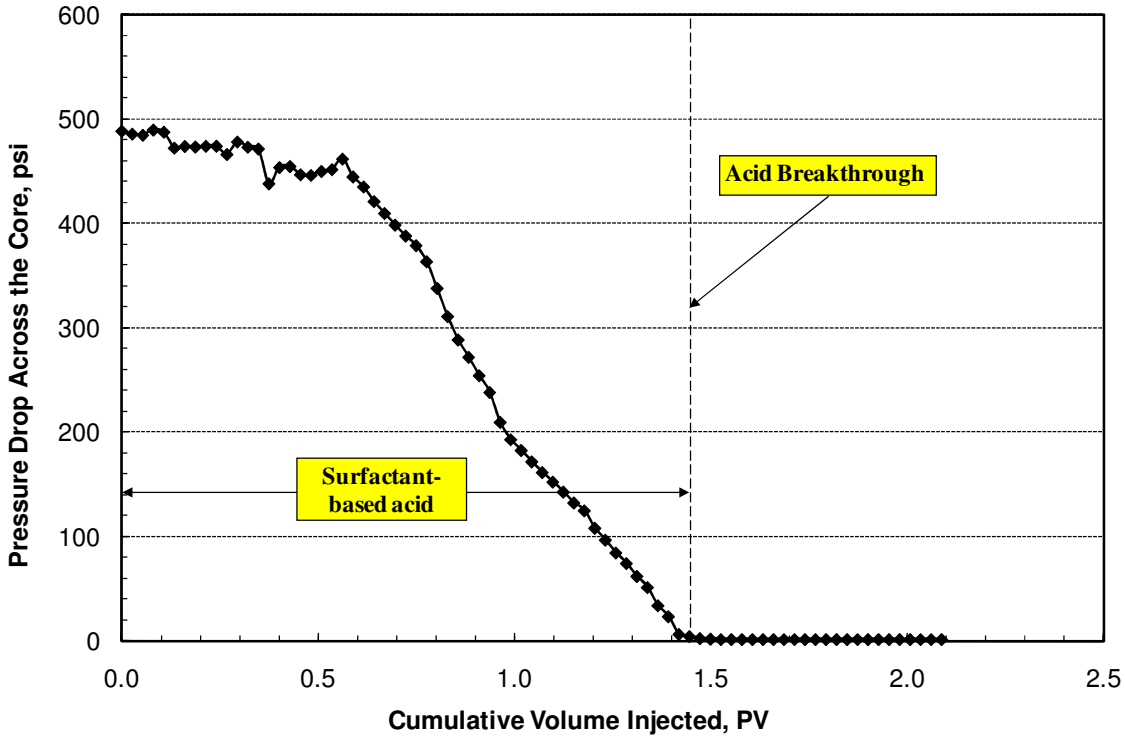

Fig. 5.6: Pressure drop across the core. Flow rate = 40 cm^3/min.

The volume of the acid needed to breakthrough varied with the acid injection rate (**Table 5.3**). **Fig. 5.7a** illustrates the pore volume of surfactant-based acid injected before acid breakthrough as a function of the acid injection flow rate. At lower flow rates, the volume of acid required to create wormhole was relatively high. As the flow rate was increased, the pore volume decreased, until it reached a minimum at 10 cm^3/min. As the flow rate was further increased, the volume increased until the flow rate reached 20 cm^3/min. This was followed by a plateau, where fewer changes in the volume were observed. The optimum flow rate was 10 cm^3/min. The existence of optimal flow rate

was consistent with the results of Hoefner et al. (1987) and Wang et al. (1993) for regular acids and Lungwitz et al. (2006) for surfactant-based acids. The latter authors noted a minimum at 1 cm^3/min. This value is different of the value noted in our work, most likely because of difference in test conditions (temperature, initial core permeability, core length, and acid additives).

Table 5.3. Surfactant retained and pore volume of surfactant-based acid at breakthrough.

Experiment	**Injection flow rate, cm^3/min**	**Shear rate, s^{-1}**	**Pore volume injected at breakthrough**	**Retained surfactant, wt%**
1	3	532	1.64	90.5
2	5	921	1.35	84.2
3	10	1,165	1.05	79.5
4	15	2,258	1.15	75.5
5	20	2,879	1.22	79.2
6	15	3,082	1.38	80.4
7	40	5,429	1.45	82.8
8	1.5	251	1.80	78.8

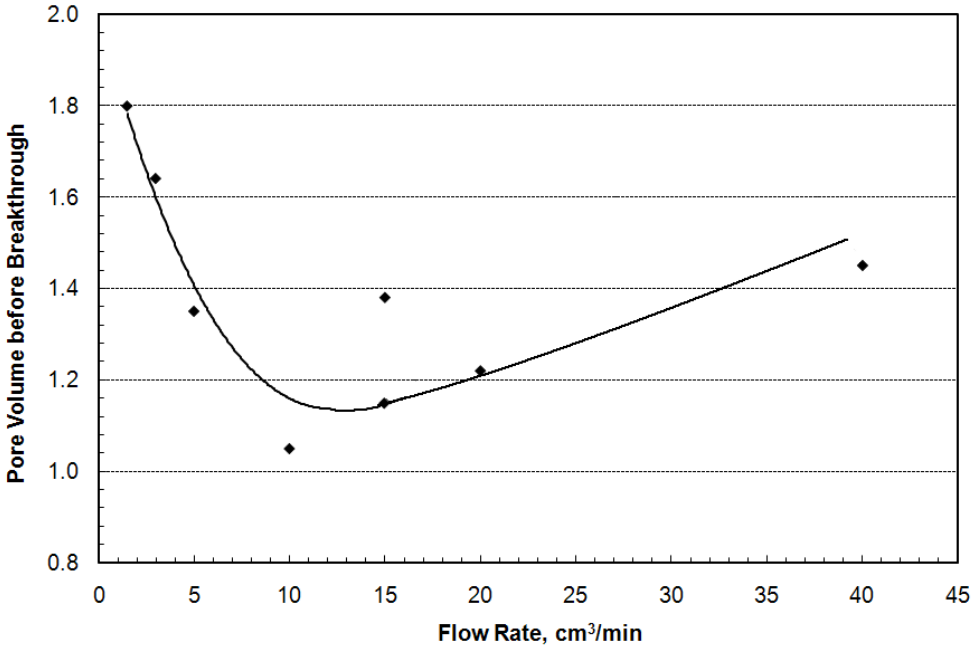

(a)

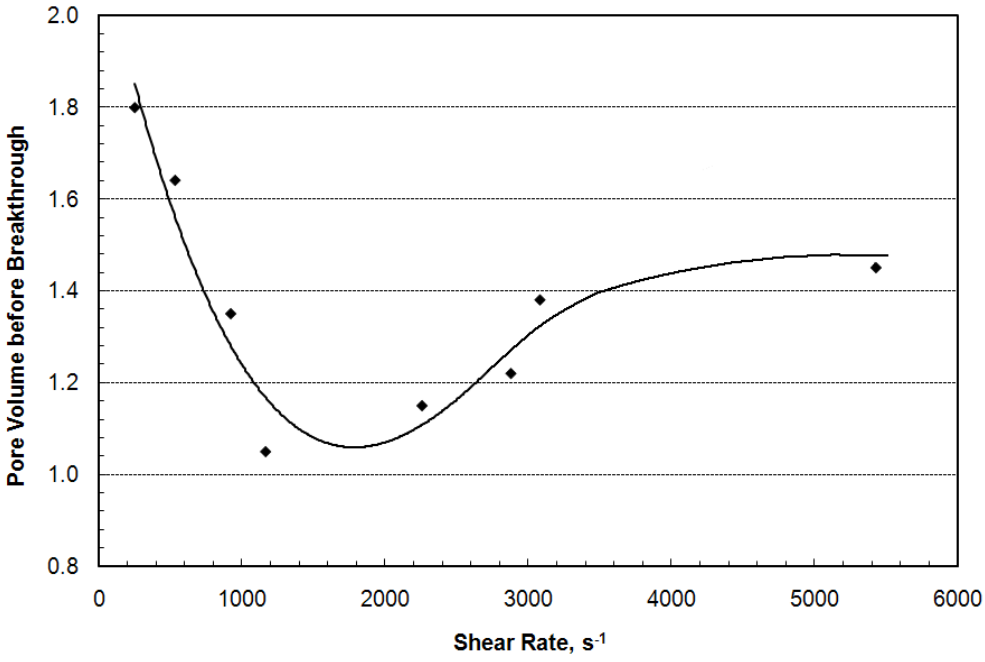

(b)

Fig. 5.7: Pore volume of injected surfactant-based acid before acid breakthrough as a function of (a) injection flow rate and (b) shear rate.

Note that two core flood tests were conducted with the same injection flow rate (15 cm^3/min); however, the volumes before breakthrough were different. This is due to the difference in the initial permeability and porosity of the two cores (Table 5.1).

Surfactant-based acids are non-Newtonian fluids. Unlike regular acids, which are Newtonian fluids, the optimum flow rate in the case of surfactant-based acids is better obtained by plotting the volume to breakthrough as a function of the shear rate. This is not needed for regular acids because the viscosity of Newtonian fluids is independent of the shear rate.

Several formulas are given in the literature to predict shear rate in porous media, including: Patruyo et al. (2002; González et al. (2005); and Rojas et al. (2008). **Eq. 5.1**, which was proposed by the latter authors, was used in the present study for its simplicity and to highlight our point.

$$\dot{\gamma} = \frac{u}{\phi L} \tag{5.1}$$

where ϕ is porosity, L (m) is characteristic length, and is given by $L = 0.05\ k_c^{0.5}$ in which k_c (md) denotes core permeability. u (m/s) is Darcy velocity given by $u = q/A$, where q (m^3/s) is flow rate, and A (m^2) is cross-sectional area of the core. Table 5.1 lists the shear rates of the different core flood experiments calculated based on the injection rates and the core properties.

Compared to Fig 5.7a, **Fig. 5.7b** shows a better trend between the pore volume to breakthrough and shear rate. It appears from these results that it is better to plot these data against shear rate instead of flow rate. It should be noted that prediction of shear

rate during acid injection is a very difficult task. The generation and propagation of wormholes in the core will change shear rate. For simplicity, the shear rate based on the initial core permeability and porosity was used.

5.2.2. Surfactant Retention as a Function of Acid Injection Rate in Calcite Cores

Surfactant and calcium concentrations in the core flood effluent are plotted in **Figs. 5.8 and 5.9** as a function of cumulative volume of injected fluids at flow rates of 10 and 40 cm^3/min, respectively. A typical surfactant concentration profile had two regions. The first region occurred before acid breakthrough, where the surfactant concentration in the core effluent was zero. This is because the core effluent was simply the fresh water that was present in the core before acid injection. The second region began following acid breakthrough. The injection fluid was fresh water and the injection rate was 10 cm^3/min (Fig. 5.8), and the surfactant concentration significantly increased from zero to 6.2 wt%. The surfactant concentration stayed at 6.3 wt% for almost 0.3 PV. It appears that this surfactant was present with the acid in the wormhole. The surfactant concentration significantly decreased with the continuous injection of fresh water.

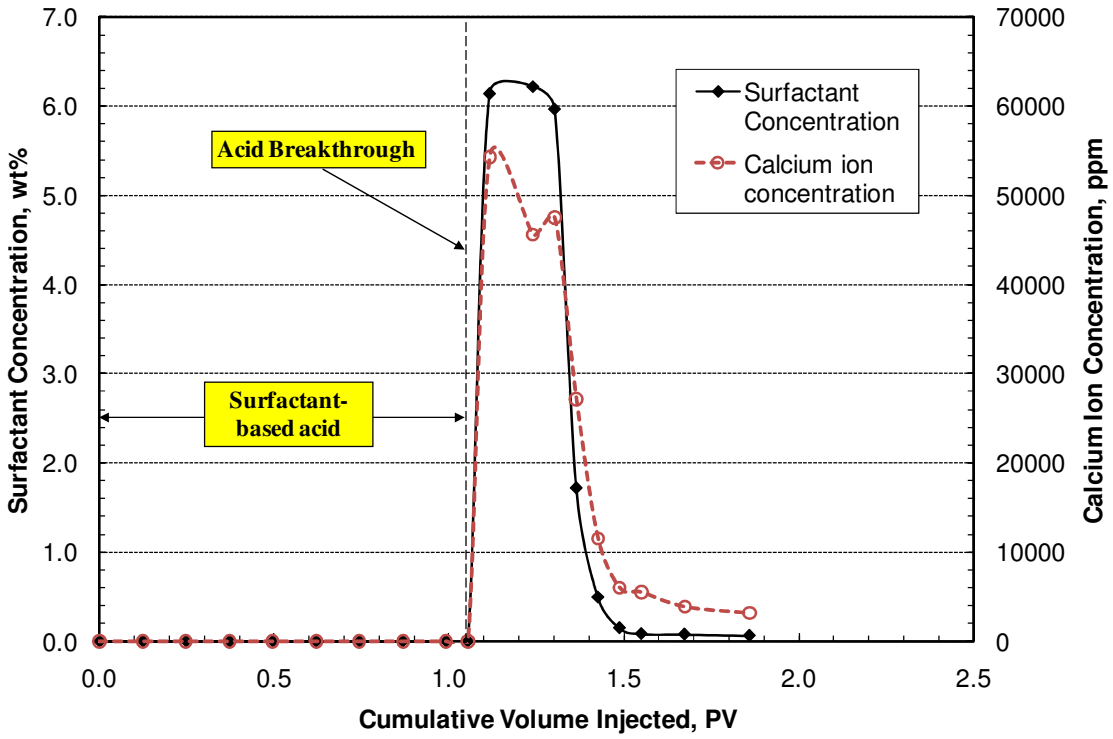

Fig. 5.8: Surfactant and calcium ion concentrations in the core effluent as a function of the cumulative pore volume injected. Flow rate = 10 cm^3/min.

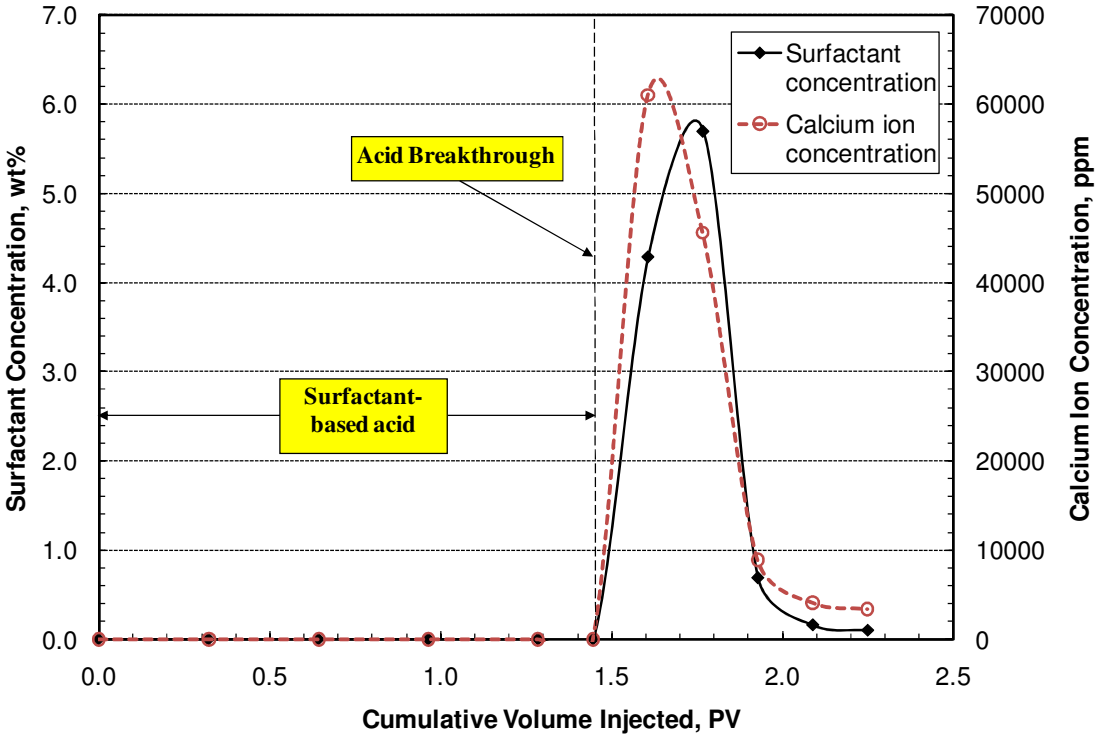

Fig. 5.9: Surfactant and calcium concentrations in the core effluent as a function of the cumulative pore volume injected. Flow rate = 40 cm^3/min.

Calcium concentration in the core effluent was analyzed by atomic adsorption (AA). The calcium concentration profile in the core effluent was similar to that noted with the surfactant and the two profiles almost coincided with each other. Visual observations of the collected samples indicated that these samples that contained both calcium and surfactant were viscous. No gel, however, was noted in these samples. It appears from these results that the surfactant produced in the core effluent did not form a gel in the core. The main source of this surfactant was the fluids present in the wormhole.

Fig. 5.9 shows the concentrations of surfactant and calcium in the core effluent at 40 cm^3/min. Similar to the results obtained at 10 cm^3/min, both profiles were close, and the calcium concentration profile exhibited tailing during the last fresh water injected into the core.

The retained surfactant was determined from material balance calculations as the percentage of the total injected surfactant (Table 5.3), and is plotted in **Fig. 5.10** as a function of the acid flow rate. The retained surfactant in the core was high ranging from 75 to 90 wt% of the total surfactant injected into the core. The retain surfactant was high at both low and high flow rates. This behavior is similar that noted with the volume of acid required to break through the core, Fig. 5.7a. A much smoother trend was noted when the percentage of the surfactant retained was plotted against shear rate, Fig. 5.10b.

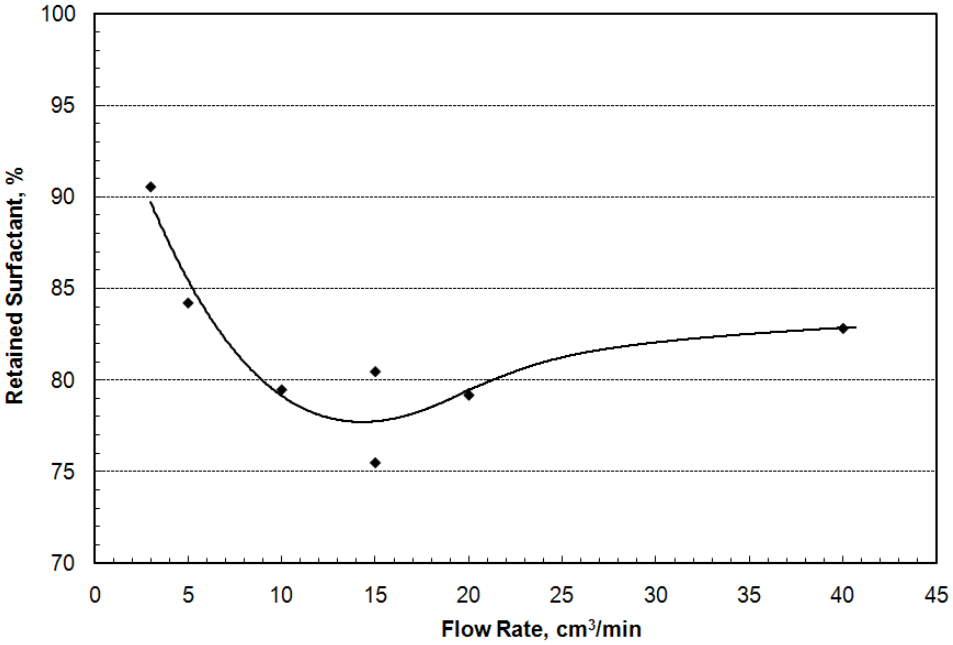

(a)

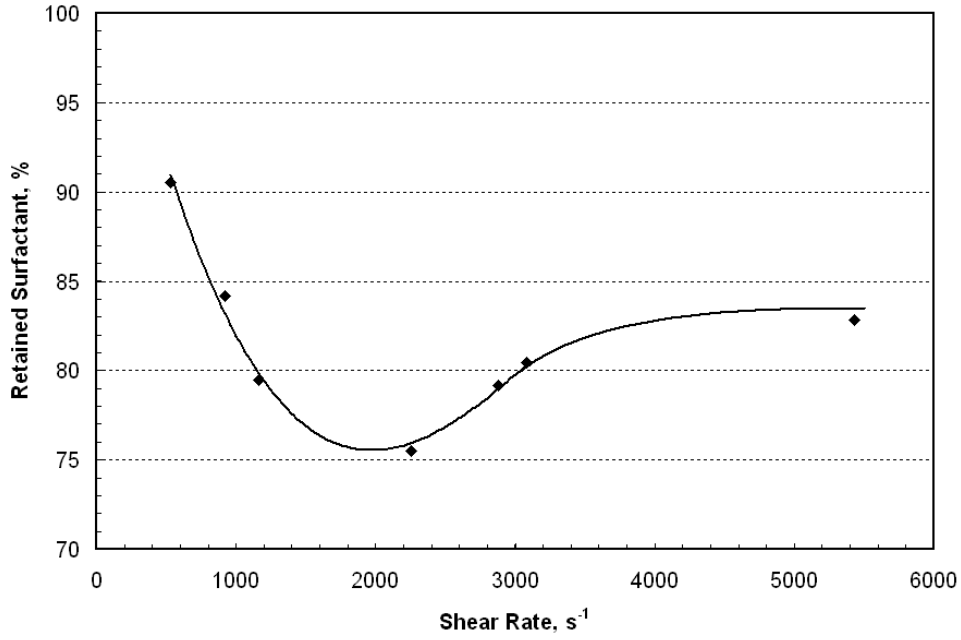

(b)

Fig. 5.10: Retained surfactant (%) in the core as a function of (a) injection flow rate and (b) shear rate.

The most important conclusion that can be inferred from Fig. 5.10 is that the amount of surfactant retained in the core following acid treatment was significant. This means that there is a need to use external (mutual solvent) or internal breakers (Crews 2005; Crews and Huang 2007b), to reduce surfactant retention, especially if a surfactant-based acid is used in power water injector or a dry gas well.

5.2.3. Effect of Mutual Solvent on Surfactant Retention in Calcite Cores

A core flood experiment (experiment #8 in Table 5.1) was conducted to determine the effect of mutual solvent on the amount of surfactant retained in the core. A Pink Desert limestone core with 20 in. length and 1.5 in. diameter was saturated with fresh water. The initial permeability was measured by injecting fresh water at a constant injection rate of 15 cm^3/min. This was followed by the injection of surfactant-based acid (Table 5.2) at a constant injection rate of 1.5 cm^3/min. Acid break through the core after the injection of 1.80 PV. This was followed by the injection of 2 PV of 10 vol% mutual solvent solution at 1.5 cm^3/min. A low flow was used in this experiment to give mutual solvent enough time to remove the surfactant retained inside the core.

The surfactant concentration in the core effluent is shown in **Fig. 5.11**. As mutual solvent propagated in the wormhole, it displaced the surfactant-based acid that was occupying the wormhole space, and dissolved part of retained surfactant in the matrix surrounding the wormhole. Therefore, the surfactant concentration increased almost 4 wt% after the injection of the mutual solvent and then decreased to nearly zero after 2.8 PV.

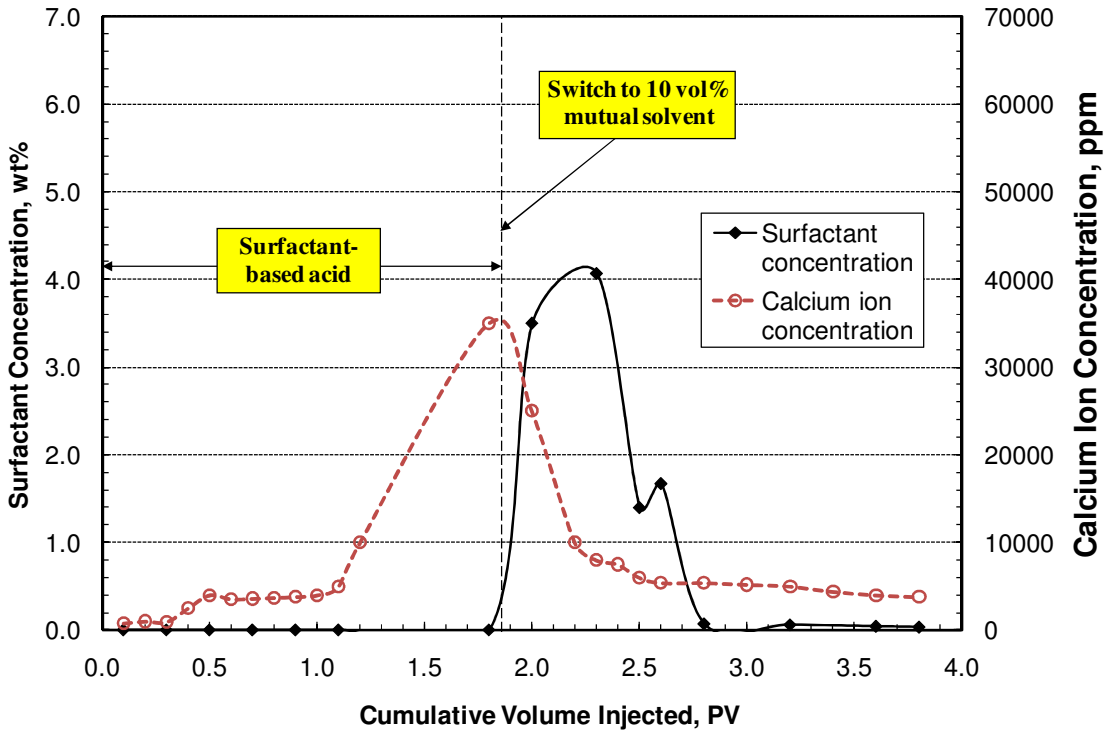

Fig. 5.11: Surfactant and calcium concentrations in the core effluent in the case of using mutual solvent. Flow rate = 1.5 cm^3/min during the whole experiment.

The surfactant concentration in the core effluent shown in Fig. 5.11 is different from those noted at 10 or 40 cm^3/min. First, the maximum surfactant concentration reached in Fig. 5.11 was 4 wt%, which is much lower than 6.2 wt% noted when the injection rate was 10 cm^3/min. Also, it took almost 1 PV for the surfactant concentration to reach zero. A third observation is that the calcium profile was ahead of that of the surfactant. On other words, the surfactant pulse was produced after that of calcium. Finally, calcium profile exhibited significant tailing that lasted to the end of the experiment.

Based on material balance calculation, the total injected surfactant was 15.85 g, and the recovered surfactant by mutual solvent was 3.36 g. Hence, the surfactant recovered by mutual solvent was 21.2%. Surfactant retention inside the core was 78.8% compared to 100% before the injection of the mutual solvent solution. Mutual solvent recovered some of the surfactant, but it did not remove all out of the core. These results mean that in a typical field treatment in water injectors, it will take longer period of time to remove the surfactant from the treated wells. This is exactly what Mohamed et al. (2002) noted in the field. Another solution is to use internal breakers to remove the surfactant (Crews 2005; Crews and Huang 2007b).

5.2.4. Propagation and Retention of Surfactant-Based Acids in Dolomite Cores

Another core flood test was performed using a dolomite core, which had a diameter of 1.5 in. and a length of 6 in. The dolomite core was saturated with fresh water. Initial permeability was measured by injecting fresh water at a constant rate of 1 cm^3/min. Core flood data are listed in **Table 5.4**.

Surfactant-based acid, Table 5.2**,** was injected at a constant injection rate of 1 cm^3/min. Temperature of acid injection was 200°F. It should be noted that we could not run this experiment at room temperature. This is mainly because of the reaction between HCl and dolomite is reaction rate is very slow at low temperatures (Lund et al. 1973; 1975). Acid breakthrough occurred after the injection of 1.44 PV of the surfactant-based acid. Injection fluid was switched to fresh water at 1.73 PV. Details of different injection

stages are given in **Table 5.5.** Photos of the inlet and outlet faces of the dolomite core after acid injection for are shown in **Fig. 5.12.**

Table 5.4. Core flood data for dolomite.

Parameter	Dolomite core flood test
Core pore volume, cm^3	46.9
Core porosity, volume fraction	0.270
Core permeability, md	100
Injection flow rate, cm^3/min	1
Back pressure, psi	1,000
Overburden (confining) pressure, psi	2,000
Temperature, °F	200

Table 5.5. Sequence of dolomite core flood tests.

Stage	Fluid type	Cumulative PV Injected	Injection pressure, psi
1	Fresh water	2.09	1,110
2	Surfactant-based acid	1.73	1,500
3	Fresh water	0.72	1,110

(a) (b)

Fig. 5.12: Dolomite core inlet (a) and outlet (b) after acid injection. Test was conducted at 1 cm^3/min and 200°F.

Fig. 5.13 shows the pressure drop across the core as a function of the cumulative volume injected. The volume of surfactant-based acid injected before breakthrough was 1.44 PV, and the core permeability increased from 100 to 550 md after acid breakthrough. It is important to mention that the increase in the pressure drop across the core, and the swings in the pressure drop were also observed by Lungwitz et al. (2007).

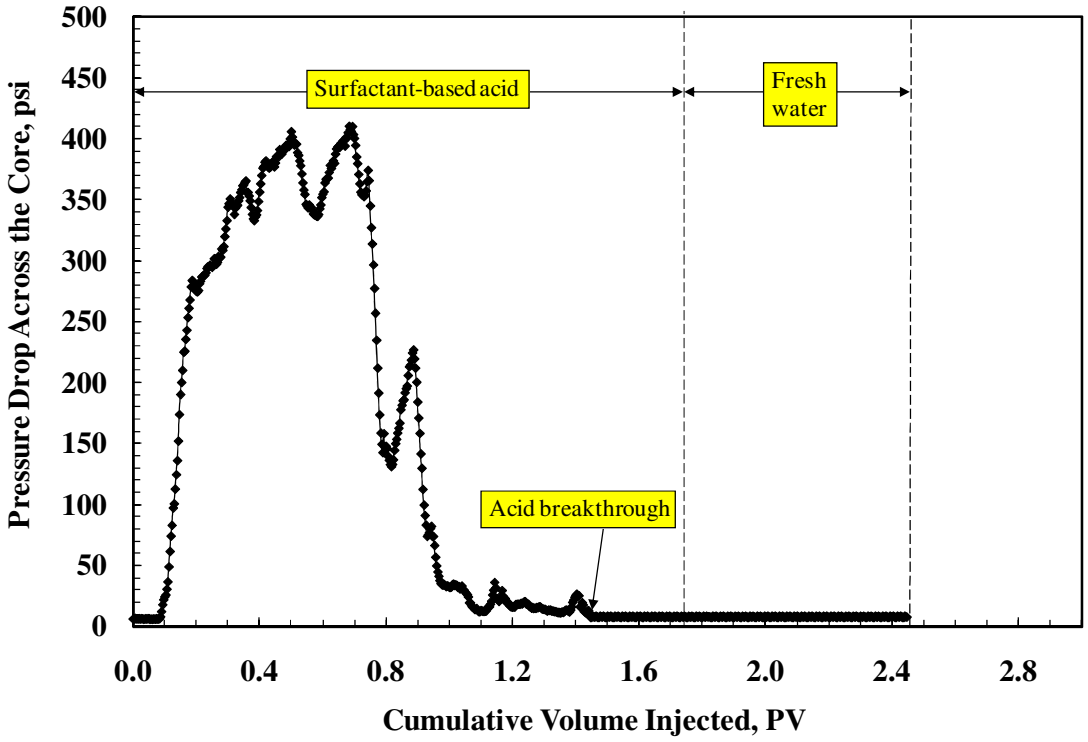

Fig. 5.13: Pressure drop across the dolomite core. Test was conducted at 1 cm^3/min and 200°F.

Fig. 5.14 shows the concentration of surfactant in the core effluent. The concentration of surfactant in the injected acid was 6.5 wt%. The surfactant concentration profile has 4 regions. In the first region (PV < 0.4), surfactant concentration was nearly zero because the effluent was the fresh water present in the core before acid injection. This was followed by the second region (0.4 < PV < 1.4), in which surfactant concentration was 0.6 to 0.7 wt%. In the third region (1.4 < PV < 2.0), surfactant concentration significantly increased to 3.53 wt%. Surfactant concentration decreased to below 0.5 wt% in the final region (PV > 2.0). According to Lund et al.

(1973; 1975), the reaction rate between dolomite and HCl is much slower than that between calcite and HCl. Apparently, the acid breakthrough in the dolomite core occurred after surfactant breakthrough. Surfactant retention in the core was determined from material balance calculations and was found to be 92 wt%. This was due to lower flow rate between dolomite matrix and the surfactant-based acid.

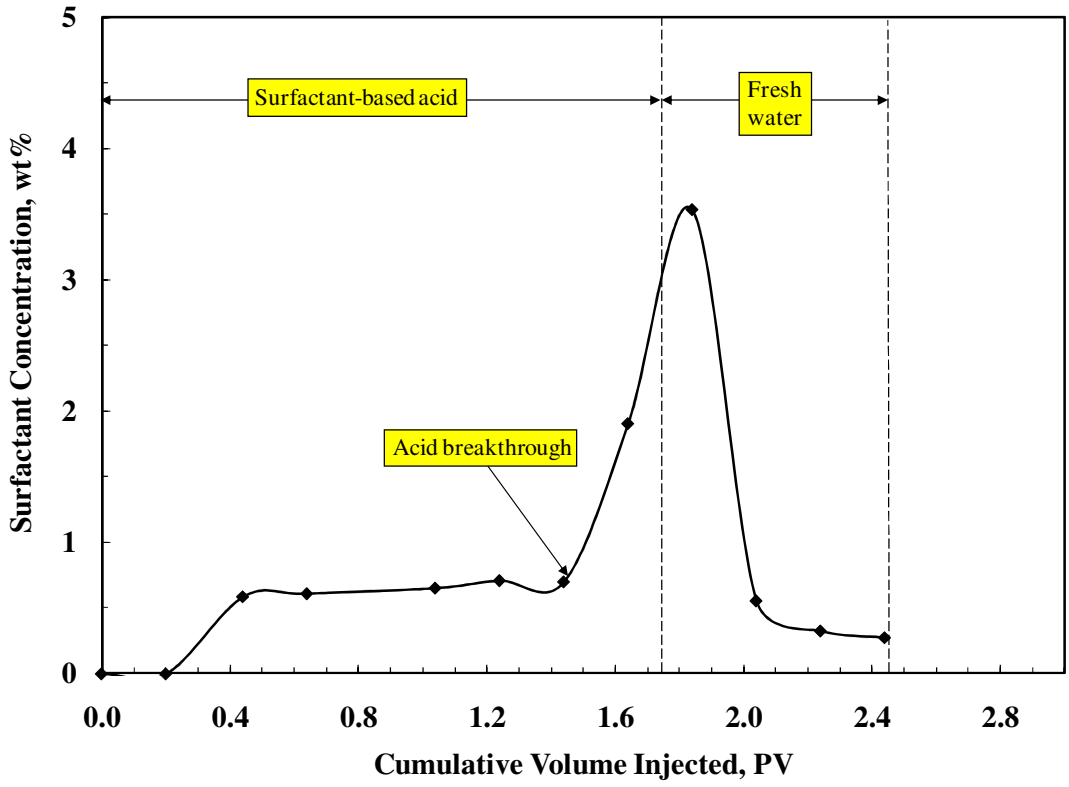

Fig. 5.14: Surfactant concentration in the dolomite coreflood effluent. This core flood experiment was conducted at 1 cm^3/min and 200°F.

5.3. Summary

Propagation and retention of a carboxybetaine surfactant in carbonate reservoirs during matrix acidizing treatments has been studied by conducting core flood experiments and measuring the surfactant concentration in acidizing fluid and core flood effluent.

Based on the results obtained, propagation of viscoelastic surfactants in linear calcite cores was found to be a function of the flow rate, or more accurately, the shear rate. The volume of acid needed to break through the core and the amount of surfactant retained varied with acid injection rate, and exhibited a minimum at 10 cm^3/min. Significant amount of surfactant was retained in the cores. The effect of injecting 2 pore volumes of 10 vol% mutual solvent removed only 20% of the surfactant injected.

6. MOLECULAR DYNAMICS SIMULATION AND ITS ROLE IN STUDYING SURFACTANT SELF ASSEMBLY

6.1. Surfactant Self-Assembly

Surfactant molecules self-assemble into micellar aggregation structures when its aqueous concentration exceeds the critical micelle concentration (CMC). CMC is a function of surfactant structure, temperature, pressure, and the ionic strength. Once the surfactant concentration reaches CMC and surfactant molecules self-assemble into micellar structures, the concentration of free surfactant monomers in the solution is nearly independent on the total surfactant concentration (Rosen 2004). The hydrophobic tails of surfactant molecules are shielded from bulk water in the interior of the aggregates, and the hydrophilic heads are exposed to water at the surface of the aggregates. Van der Waals interactions, hydrogen-bonding and electrostatic interactions have certain contribution to the self-assembly process of surfactant molecules in aqueous solutions, whereas the driving force is primarily the hydrophobic interactions (Holmberg et al. 2003).

Micelles exist as different forms, including spherical or globular micelles at relatively low surfactant concentrations, and worm-like or planar disk-like micelles at high surfactant concentrations. For ionic surfactants (cationic, anionic and zwitterionic surfactants), addition of counterions is able to reduce the electrostatic repulsion between surfactant head groups and lead to a phase transition between spherical micelles and worm-like/disk-like micelles (Holmberg et al. 2003).

Surfactant self-assembly is of tremendous interest for many natural and industrial applications. For example, self-assembly of surfactant molecules at liquid-liquid or liquid-gas interfaces is essential in the preparation and stabilization of emulsions and foams. Another example is the viscoelastic surfactant self-assembly in aqueous solutions to form worm-like micelles, which significantly enhances the elasticity and viscosity of the fluid. The importance of these surfactant self-assembly processes is reflected through their wide applications in the petroleum, chemical, food, cosmetic, pharmaceutical, and coating industries (Tadros 2005).

Although the fundamentals of surfactant micelles and their phase transitions are extensively explored, the dynamics and mechanism of surfactant self-assembly processes are not well understood. One of the challenges remained is to reveal and reproduce the surfactant self-assembly processes. Molecular dynamics (MD) simulations is therefore employed to overcome this challenge by studying surfactant self-assembly on the molecular level.

6.2. Introduction to Molecular Dynamics Simulation

Molecular dynamics (MD) simulation is carried out to understand the structures and interactions of molecular assemblies. It acts as a complement to conventional experimental approaches and enables us observe the self-assemble processes microscopically.

MD simulations of molecular systems serve as a linkage between microscopic and macroscopic scales of time and length (**Fig. 6.1**). Predictions on the bulk properties

can be provided by simulating molecular interactions and behaviors, which is subjected to limitations in computational power. MD simulations also serve as a linkage between theoretical hypothesis and experimental results. The proposed model can be proven by conducting computer simulations, while the accuracy of the simulations can be tested by carrying out experimental studies. MD simulation is a useful tool when the required experimental conditions are difficult or even impossible to achieve in the laboratory; for example, extremely high/low temperatures and pressures.

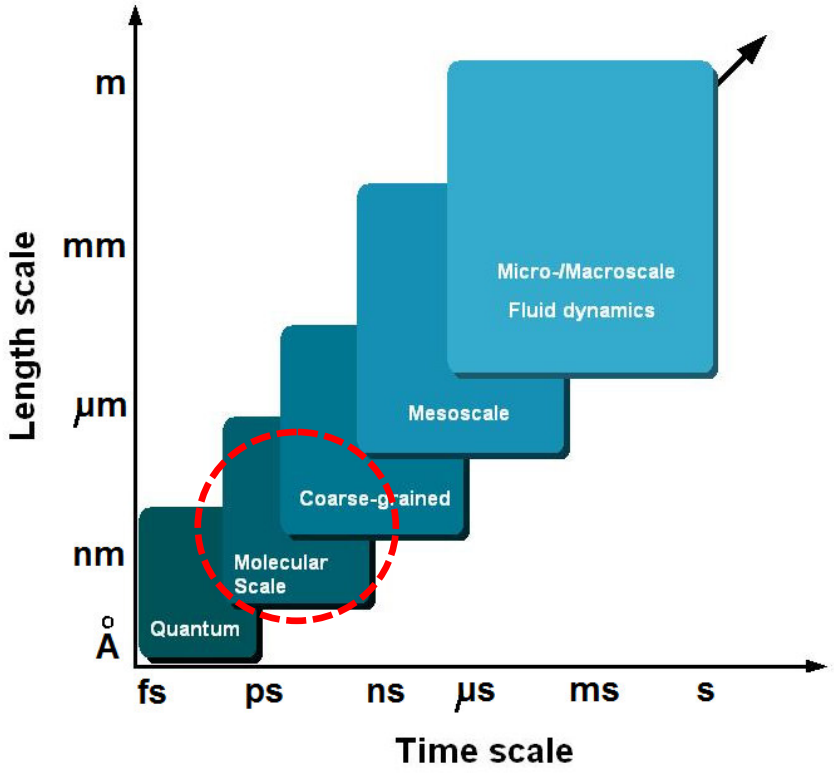

Fig. 6.1: Time and length scales of simulation and experimental systems. The red circle highlights the time and length scale for atomic and coarse-grained molecular dynamics simulations.

6.2.1. Forcefields – Molecular Interactions

MD simulation consists of solving the numerical, time-dependent Newtonian equations of motion for an ensemble of particles. For a molecular system, the equations of motion are (**Eq. 6.1**) (Allen 2004)

$$m_{a,i}\ddot{r}_i = f_i \qquad f_i = -\frac{\partial}{\partial r_i} E \tag{6.1}$$

where m_a is the atomic mass, $\ddot{r}$ is the acceleration, f is the force acting on the atom and E is the total potential energy of the atom. The subscript i denotes the ith atom. In order to calculate the forces f_i acting on the atoms, potential energies $E(r^N)$ should be obtained for all N atoms, where $r^N = (r_1, r_2, \ldots r_N)$ for a complete set of $3N$ atomic coordinates. Molecular interactions can be written in two parts, namely intermolecular and intramolecular interactions (**Eq. 6.2**).

$$\begin{aligned} E &= \sum E_{\text{intermolecular}} + \sum E_{\text{intramolecular}} \\ &= \left(\sum E_{\text{stretch}} + \sum E_{\text{bend}} + \sum E_{\text{torsion}} + \sum E_{\text{out-of-plane}}\right) + \left(\sum E_{\text{vdW}} + \sum E_{\text{Coulombic}}\right) \end{aligned} \tag{6.2}$$

Intermolecular interaction is the sum of effect of all atomic movements, including bond stretching, angle bending, torsional angles and out-of-plane movements. Intramolecular interaction involves two parts, van der Waals interactions and Coulombic electrostatic interactions.

Various kinds of forcefields are available for MD simulations, in which different expressions for the potential energies terms are developed for the applications on different molecular systems. For example, the consistent-valence forcefield (cvff) is suitable for handling peptides, proteins and various organic systems (Hagler et al. 1974).

It has been extensively used for many years, and is primarily intended for organic crystals, aqueous solutions and gas phase systems. The Condensed-phase Optimized Molecular Potentials for Atomistic Simulation Studies (COMPASS) is a forcefield that enables accurate prediction of gas-phase and condensed phase properties, such as structure, conformation, equation of state and cohesive energies etc. (Sun et al. 1998). It is also applicable for a wide range of organic/inorganic and polymer systems.

6.2.2. Periodic Boundary Conditions

Periodic boundary conditions (PBC) are useful to handle large simulation systems by simulating small repetitive units (Haile 1992). Most commonly, the shape of the repetitive simulation units is a cube, which is surrounded by replicas of itself on two or three dimensions. Minimum image convention in which each atom can interact with the nearest atom or image in the periodic array can be adopted, as long as the potential range does not exceed the smallest box length. During an MD simulation, if one atom/particle leaves the unit simulation box, it is considered as being replaced by an incoming particle image from the opposite side (**Fig. 6.2**). Both real and image neighbors are included when calculating particle interactions within the cutoff range.

6.3. Studying Surfactant Self Assembly by MD Simulations

Surfactants have been extensively studied using various kinds of theoretical techniques, including Monte Carlo simulations (Floriano and Caponetti 1999; Rodríguez-Guadarrama et al. 1999) and molecular dynamics (MD) simulations

(Watanabe et al. 1988, Shelley et al 1990, MacKerell 1995, Shelley and Shelley 2000). The physical properties of micelles have been therefore interpreted from the perspective of the structures of organized assemblies.

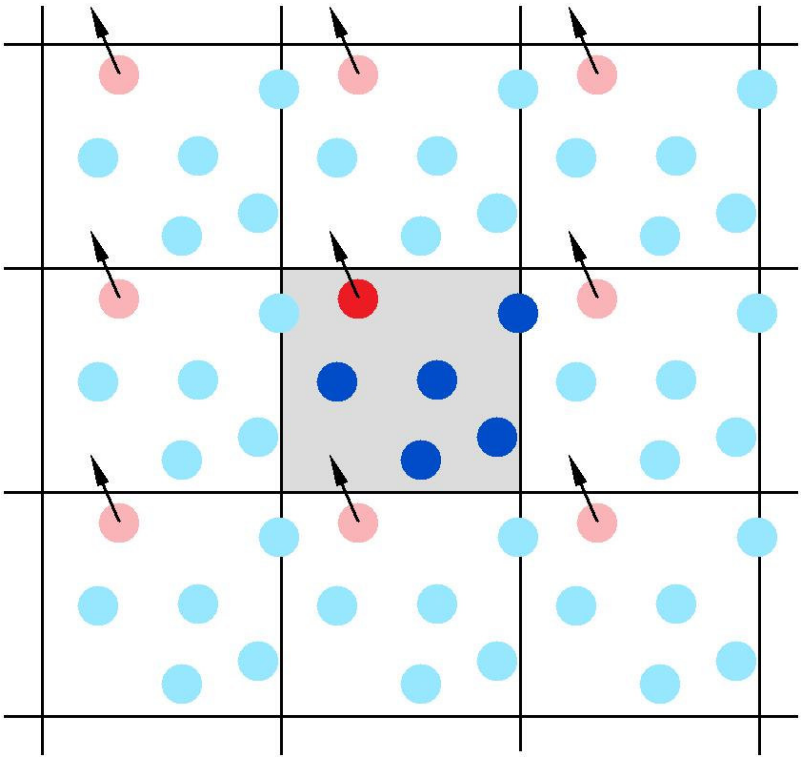

Fig. 6.2: Periodic boundary conditions. When a particle moves out of the unit simulation box, it is replaced by an image particle that moves in from the opposite side.

MD simulations have been increasingly employed in studying surfactant micelle structures with the development of computing powers (Tieleman et al 2000, Bogusz et al 2000; 2001). MD simulation is a very useful tool to study the behavior of surfactants in

solutions, which allows us not only to observe the microscopic aggregation process of surfactants but also analyze the formed aggregation structures at atomic level (Maillet et al. 1999; Stevens et al. 2003; Klein and Shinoda 2008; Lane et al. 2008; Shinoda et al. 2008). Surfactant categories investigated by MD simulations include nonionic, cationic, anionic and zwitterionic surfactants.

6.3.1. Nonionic Surfactants

To date, there has not been a significant number of simulations on this category of surfactants. However, based on current computational power, comparatively larger simulation systems and longer simulation time is manageable for nonionic surfactants.

Bogusz et al. (2000) performed MD simulations of over 4 nanosecond on micelles composed of 1 to 75 nonionic octyl glucoside surfactant molecules, and found that those micelles consisting of more than 10 surfactant molecules were stable. Ryjkina et al. (2002) studied nonionic surfactant (dodecyldimethylamine oxide) phase structures by MD simulations, and reproduced the aggregation behavior of micellar, hexagonal and lamella surfactant mesostructures. Srinivas et al. (2006) studied adsorption of nonionic surfactants, alkylpoly(ethylene oxide) ($H(CH_2)_m(OCH_2CH_2)_nOH$, shorted for C_mE_n), onto a granite surface by the means of coarse-grained (CG) MD simulation. Due to the simplified nature of CG molecules, relatively large systems consisting of 400 CG surfactant molecules and 14,400 CG water sites were investigated in their simulations. Klein and Shinoda (2008) conducted large-scale MD simulation on alkylpoly(ethylene oxide) ($C_{12}E_6$) surfactant systems containing over 62,000 CG $C_{12}E_6$ molecules and more

than 500,000 CG water particles, corresponding to atomic systems of ~5 million atoms. A transition from hexagonal to lamellar phases was observed at 500 nanosecond.

6.3.2. Anionic Surfactants

Compared with nonionic surfactants, many MD simulations have been performed on cationic and anionic surfactant systems over the past 20 years. However, the systems were relatively small in general, and were not studied over very long time scales. Much of the prior work consisted of MD simulations that included around 50 surfactant molecules and were hundreds of picoseconds to several nanoseconds in simulation duration. In fact, the reason for the lack of larger and longer simulations is the computational effort required for handling long range electrostatic interactions.

Early investigations of anionic surfactant systems by MD simulations can be dated back to 1990s. Shelley et al. (1990) reported a 182-picosecond MD simulation of a micelle consisting of 42 sodium dodecyl sulfate (SDS) surfactant molecules; in 1995, MacKerrell conducted similar MD simulations of 120 picoseconds on a micelle consisting of 60 SDS surfactant molecules. In both studies, sodium ions were added to the systems as surfactant counterions, and stable micellar structures over simulation time were observed.

Bruce et al. (2002) focused on the structures of SDS micelles in water and the distribution of counterions. Their system consisted of 60 SDS molecules and ~7,500 water molecules, MD simulations trajectories were as long as 5 nanoseconds. Long equilibration time was required for the distribution of counterions. The counterions

formed two layers of shells outside the SDS micelles.

Kaznessis et al. (2002) carried out MD simulations on the aggregation behavior of anionic surfactant dipalmitoylphosphatidylglycerol (DPPG) and zwitterionic surfactant dipalmitoylphosphatidylcholine (DPPC) at water-air interface, which can greatly facilitate the investigation of phospholipid monolayer properties. Their simulation systems included 40 surfactant molecules and ~2,800 water molecules, and the simulation time was over 1 nanosecond for all systems.

The influence of calcium ions on foam stability of three common surfactants (linear alkylbenzene sulfonate (LAS), SDS, and $C_{12}E_7$) was examined by Yang and Yang (2010) by simulating film rupture during which critical thickness was measured. It was found that Ca^{2+} significantly reduced the foam stability of SDS, while it has little-to-no effect on the foam stability of LAS and $C_{12}E_7$.

6.3.3. Cationic Surfactants

MD simulation of the dynamics of self-assembly processes of two kinds of cationic surfactants (n-nonyltrimethylammonium chloride (C_9TAC) and erucyl-bis[2-hydroxyethyl]methylammonium chloride (EMAC)) was carried out by Maillet et al. (1999). Among the two cationic surfactants, EMAC has the capability of forming worm-like micelles. Around 50 surfactant molecules and ~3000 surfactant molecules were included in each system, and the simulation time was over 1 nanosecond. Worm-like micelle structure was observed for EMAC surfactant systems that started from a random initial surfactant distribution.

A mixed surfactant system of anionic/cationic surfactants was studied by MD simulation by Yakovlev and Boek (2007). A wide range of surfactant ratios were included in this study. Different surfactant worm-like aggregation structures were obtained for systems with different surfactant ratios, including symmetric worm-like micelles (34/66 cationic/anionic) and flattened worms (50/50 cationic/anionic). It was found that adding a small amount of anionic surfactant with short tail (C8) to the cationic surfactant is helpful in forming more stable worm-like micelles.

The impact of dicationic alkylammonium bromide gemini surfactants on DPPC lipid membranes was examined by Almeida et al. (2010) by both experimental and MD simulation studies. Experimentally, a disrupting effect upon the overall order of the lipid bilayer was observed for short-tail dicationic gemini surfactants (C12), while the formation of more ordered structures can be resulted from the addition of long-tail dicationic gemini surfactants (C16 and C18). MD simulation further supported this experimental observation by providing insights into the mechanism of the surfactant-lipid interactions.

6.3.4. Zwitterionic Surfactants

MD simulation on zwitterionic surfactant can be dated back to 1989, when Wendoloski et al conducted a 100 picosecond simulation of a phospholipid micelle of lysophosphatidylethanolamine (LPE). Tieleman et al. (2000) studied micelle formation from the dodecylphosphocholine (DPC) zwitterionic surfactant by MD simulations of at least 500 picoseconds. Differences in micellar shapes, accessible surface areas, and

monomer packing was analyzed for simulation systems consisting of 40, 54, and 65 surfactant monomers. DPC surfactant micelle formation has been the subject of MD simulation studies conducted by Marrink et al. (2000) as well. Xu et al. (2007) reported CG MD simulation of spontaneous micelles formation of zwitterionic surfactant 3-(N,N-dimethyldodecylammonio)-2-hydroxy-propanesulfonate (DSB) in NaCl aqueous solution. Stable bipolar micellar structures were observed in their study. Adsorption of zwitterionic surfactant dodecyl sulfobetaine (DBS) on a silica/solution interface in the presence of Ca^{2+}, Mg^{2+} divalent cations in aqueous solution was explored by Hu et al. (2010) by atomic MD simulations. All of these studies have significantly advanced the understanding of the structure and dynamics on the molecular-level for categories of surfactants.

7. IMPACT OF HYDROLYSIS AT HIGH TEMPERATURES ON THE APPARENT VISCOSITY OF CARBOXYBETAINE VISCOELASTIC SURFACTANT-BASED ACID: EXPERIMENTAL AND MOLECULAR DYNAMICS SIMULATION STUDIES

It is well known that in aqueous solutions, peptide bond (-CO-NH-) can be easily broken in acidic environments at high temperatures, which is referred to as acidic hydrolysis reaction (Long and Truscott 1968; Qian et al. 1993). Because of the existence of peptide bonds in amido-carboxybetaine viscoelastic surfactants, acid hydrolysis reaction occurs for this type of surfactant at high temperatures. Hydrolysis reaction of amido-type viscoelastic surfactant at high temperature may lead to changes in fluid apparent viscosity. If fully taken into consideration, hydrolysis of surfactant at high temperature helps breaking down the gel, and no additional breaker or mutual solvent is needed for gel cleanup; otherwise, it would adversely affect the outcome of the treatment by altering the fluid apparent viscosity.

The objectives of the research are to (Yu et al. 2011)

(1). experimentally determine the viscosity alteration of amido-carboxybetaine acid fluids by high temperatures; and

(2). determine the mechanism for viscosity changes on molecular level by carrying out molecular dynamics (MD) simulations.

7.1. Experimental Studies

7.1.1. Materials

The original surfactant sample, whose active ingredient is oleamidopropyl dimethyl betaine (ODB), was supplied by Rhodia Inc. Winder, Georgia. It contained nearly 30 wt% active ingredient. **Fig. 7.1(a)** shows the molecular formula of ODB surfactant. Other materials used in the experimental studies included hydrochloric acid (HCl, 36.8 wt%, Mallinckrodt Backer Inc.) and calcium carbonate ($CaCO_3$, ACS reagent grade, > 99.0%, Sigma Aldrich Inc.). All solutions were prepared using deionized water with a resistivity of 18.2 mΩ-cm at 25°C.

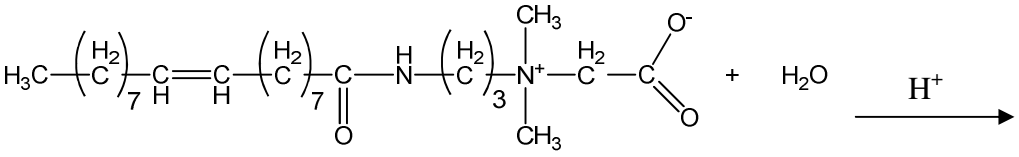

(a)

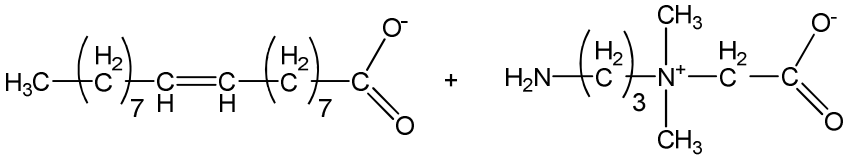

(b) (c)

Fig. 7.1: High temperature hydrolysis reaction of (a) oleamidopropyl dimethyl betaine (ODB), into (b) oleic acid (OA) and (c) aminopropyl dimethyl betaine.

7.1.2. Method

Surfactant-acid solutions were prepared such that HCl concentration was 15 wt%, and ODB surfactant concentrations were 4, 6 and 8 wt%, respectively. The components of these solutions are shown in **Table 7.1**. Immediately after the solutions were prepared, they were placed in water baths to be hydrolyzed under reflux (**Fig. 7.2**). Hydrolysis temperature was 190°F, and hydrolysis times included 1, 2, 3 and 6 hours. Samples were cooled to room temperature after hydrolysis, and partially spent by $CaCO_3$ until the pH value of the sample was 4.5. After centrifuging at 3000 rpm for 40 minutes, foam and excessive $CaCO_3$ solid in the partially spent samples could be removed. The control experiments were conducted on samples with the same composition and preparation procedure, but not subjected to hydrolysis at 190°F.

Table 7.1. Composition of ODB sample solutions.

Component	Concentration		
	4 wt% ODB	6 wt% ODB	8 wt% ODB
ODB sample as received	13 wt%	20 wt%	27 wt%
36.8 wt% HCl	41 wt%	41 wt%	41 wt%
DI water	46 wt%	39 wt%	32 wt%

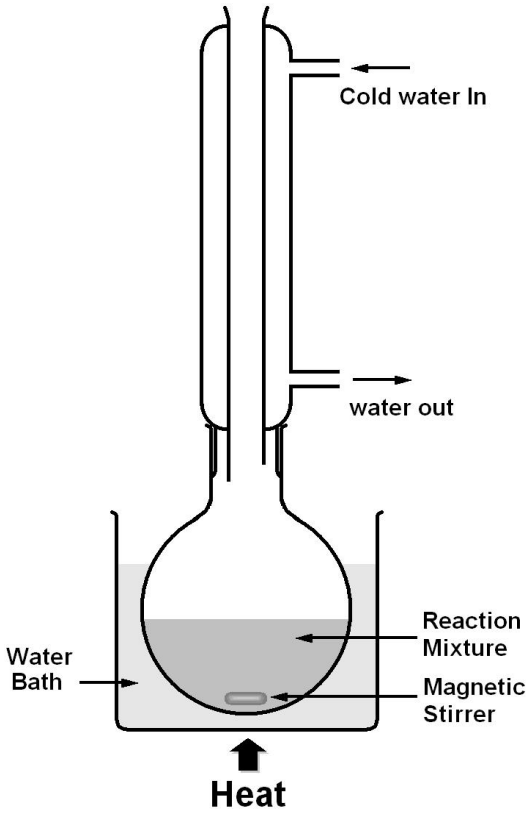

Fig. 7.2: Experimental setup for surfactant-acid hydrolysis reaction.

After sample preparation, the apparent viscosity vs. shear rate was measured on a rheometer at 25°C, 1 atm, with shear rates from 0.1-900 s^{-1}. For samples with phase separation, the apparent viscosity of only the aqueous phase was measured. For each sample, the results were averaged from 3 parallel trials.

7.1.3. Results and Discussion

Photos of 4, 6 and 8 wt% ODB surfactant samples with or without hydrolysis are shown in **Figs. 7.3 to 7.5**. Compared to the colorless and transparent samples without hydrolysis, samples subjected to 1 hour hydrolysis at 190°F had a yellow color and

became cloudy. Judging from samples after 1, 2 and 3 hours of hydrolysis, this phenomenon was increasingly intensified with time. Phase separation took place for the 8 wt% ODB sample hydrolyzed for 3 hours at 190°F, as 2 immiscible liquids with different colors were presented (Fig. 7.5(e)). After 6 hours of hydrolysis at 190°F, all samples showed phase separation. The upper layer of the sample was a viscous organic phase with brown color, and consisted of the hydrolyzed reaction product, oleic acid (OA, **Fig. 7.1(b)**). The amount of the organic phase increased with the initial surfactant concentration. The lower layer was an aqueous phase, which was colorless and transparent.

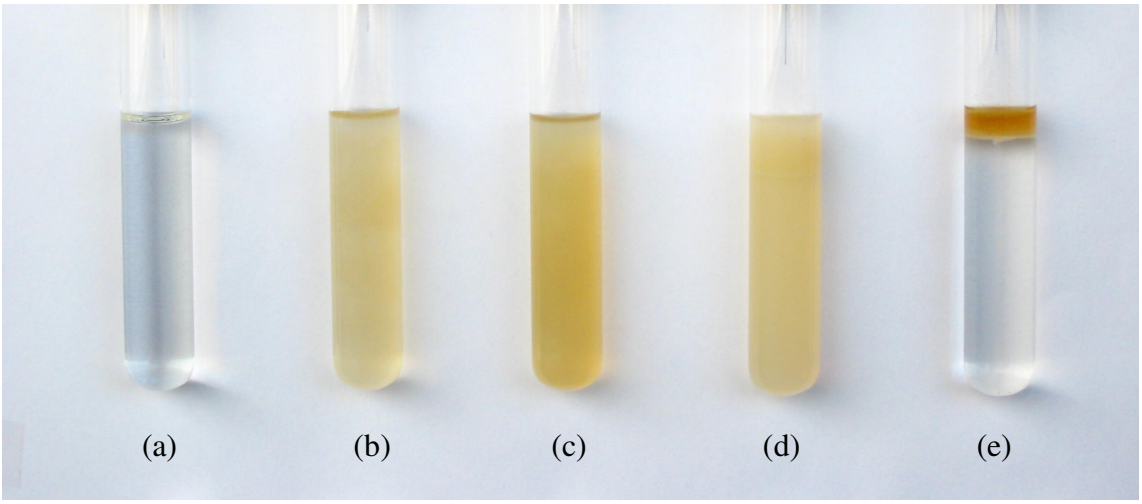

Fig. 7.3: 4 wt% surfactant samples that were hydrolyzed at 190°F for (a) 0 hour (no hydrolysis); (b) 1 hour; (c) 2 hours; (d) 3 hours; (e) 6 hours. Samples were partially spent after hydrolysis (pH 4.5).

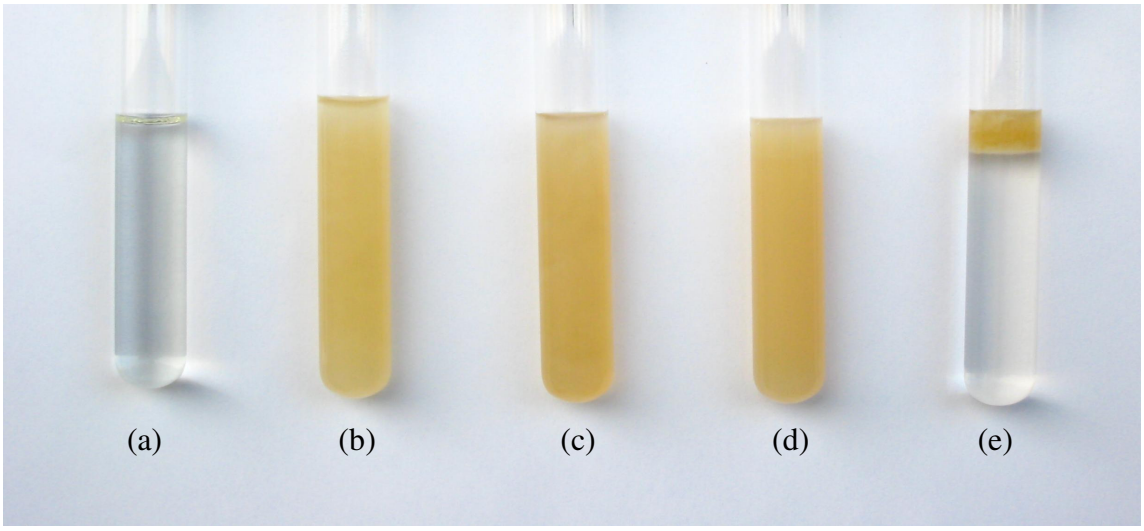

Fig. 7.4: 6 wt% surfactant samples that were hydrolyzed at 190°F for (a) 0 hour (no hydrolysis); (b) 1 hour; (c) 2 hours; (d) 3 hours; (e) 6 hours. Samples were partially spent after hydrolysis (pH 4.5).

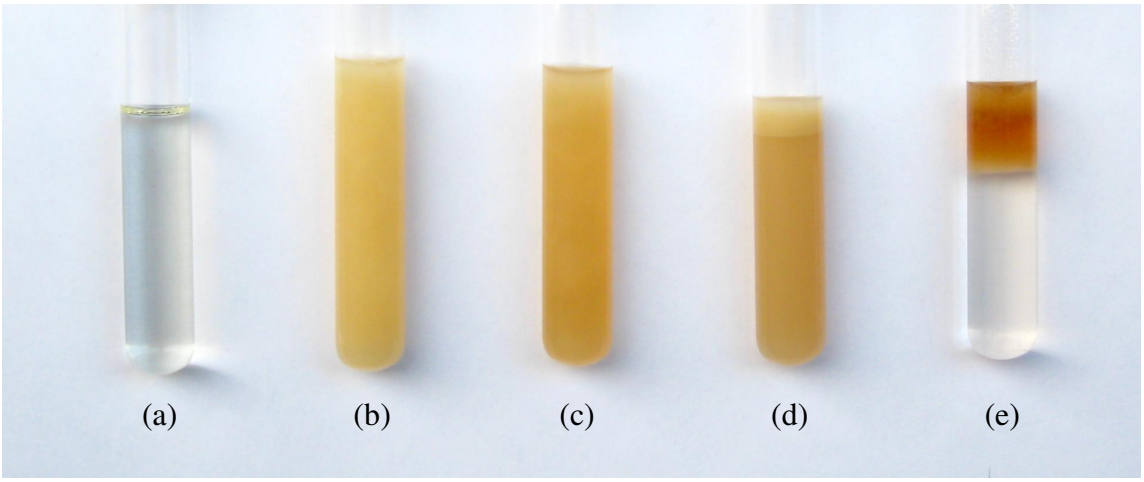

Fig. 7.5: 8 wt% surfactant samples that were hydrolyzed at 190°F for (a) 0 hour (no hydrolysis); (b) 1 hour; (c) 2 hours; (d) 3 hours; (e) 6 hours. Samples were partially spent after hydrolysis (pH 4.5).

Viscosity at different shear rates for all samples is listed in **Tables 7.2 to 7.4**. **Fig. 7.6** is the sample apparent viscosity profile at 300 s^{-1} as a function of hydrolysis time at 190°F. For three samples with different initial surfactant concentrations, maximum apparent viscosity appeared after 1 hour of hydrolysis. Clearly, apparent viscosity of ODB samples without hydrolysis was relatively lower compared to that of the samples with short time (1-2 hours) hydrolysis. Sample viscosity significantly decreased to less than 10 cP after 3 hours of hydrolysis. Generally speaking, at any hydrolysis time, sample with higher initial surfactant concentration possessed higher apparent viscosity.

In summary, when subjected to hydrolysis at 190°F, ODB surfactant-acid fluid experienced early enhancement and then reduction in the apparent viscosity. The maximum apparent viscosity appeared when surfactant-acid fluid was hydrolyzed for 1 hour at 190°F. Since hydrolysis reaction involves breaking of ODB molecules and generation of OA molecules, intuitively, it can be assumed that the mix of ODB and OA molecules within a certain ratio range is capable of enhancing the apparent viscosity of the surfactant fluid. In other words, the addition of OA molecules to ODB solution helps forming stronger and more stable worm-like micelles. To confirm this hypothesis, MD simulations were carried out on ODB and OA systems and are discussed in the next section.

Table 7.2. Apparent viscosity of 4 wt% ODB samples hydrolyzed at 190°F for different times. Samples were partially spent by $CaCO_3$ (pH 4.5), and their apparent viscosity was measured under ambient conditions.

Shear Rate (s^{-1})	Apparent viscosity (cP)				
	0 hour	1 hour	2 hours	3 hours	6 hours
0.1	1371.5	23334.4	8406.2	543.6	82.1
1	1119.6	3933.8	1643.5	54.0	47.2
10	636.9	617.6	313.0	12.7	7.2
50	276.2	269.9	212.1	7.1	3.8
100	178.4	323.7	232.0	6.5	3.2
300	87.5	159.3	117.4	6.6	3.2
500	63.7	112.0	78.0	6.7	3.4
700	52.3	88.0	60.8	6.9	3.6
900	45.8	72.5	51.4	7.1	3.7

Table 7.3. Apparent viscosity of 6 wt% ODB samples hydrolyzed at 190°F for different times. Samples were partially spent by $CaCO_3$ (pH 4.5), and their apparent viscosity was measured under ambient conditions.

Shear Rate (s^{-1})	Apparent viscosity (cP)				
	0 hour	1 hour	2 hours	3 hours	6 hours
0.1	1317.0	125107.0	5851.7	100.0	377.9
1	1775.2	13208.9	1339.3	10.0	62.7
10	1099.3	2653.5	313.6	1.0	11.0
50	478.9	856.2	231.6	5.4	5.7

Table 7.3. continued

Shear Rate (s^{-1})	Apparent viscosity (cP)				
	0 hour	0 hour	0 hour	0 hour	0 hour
100	306.7	583.9	234.2	6.7	3.5
300	144.3	276.2	132.1	7.9	3.4
500	102.2	190.8	94.1	8.4	3.7
700	82.2	150.8	76.1	8.7	4
900	70.5	127.9	65.6	8.9	5

Table 7.4. Apparent viscosity of 8 wt% ODB samples hydrolyzed at 190°F for different times. Samples were partially spent by $CaCO_3$ (pH 4.5), and their apparent viscosity was measured under ambient conditions.

Shear Rate (s^{-1})	Apparent viscosity (cP)				
	0 hour	1 hour	2 hours	3 hours	6 hours
0.1	450.1	171894.3	49540.1	100.0	43.6
1	819.0	28027.3	5569.9	4.4	8.3
10	748.0	3528.6	814.6	11.5	5.1
50	479.5	972.6	404.5	10.6	4.0
100	349.7	698.0	337.1	10.4	3.7
300	189.0	404.1	211.1	10.2	3.7
500	138.7	292.9	146.2	10.4	3.9
700	113.5	233.8	124.6	10.5	4.7
900	98.3	195.4	108.0	10.6	5.4

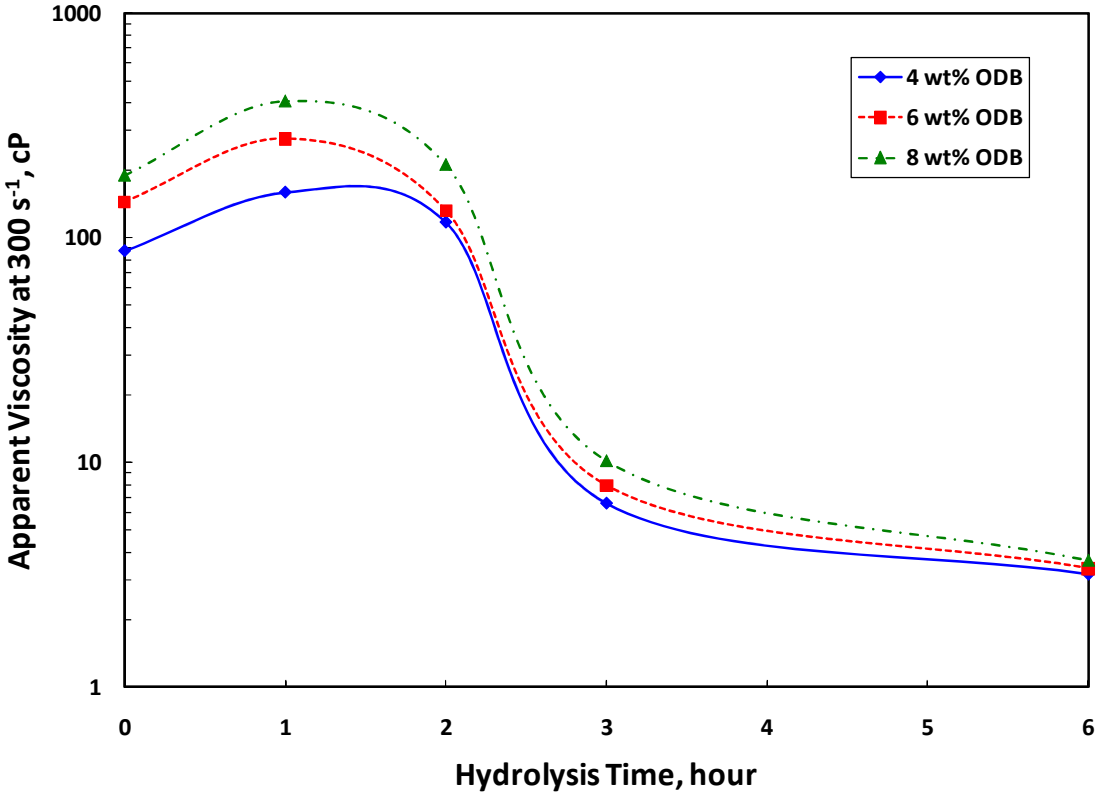

Fig. 7.6: Effect of hydrolysis time on the apparent viscosity of surfactant solutions containing 4, 6, and 8 wt% ODB surfactant, respectively. Shear rate = 300 s^{-1}. Measurements were carried out at ambient conditions.

7.2. Molecular Dynamics Simulation Studies

The aggregation behaviors of an amido-carboxybetaine surfactant and the corresponding fatty acid soap under different conditions were studied by MD simulations. Two typical aggregation structures were observed in our simulations, including infinite worm-like micelle and finite micelle. It was found that there exists an optimal molar ratio between amido-carboxybetaine and fatty acid soap at which the

worm-like micelle structure can be formed. The simulation results are qualitatively in agreement with the experimental results.

7.2.1. System Setup

Aggregation behavior of ODB and OA surfactant molecules in aqueous solution was studied with MD simulations in this paper. Each simulation system was constructed with 48 surfactant molecules and 3053 water molecules, which were placed into a cubic box with three-dimensional periodic boundary conditions (boundary conditions that are used to handle a large system by simulating small repetitive unit cells) (**Fig. 7.7**). The ODB/OA molar ratios considered in the current study were 1:0, 3:1, 1:1 and 1:3, respectively.

Water molecules are represented by the Jorgensen TIP3P (transferable intermolecular potential 3P) model (Jorgensen et al. 1983). In all cases, divalent electrolyte ($CaCl_2$) was added to the solution, and the number of Ca^{2+} cations was 100. The corresponding numbers of ions in each system are listed **Table 7.5**. The initial density of all constructed systems was 1.0 g/cm^3. The initial sizes of the systems and the numbers of molecules of different species contained in each system are listed in Table 7.5. In all initial system configurations, these surfactant molecules were randomly distributed in the simulation box.

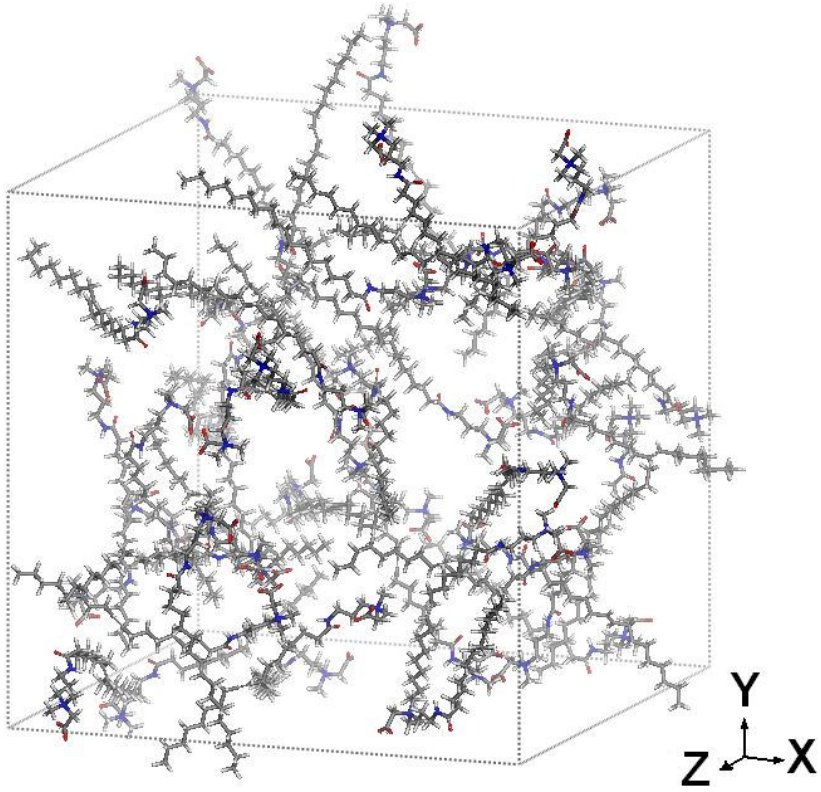

Fig. 7.7: A typical simulation system with 48 ODB molecules constructed in the current study. For clarity, only surfactant molecules are shown. In this figure and all subsequent simulation snapshots, carbon atoms are depicted in grey, oxygen atoms in red, nitrogen atoms in blue and hydrogen atoms in white. The grey dashed lines represent the simulation box.

Table 7.5. Setup of the simulation systems.

Initial box side length, Å	# ODB	# OA	# TIP3P water	# Ca^{2+}	# Cl^-	ODB concentration*, wt%
52.4	48	0	3053	100	200	25.0
51.9	36	12	3053	100	188	18.8
51.5	24	24	3053	100	176	12.5
51.0	12	36	3053	100	164	6.4

* ODB concentrations are based on live acids.

7.2.2. Simulation Details

MD simulations were carried out using Materials Studio 5.0 software (2009). The consistent-valence forcefield (cvff) was employed in the current study (Hagler et al. 1974). All atoms are included explicitly in this forcefield. The total potential energy of the system is expressed by **Eq. 7.1**:

$$\begin{aligned} E &= \sum E_{\text{intermolecular}} + \sum E_{\text{intramolecular}} \\ &= \left(\sum E_{\text{stretch}} + \sum E_{\text{bend}} + \sum E_{\text{torsion}} + \sum E_{\text{out-of-plane}}\right) + \left(\sum E_{\text{vdW}} + \sum E_{\text{Coulombic}}\right) \\ &= \left\{\sum_b H_b (b - b_0)^2 + \sum_\theta H_\theta (\theta - \theta_0)^2 + \sum_\varphi H_\varphi \left[1 + S\cos(n\phi_a)\right] + \sum_\chi H_\chi \chi^2\right\} \\ &\quad + \left\{\sum \varepsilon \left[\left(\frac{r^*}{r}\right)^{12} - 2\left(\frac{r^*}{r}\right)^6\right] + \sum \frac{q_i q_j}{\varepsilon r_{ij}}\right\} \end{aligned} \tag{7.1}$$

where

H_b = bond stretching force constant;

b = equilibrium bond length;

b_0 = actual bond length;

H_θ = bond bending force constant;

θ = equilibrium bond angle;

θ_0 = actual bond angle;

H_φ = torsional force constant;

S = phase factor (1 or –1 based on the dihedral angle);

ϕ_a = torsional angle;

H_χ = bending constant;

χ = bending angle;

ε = strength of the vdW potential;

r^* = distance at which the potential reaches its minimum;

r = distance between two particles;

q_i and q_j = point charge;

r_{ij} = separation distance.

After the systems were constructed, energy minimization was carried out to eliminate energetically unfavorable configurations. This in turn generated a starting point with reasonably low potential energy for MD simulations. All MD simulations were performed under NPT ensemble (in which the number of particle, pressure and temperature were fixed). The pressure was set to 1 atm and the temperature was fixed at 300K, and these parameters were chosen to simulate the condition at which the apparent viscosity of surfactant sample was measured. In the current study, temperature and

pressure were controlled using the Nosé algorithm (Nosé and Klein 1983; Nosé 1984a, b) and Berendsen algorithm (Berendsen et al. 1984), respectively. At the beginning of MD simulation, each atom in the system was assigned a random velocity based on Maxwellian distribution at 300K. A time step of 1 fs (1×10^{-15} s) was used to integrate Newtonian equations of motion for all atoms. The particle mesh Ewald method (Ewald 1921) was employed to handle the long-range Coulombic interactions, and the atom-based method was used to calculate the van der Waals interactions. A cut-off radius of 9.5Å was used for the calculations of the van der Waals interactions. For most MD trajectories, the total simulation time was more than 1 ns (1×10^{-9} s).

7.2.3. Results and Discussion

Structure and Dynamics of ODB Surfactant Systems

48-ODB systems with the addition of electrolyte ($CaCl_2$) were studied first. It took 140 ps for the total energies to reach stable values (**Fig. 7.8(a)**). **Fig. 7.9** shows the snapshots of evolution process of a 48-ODB system at 0, 200, 400, 600, 800 ps and 1 ns. For clarity, only surfactant backbone atoms, namely C, O and N atoms, are displayed in Fig. 7.9 and all subsequent snapshots. Water molecules and Ca^{2+}/Cl^{-} ions are omitted. Amorphous aggregation, which is composed of randomly packed surfactant molecules, emerged at 200 ps. After 600 ps, relatively organized structures appeared. These aggregates were sheet-like structures composed of 3 to 5 parallelly aligned surfactant molecules.

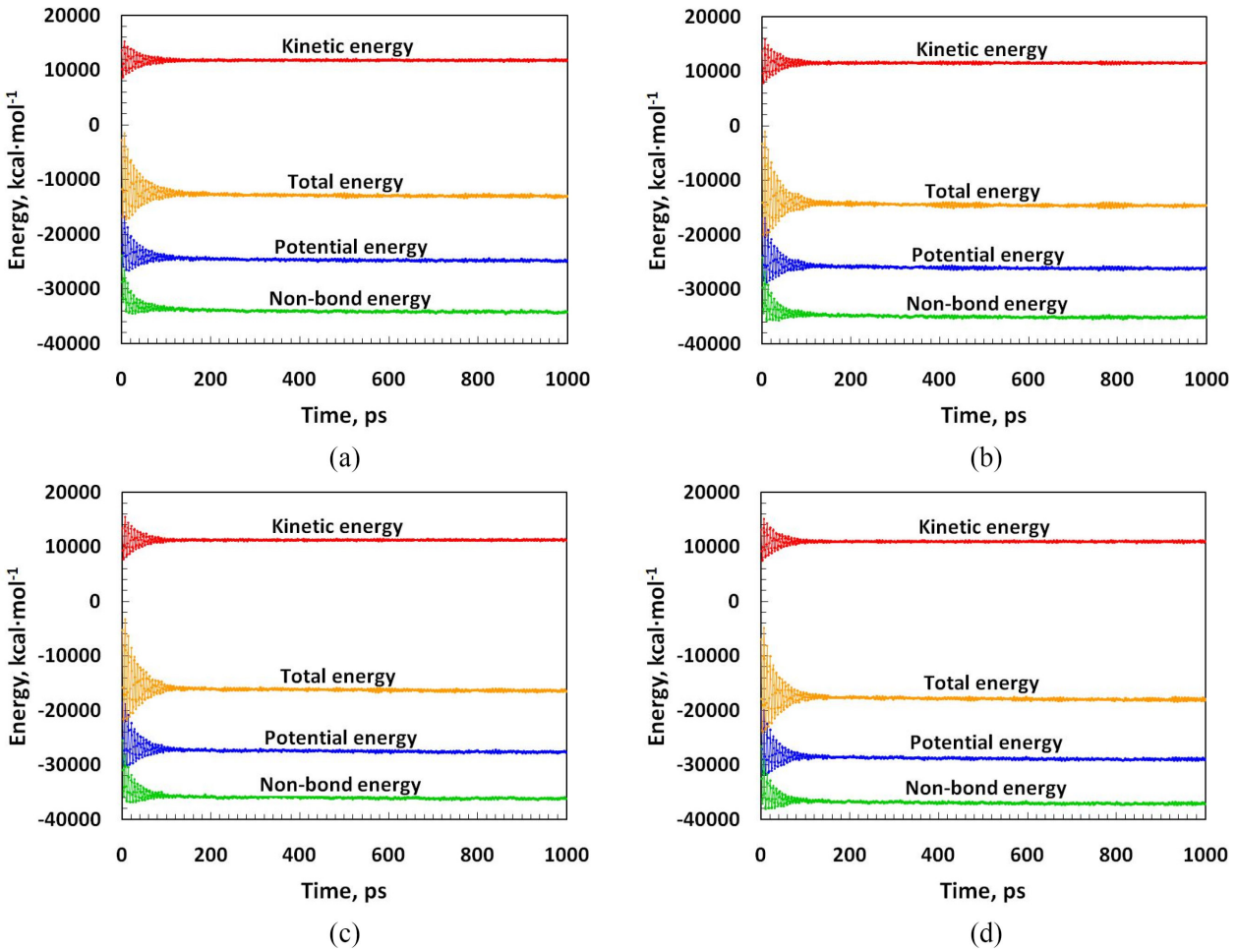

Fig. 7.8: Energy profiles as a function of simulation time for (a) 48-ODB system; (b) 36-ODB/12-OA system; (c) 24-ODB/24-OA system and (d) 12-ODB/36-OA system.

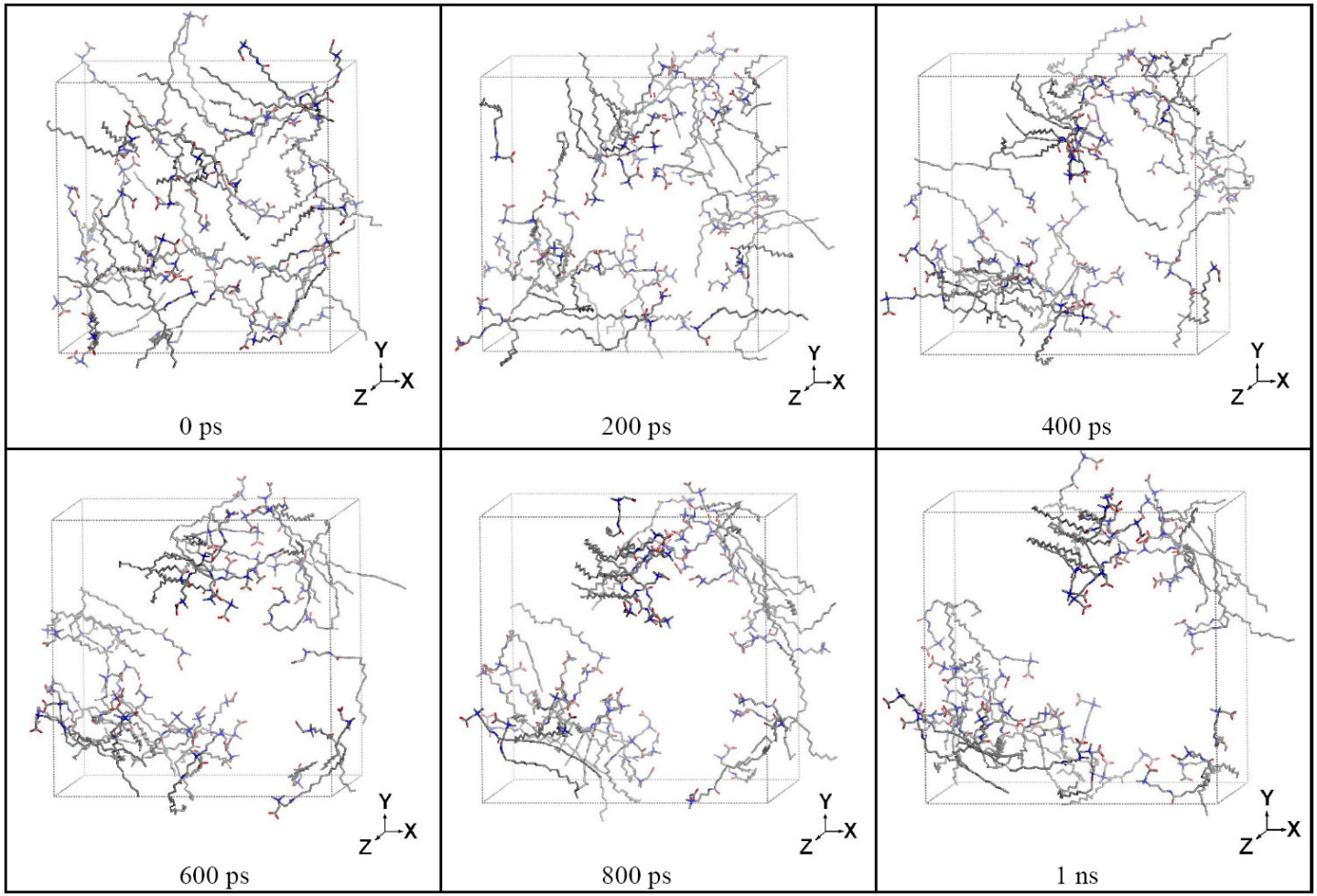

Fig. 7.9: Snapshots from the simulation trajectory of 48-ODB system at 0, 200, 400, 600, 800 ps and 1 ns. Only surfactant backbones are displayed. Water molecules and Ca^{2+}/Cl^{-} ions are omitted.

Fig. 7.10 is the system configuration after 1 ns of MD simulation viewed along the *y*-direction, and the simulation box was repeated on the *x* and *z* directions due to periodic boundary conditions. Fig. 7.10 demonstrates that an ellipsoid-shape aggregate was finally formed, whose long axis is along the z-direction. The hydrophilic heads of the surfactant molecules extended towards the bulk water that occupied the blank space. There was a tendency of the formation of an organized structure, but no worm-like structure was observed in this case.

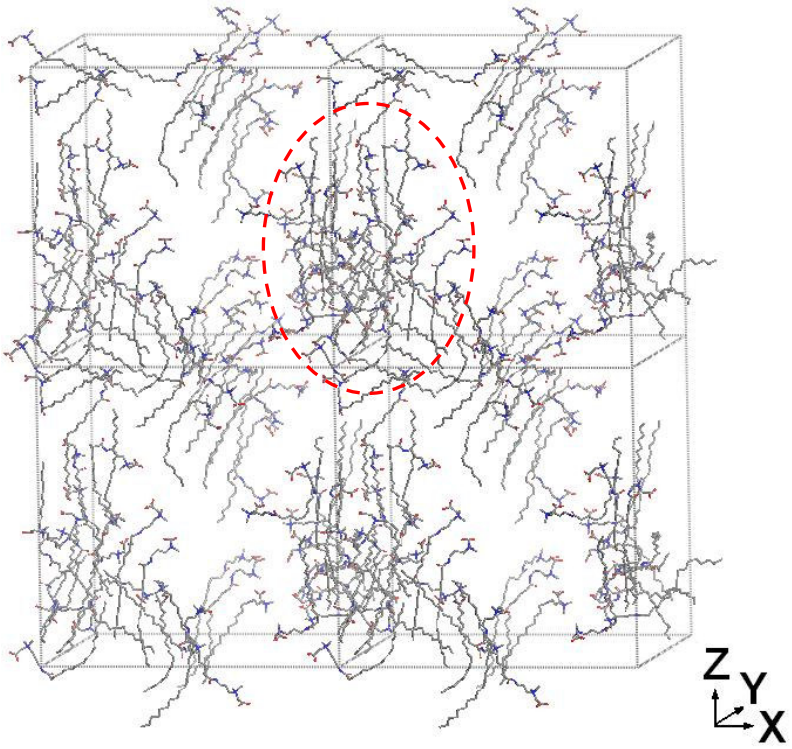

Fig. 7.10: Aggregation structures of the 48-ODB system at 1 ns. The ellipsoid-shape aggregate is highlighted by the red dash line. Only surfactant backbones are displayed. Water molecules and Ca^{2+}/Cl^{-} ions are omitted.

Structure and Dynamics of ODB/OA Mixed Surfactant Systems

Three types of ODB/OA mixed surfactant systems were studied in this paper. The total number of surfactant molecules was 48 for all mixed surfactant systems, and the ODB/OA molar ratios were 3:1, 1:1 and 1:3, respectively. Electrolyte ($CaCl_2$) was added to each mixed surfactant system. The time required for system total energies to equilibrate was nearly 140 ps for all systems (**Fig. 7.8(b) (c) (d)**).

Fig. 7.11 shows snapshots taken from a typical 36-ODB/12-OA simulation trajectory at 0, 200, 400, 600, 800 ps and 1 ns. Relatively ordered surfactant aggregates started to appear after 200 ps. At 400 ps, small sheet-like structures were formed. They further self-organized into two large aggregation structures at 600 ps. These aggregations can be regarded as stacks of sheet-like structures. Viewed along the *z*-direction towards the *xy*-plane, two distinct "surfaces" existed for these structures: a hydrophilic surface on which most surfactant head groups are exposed, and a hydrophobic surface where the surfactant tails are aligned together. If the simulation box was repeated in the *x*- and *y*-directions, it can be seen that these two aggregation structures faced each other with the hydrophobic surfaces. At 800 ps, they further merged into one large aggregate. Finally, at 1000 ps, a micelle-like structure was formed, in which all hydrophilic heads of surfactants exposed to water molecules and hydrophobic tails were buried in the central area of this aggregate. From **Fig. 7.12**, it can be seen that the micelle-like structure is infinitely extended along the *z*-direction to form a worm-like micelle due to periodic boundary conditions, and all surfactant molecules were included in the micelle-like structure.

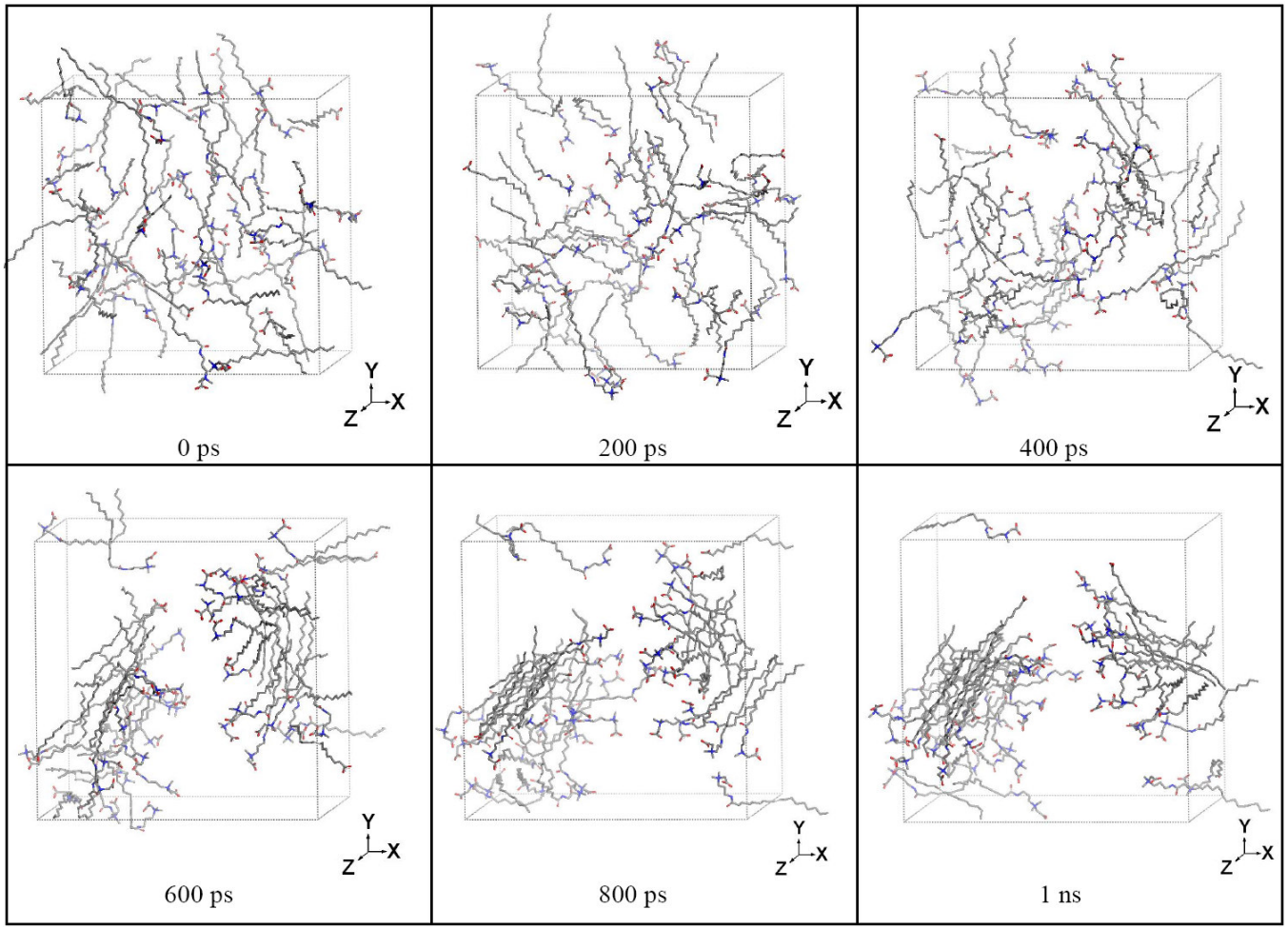

Fig. 7.11: Snapshots from the simulation trajectory of 36-ODB/12-OA system at 0, 200, 400, 600, 800 ps and 1 ns. Only surfactant backbones are displayed. Water molecules and Ca^{2+}/Cl^{-} ions are omitted.

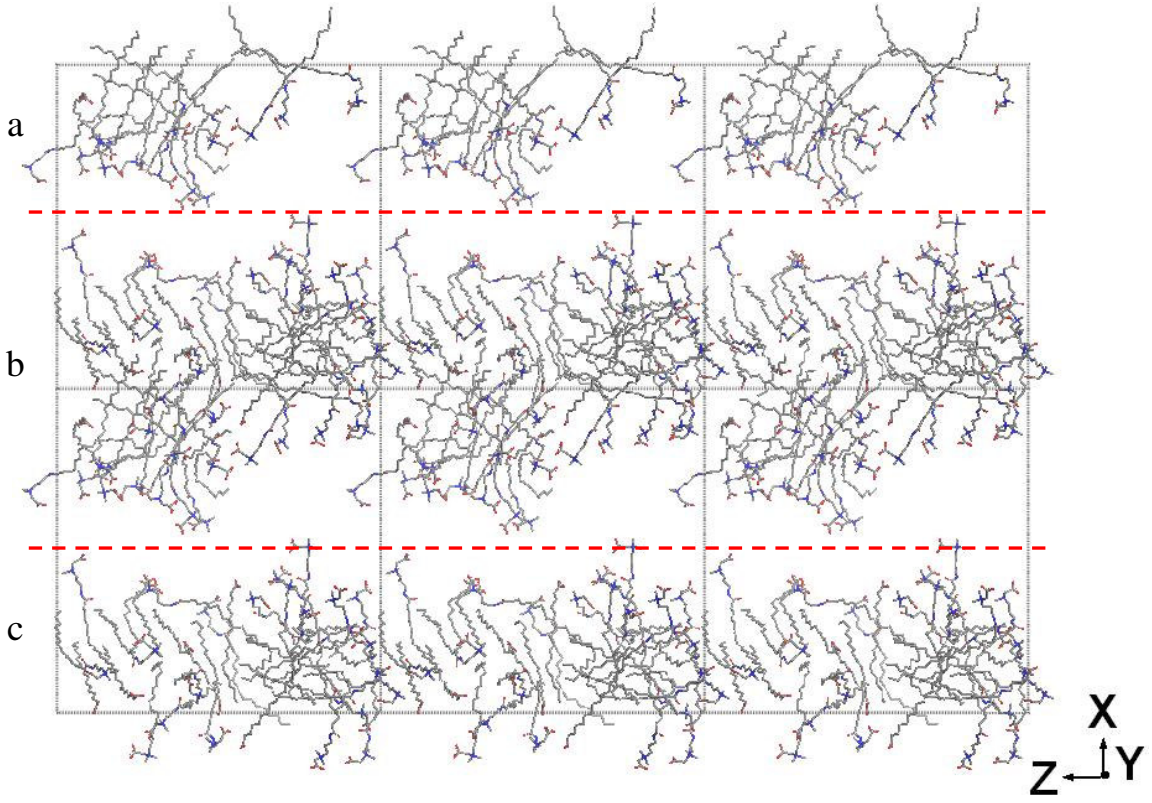

Fig. 7.12: Aggregation structure of the 36-ODB/12-OA system at 1 ns. A complete worm-like micelle is shown in section b. Due to the periodic boundary condition in x-direction, sections a and c belong to two other complete worm-like micelles. Only surfactant backbones are displayed. Water molecules and Ca^{2+}/Cl^{-} ions are omitted.

To demonstrate the aggregation structures in solutions, we calculated the radial distribution function (RDF) g(r) for 36-ODB/12-OA system. RDF is a physical quantity that describes the variation of atomic density as a function of the distance from one particular atom. **Fig. 7.13** shows the RDF curves between carboxyl oxygen atoms and respectively, calcium ions, chlorine ions and oxygen atoms of water molecules. **Fig. 7.14** shows the RDF curves between olefinic carbon atoms and respectively, calcium ions, chlorine ions and oxygen atoms of water molecules. All data were computed over the last 200 ps of trajectory. As shown in Figs. 7.13 and 7.14, the first peak of O-water RDF curve is much higher than that of C-water RDF curve, and the O-water distance is closer than the C-water distance. This indicates that the hydrophilic heads of surfactants were exposed to water solutions and the hydrophobic tails were basically buried inside the aggregation structure. Moreover, the relatively higher peaks of C-Ca and C-Cl RDF curves suggest that compared to water molecules, calcium and chlorine ions were in closer vicinity to the surfactant hydrophobic tails.

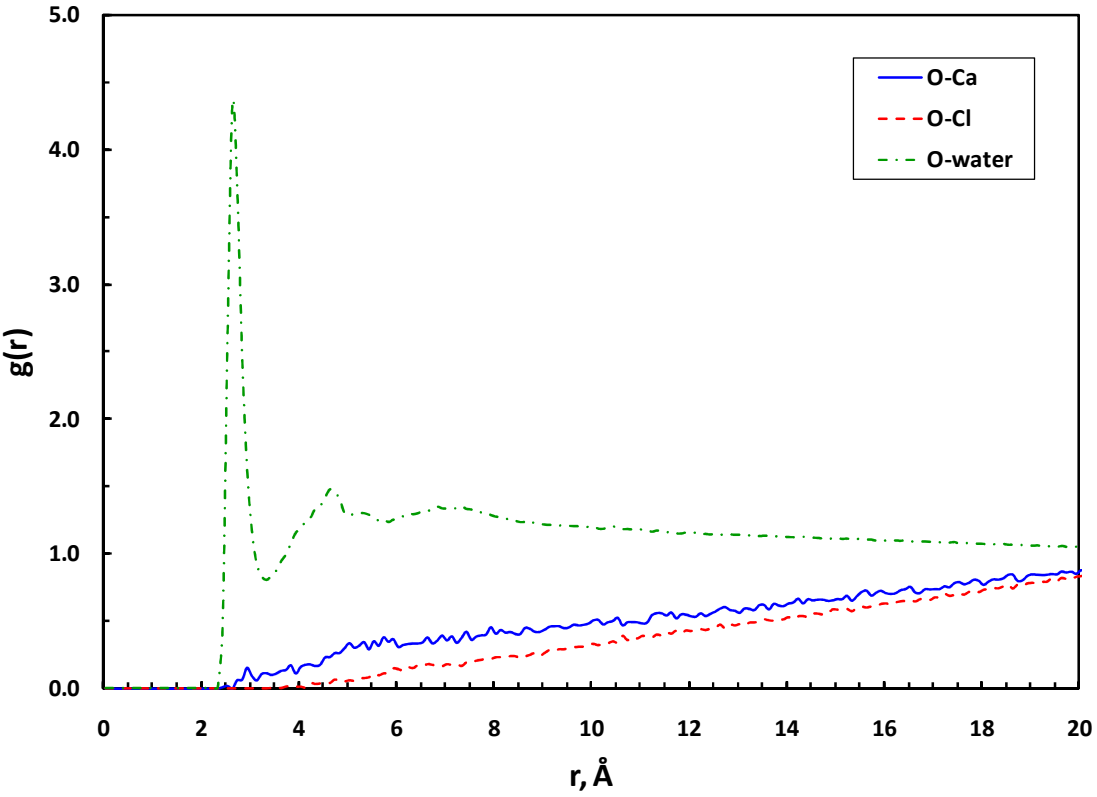

Fig. 7.13: Radial distribution function for 36-ODB/12-OA system between carboxyl oxygen atoms/calcium ions (——), carboxyl oxygen atoms/chlorine ions (- - - -) and carboxyl oxygen atoms/water oxygen atoms (—·—·). Data were obtained by averaging over the last 200 ps of trajectory.

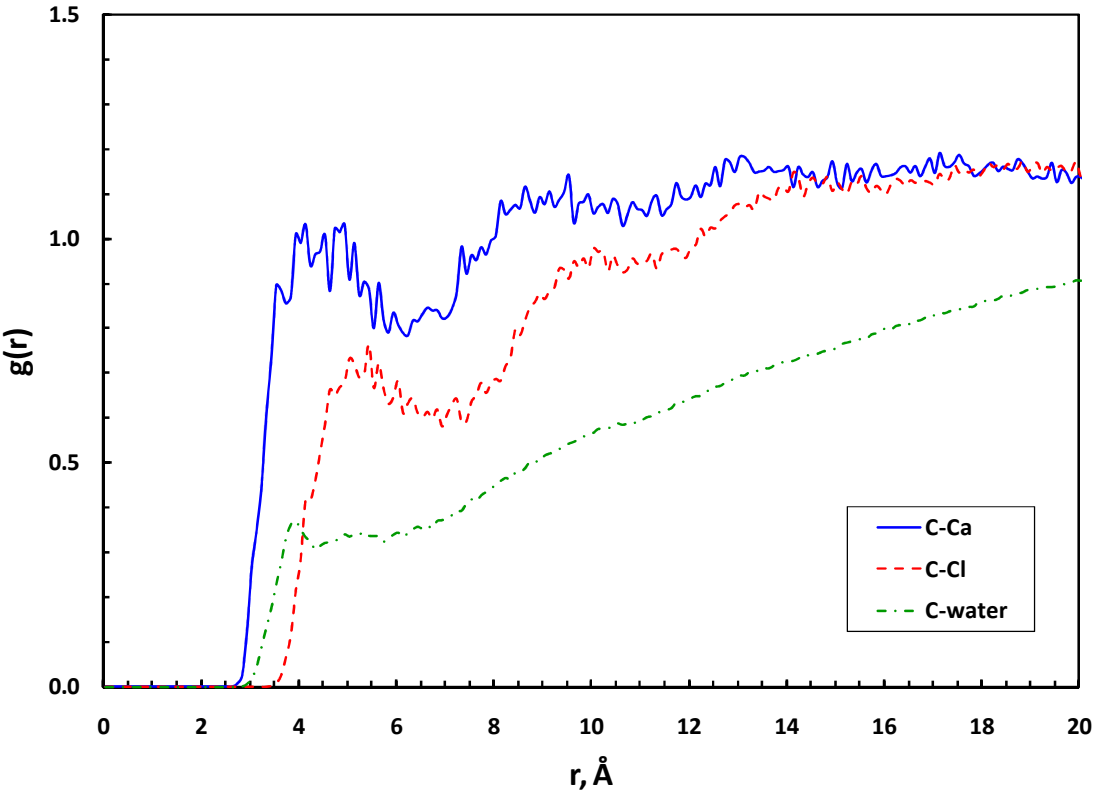

Fig. 7.14: Radial distribution function for 36-ODB/12-OA system between olefinic carbon atoms/calcium ions (——), olefinic carbon atoms /chlorine ions (- - - -) and olefinic carbon atoms /water oxygen atoms (—·—·). Data were obtained by averaging over the last 200 ps of trajectory.

Figs. 7.15 and 7.16 are the snapshots at 0, 200, 400, 600, 800 ps and 1 ns from an 24-ODB/24-OA system and an 12-ODB/36-OA system, respectively. In both cases, amorphous aggregates appeared at 200 ps, and gradually self-organized into small sheet-like structures at 400 ps. Subsequently, these small sheet-like structures have grown into large aggregation structures by attracting free surfactant molecules. For the 24-ODB/24-OA system, two large sheet-like structures were formed at the end of simulation (1 ns), containing 20 and 28 surfactant molecules, respectively (**Fig. 7.17**). For the 12-ODB/36-OA system, a large sheet-like structure formed by 34 surfactant molecules and an amorphous aggregate consisting of 14 surfactants were obtained (**Fig. 7.18**). Similar to the case of the 48-ODB system, no worm-like structure was observed in these two systems, although some finite aggregation structures were obtained.

In summary, worm-like micelle was quickly formed in mixed surfactant systems with an ODB/OA molar ratio of 3:1. For systems with ODB/OA molar ratios of 1:0, 1:1 and 1:3, only finite aggregates were formed, whose contribution to the system apparent viscosity was significantly less than that of the worm-like micelles.

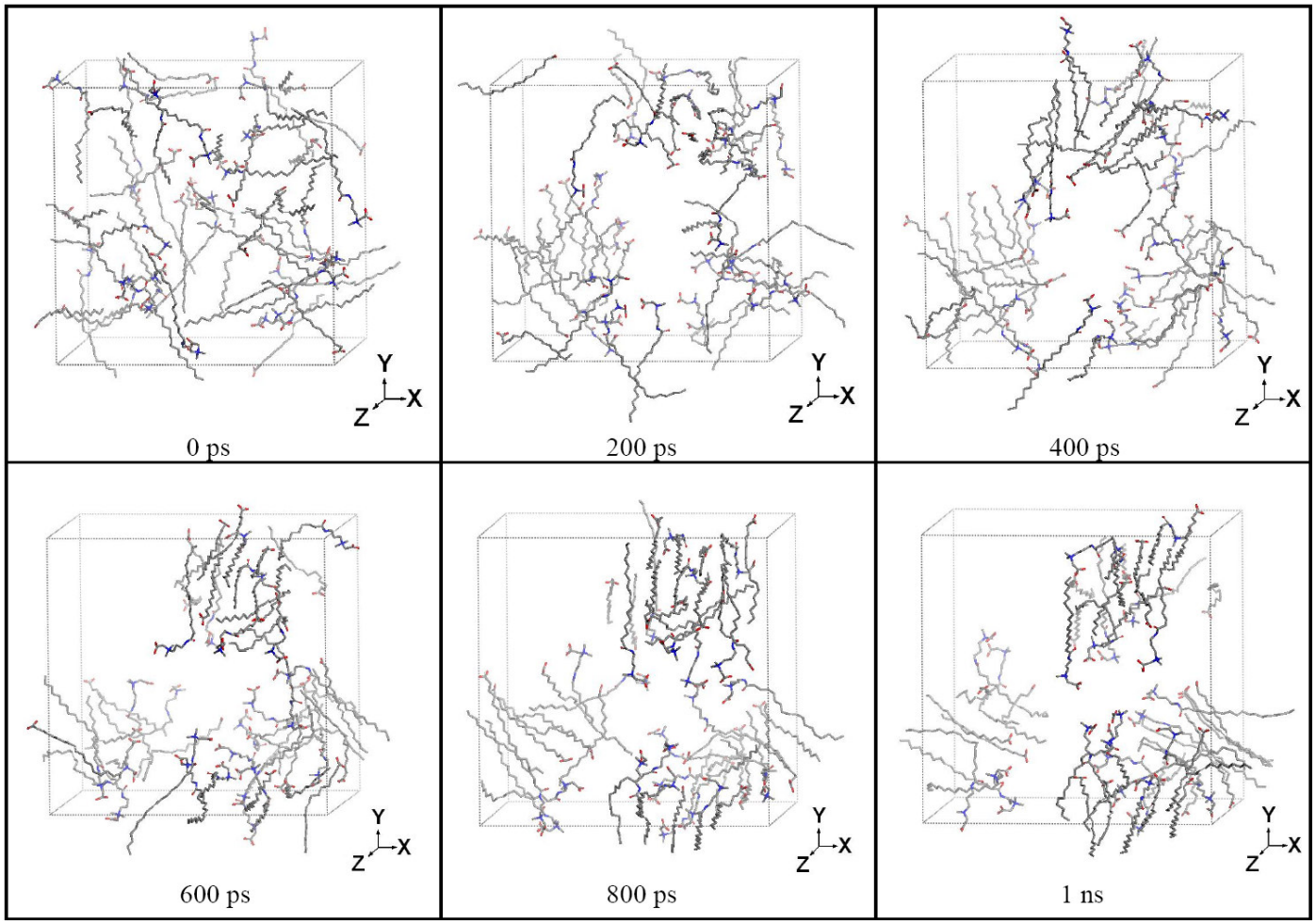

Fig. 7.15: Snapshots from the simulation trajectory of 24-ODB/24-OA system at 0, 200, 400, 600, 800 ps and 1 ns. Only surfactant backbones are displayed. Water molecules and Ca^{2+}/Cl^{-} ions are omitted.

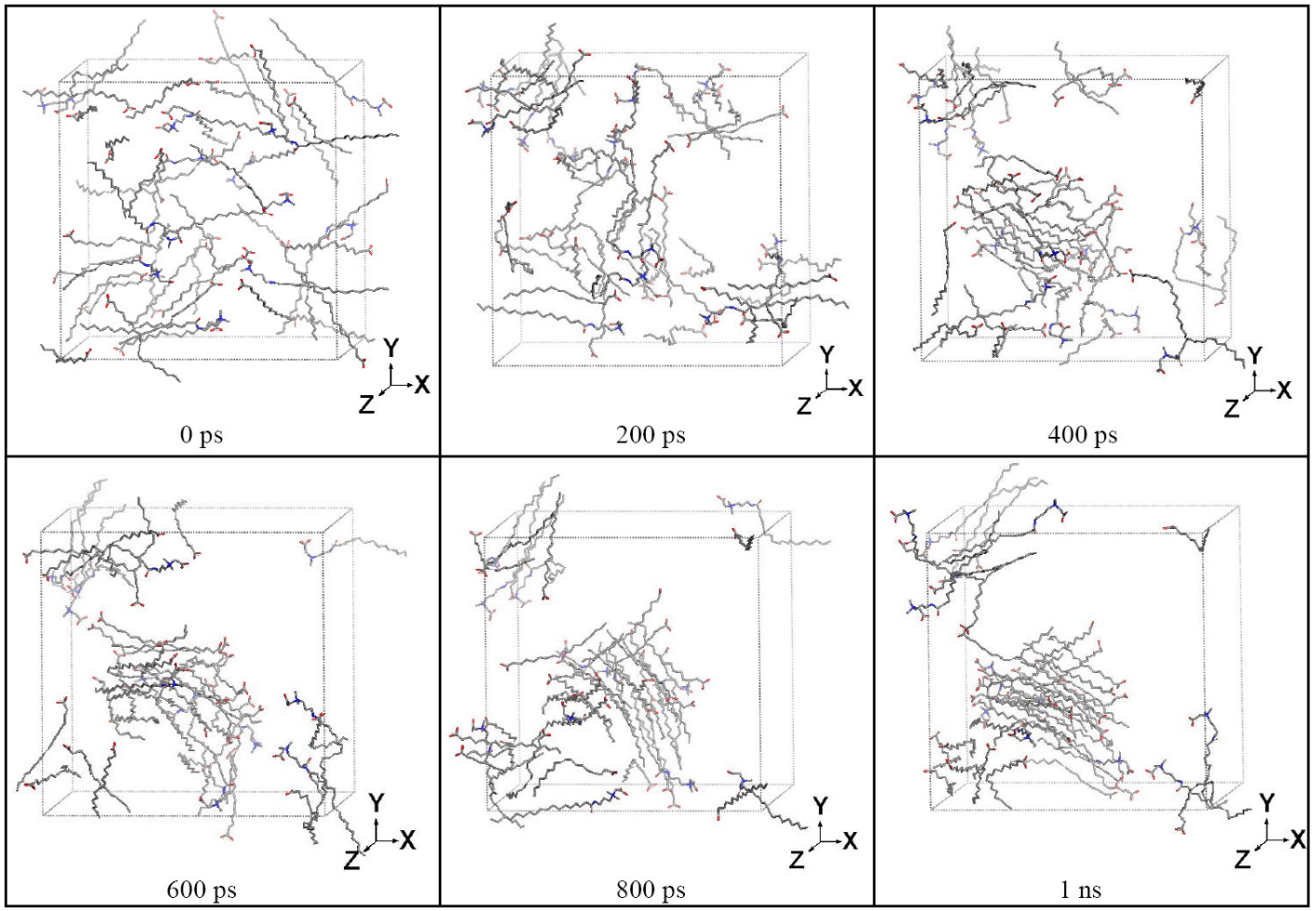

Fig. 7.16: Snapshots from the system simulation trajectory of 12-ODB/36-OA at 0, 200, 400, 600, 800 ps and 1 ns. Only surfactant backbones are displayed. Water molecules and Ca^{2+}/Cl^{-} ions are omitted.

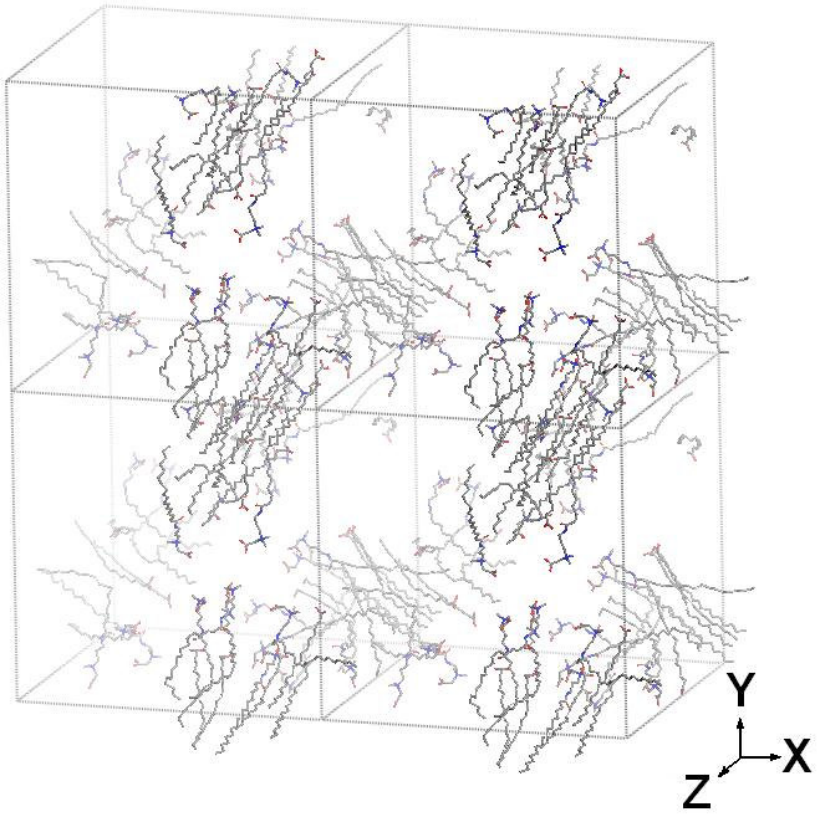

Fig. 7.17: Aggregation structures of the 24-ODB/24-OA system at 1 ns. Only surfactant backbones are displayed. Water molecules and Ca^{2+}/Cl^{-} ions are omitted.

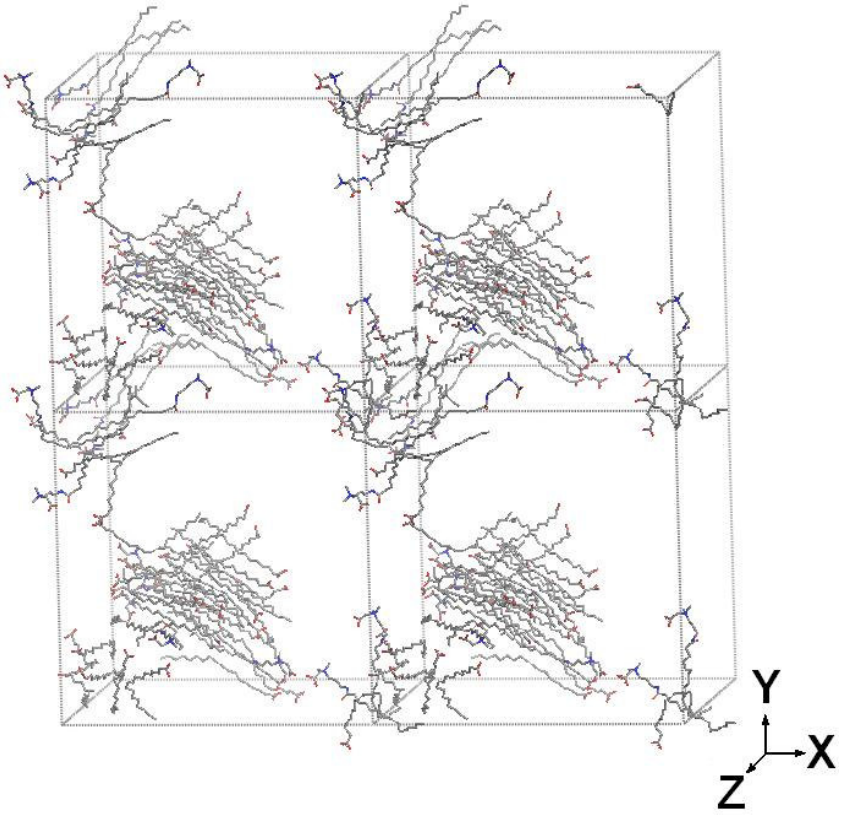

Fig. 7.18: Aggregation structures of the 12-ODB/36-OA system at 1 ns. Only surfactant backbones are displayed. Water molecules and Ca^{2+}/Cl^{-} ions are omitted.

The sterical hindrance inside worm-like micelle structures is relatively larger for pure ODB surfactants due to their long tails. By substituting certain amount of ODB molecules with shorter OA molecules, the sterical-hindrance effect can be significantly lowered, resulting in the formation of stable worm-like micelle structures composed of both ODB and OA surfactants. However, if too many ODB molecules are substituted by OA molecules, since OA is not capable of forming worm-like micelles at ambient conditions, worm-like micelles are destabilized, and finite surfactant micelles are preferred.

As a result, the formation of worm-like micelles in mixed surfactant systems is more structurally favorable only with certain surfactant molar ratios. Based on current simulation results, the optimum ODB/OA molar ratio was nearly 3:1. The results in the current study are in accordance with previous work, in which the mixture of zwitterionic and anionic surfactants was found to form worm-like micelles synergistically (Saul et al. 1974; Hoffmann et al. 1992; 1994).

Compare Experimental and MD Simulation Results

The MD simulation results are qualitatively in agreement with our experimental results. In the ODB hydrolysis experiments, the value of ODB/OA molar ratio continuously decreased with hydrolysis time. Unhydrolyzed surfactant samples exhibited low apparent viscosity at ambient conditions. This corresponds to the MD simulation systems which show the formation or relatively ordered aggregates but no worm-like micelle. After short-time hydrolysis, when the optimum ODB/OA molar ratios (nearly

3:1) were achieved, stable worm-like micelles were formed quickly, resulting in much higher apparent viscosity of the solution. This can be proved by the existence of maximum apparent viscosity in Fig. 7.6. If hydrolysis reaction continued, as ODB/OA molar ratio became lower, the already-formed worm-like micelle structures were no longer stable and decomposed into finite micelles, which inevitably causes the loss of large viscosity of solution. This is reflected by the significant decrease in the fluid apparent viscosity as shown in Fig. 7.6.

7.3. Summary

Both experimental studies and theoretical studies (MD simulations) were carried out to study the impact of hydrolysis at high temperature on the apparent viscosity of amido-carboxybetaine surfactant-based acid. The following observations are noted:

Samples (15 wt% HCl and 4, 6, 8 wt% surfactant) were hydrolyzed at 190°F and partially spent (pH 4.5). After 1 hour hydrolysis, the apparent viscosity reached the maximum, while a significant viscosity reduction occurred after 3 hours hydrolysis. In addition, phase separation occurred after 3 hours of hydrolysis.

MD Simulation results revealed the formation of different micelle structures in surfactant systems with different amido-carboxybetaine/fatty acid soap molar ratios. The optimal surfactant molar ratio (ODB:OA) was nearly 3:1, at which the worm-like micelle structure was formed in a short time (less than 1 ns). Other surfactant molar ratios, including 1:0, 1:1 and 1:3, only resulted in the formations of finite surfactant aggregates.

8. CONCLUSIONS AND RECOMMENDATIONS

In regarding to its applications in matrix acidizing treatments, two properties of viscoelastic surfactant have been investigated, including:

1. Propagation and retention of viscoelastic surfactant in carbonate reservoirs following matrix acidizing treatments; and
2. Impact of acid hydrolysis reaction at high temperatures on the apparent viscosity of viscoelastic surfactant fluids.

First, the optimized two-phase titration method was used to measure surfactant concentration, and examined the impact of acid additives, reaction products, and contaminants on these measurements. Based on results obtained, the following conclusions can be drawn:

1. The two-phase titration method was optimized and successfully applied to measure surfactant concentration in solutions of live and spent HCl acid. The accuracy of the method was found to be ±1.33%.
2. Typical acid additives (corrosion inhibitor, mutual solvent, and methanol); reaction products ($CaCl_2$, $MgCl_2$ and $FeCl_2$), contaminants (mainly Fe^{3+}); HCl and HTO acid (high temperature organic acid) did not interfere with measurement of the surfactant.

With the surfactant concentration analysis method well developed, extensive laboratory work was conducted to study retention of a carboxy-betaine surfactant that is commonly used in acid diversion in carbonate reservoirs. Long carbonate cores of 20 in.

length were used in the present study. Based on the results obtained, the following conclusions can be drawn:

1. Propagation of viscoelastic surfactants in linear calcite cores was found to be a function of flow rate. Surfactant lagged calcium in the core effluent samples.
2. The volume of acid needed to break through the core and the amount of surfactant retained varied with acid injection rate, and exhibited a minimum at 10 cm^3/min.
3. A significant amount of surfactant was retained in the cores.
4. Injection of 2 pore volumes of 10 vol% mutual solvent removed only 20% of the surfactant injected.

Based on these results, there is a need to use internal breakers when surfactant-based acids are used in dry gas wells or water injectors.

On the other hand, the impact of hydrolysis at high temperature on the apparent viscosity of amido-carboxybetaine surfactant-based acid was studied both experimentally and theoretically by MD simulations. The following conclusions can be drawn based on the results obtained:

1. For all samples with 15 wt% HCl and 4, 6, 8 wt% surfactant that were hydrolyzed at 190°F and partially spent (pH 4.5), the maximum apparent viscosity was obtained after 1 hour hydrolysis. A significant viscosity reduction occurred after 3 hours hydrolysis.
2. Phase separation occurred for samples that were hydrolyzed at 190°F for more than 3 hours and partially spent (pH 4.5).

3. Simulation results show that different micelle structures can be observed in surfactant systems with different amido-carboxybetaine/fatty acid soap molar ratios. The optimal surfactant molar ratio was nearly 3:1, at which the worm-like micelle structure was formed in a short time (less than 1 ns).

As a result, high temperature hydrolysis reaction should be taken into consideration when amido-type viscoelastic surfactants are applied in carbonate matrix acid treatments. The following are recommended:

1. At 190°F, treatments should be completed within 3 hours to avoid significant viscosity reduction and phase separation of the amido-surfactant gel.
2. Short-time viscosity enhancement of the amido-surfactant gel can be achieved within 1-2 hours of treatments at 190°F.
3. Amido-surfactant fluid viscosity can be effectively reduced after 3 hours of acid treatments at 190°F. In this case, no additional breaker is needed to break down the surfactant gel.

REFERENCES

Al-Ghamdi, A.H., Nasr-El-Din, H.A., Al-Qahtani, A.A., and Samuel, M. 2004. Impact of Acid Additives on the Rheological Properties of Viscoelastic Surfactants and Their Influence on Field Application. Paper SPE 89418 presented at the SPE/DOE Symposium on Improved Oil Recovery, Tulsa, 17-21 April.

Allen, M.P. 2004. Introduction to Molecular Dynamics Simulation. In *Computational Soft Matter: From Synthetic Polymers to Proteins, Lecture Notes*, ed. N. Attig, K. Binder, H. Grubmüller, and K. Kremer, **23**: 1-28. Jülich, Germany: John von Neumann Institute for Computing.

Almeida, J.A.S., Marques, E.F., Jurado, A.S., and Pais, A.A.C.C. 2010. The Effect of Cationic Gemini Surfactants upon Lipid Membranes. An Experimental and Molecular Dynamics Simulation Study. *Phys. Chem. Chem. Phys*. **12** (43): 14462-14476.

Al-Muhareb, M.A., Nasr-El-Din, H.A., Samuel, E., Marcinew, R.P., and Samuel, M. 2003. Acid Fracturing of Power Water Injectors: A New Field Application Using Polymer-Free Fluids. Paper SPE 82210 presented at the SPE European Formation Damage Conference, The Hague, The Netherlands, 13-14 May.

Al-Mutawa, M., Al-Anzi, E., Jemmali, M., Chang, F., Samuel, E., and Samuel, M. 2005. Zero-Damaging Stimulation and Diversion Fluid: Field Cases from the Carbonate Formations in North Kuwait. *SPE Prod & Fac* **20** (2): 94-105.

Arangath, R., Hopkins, K.W., Lungershausen, D., and Bolyspayev, N.T. 2008. Successful Stimulation of Thick, Naturally-Fractured Carbonates Pay Zones in Kazakhstan. Paper SPE 112419 presented at the SPE International Symposium and Exhibition on Formation Damage Control, Lafayette, Louisiana, 13-15 February.

Artola, P., Alvarado, O., Huidobro, E., and Salmorán, A. 2004. Nondamaging Viscoelastic Surfactant-Based Fluids Used for Acid Fracturing Treatments in Veracruz Basin, Mexico. Paper SPE 86489 presented at the SPE International Symposium and Exhibition on Formation Damage Control, Lafayette, Louisiana, 18-20 February.

Berendsen, H.J.C.; Postma, J.P.M.; Gunsteren, W.F.v.; DiNola, A.; Haak, J.R. **1984**. Molecular Dynamics with Coupling to External Bath. *J. Chem. Phys.* **81**: 3684-3690.

Bogusz, S., Venable, R.M., and Pastor R.W. 2000. Molecular Dynamics Simulations of Octyl Glucoside Micelles: Structural Properties. *J. Phys. Chem. B* **104** (23): 5462-5470.

Bogusz, S., Venable, R.M., and Pastor R.W. 2001. Molecular Dynamics Simulations of Octyl Glucoside Micelles: Dynamic Properties. *J. Phys. Chem. B* **105** (35): 8312-8321.

Bruce, C.D., Berkowitz, M.L., Perera, L., and Forbes, M.D.E. 2002. Molecular Dynamics Simulation of Sodium Dodecyl Sulfate Micelle in Water: Micellar Structural Characteristics and Counterion Distribution. *J. Phys. Chem. B* **106** (15): 3788-3793.

Bulat, D., Chen, Y., Graham, M.K., Marcinew, R., Adeogun, G., Sheng, J., and Abad, C. 2008. A Faster Cleanup, Produced-Water-Compatible Fracturing Fluid: Fluid Designs and Field Case Studies. Paper SPE 112435 presented at the 2008 SPE International Symposium and Exhibition on Formation Damage Control, Lafayette, Louisiana, 13-15 February.

Buschmann, N. 1995. Does the Two-Phase Titration of Surfactants Require a Mutagenic Indicator? *J. Am. Oil Chem. Soc.* **72** (10): 1243.

Buschmann, N. and Schulz, R. 1992. Determination of Cationic and Zwitterionic Surfactants Using Ion Selective Electrodes. *Tenside, Surfactants, Deterg.* **29** (2): 128-130.

Bustos, O., Chen, Y., Stewart, M., Heiken, K., Bui, T., Mueller, P., and Lipinski, E. 2007. Case Study: Application of a Viscoelastic Surfactant-Based CO_2-Compatible Fracturing Fluid in the Frontier Formation, Big Horn Basin, Wyoming. Paper SPE 107966 presented at the SPE Rocky Mountain Oil & Gas Technology Symposium, Denver, Colorado, 16-18 April.

Campeau, D., Gruda, I., Thibeault, Y., and Legendre, F. 1987. Analysis of Amphoteric Surfactants of the Alkylaminopropylglycine Type by Gas Chromatography. *J. Chromatogr.* **405**: 305-310.

Card, R.J, Brown, J.E., Vinod, P.S., Willberg, D.M., Samuel, M.M., and Chang, F.F. 1999. Methods for Limiting the Inflow of Formation Water and for Stimulating Subterranean Formation. US Patent No. 5,979,557.

Chang, F.F., Thomas, R.L., and Fu, D.K. 1998. A New Material and Novel Technique for Matrix Stimulation in High-Water-Cut Oil Wells. Paper SPE 39592 presented at the SPE Formation Damage Control Conference, Lafayette, Louisiana, 18-19 February.

Chang, F.F., Love, T., Affeld, C.J., Blevins, J.B. III, Thomas, R.L., and Fu, D.K. 1999. Case Study of a Novel Acid-Diversion Technique in Carbonate Reservoirs. Paper SPE 56529 presented at the SPE Annual Technical Conference and Exhibition, Houston, Texas, 3-6 October.

Chang, F.F., Acock, A.M., Geoghagan, A., and Huckabee, T. 2001a. Experience in Acid Diversion in High Permeability Deep Water Formations Using Visco-Elastic-Surfactant. Paper SPE 68919 presented at the SPE European Formation Damage Conference, The Hague, The Netherlands, 21-22 May.

Chang, F.F., Qi, Q., and Frenier, W. 2001b. A Novel Self-Diverting-Acid Developed for Matrix Stimulation of Carbonate Reservoirs. Paper SPE 65033 presented at the SPE International Symposium on Oilfield Chemistry, Houston, Texas, 13-16 February.

Chilingarian, G.V., Robertson, J.O., and Kumar, S. 1989. *Surface Operations in Petroleum Production*, *II*. New York: Elsevier Science Publishing Company Inc.

Crews, J.B. 2005. Internal Phase Breaker Technology for Viscoelastic Surfactant Gelled Fluids. Paper SPE 93449 presented at SPE International Symposium on Oilfield Chemistry, Houston, Texas, 2-4 February.

Crews, J.B. 2007. Saponified Fatty Acids as Viscosity Modifiers for Viscoelastic Surfactant-Gelled Fluids. US Patent No. 20080108526A1.

Crews, J.B., and Huang, T. 2007a. Methods and Composition for Diverting Acid Fluids in Wellbores. US Patent No. 20070151726A1.

Crews, J.B. and Huang, T. 2007b. Internal Breakers for Viscoelastic-Surfactant Fracturing Fluids. Paper SPE 106216 presented at the SPE International Symposium on Oilfield Chemistry, Houston, Texas, 28 February-2 March.

Cross, J.T. 1998. The Volumetric Analysis of Anionic Surfactants. In *Anionic Surfactant*, second edition, ed. J. Cross. 35-88. New York: Marcel Dekker, Inc.

Crowe, C.W., Hutchinson, B.H., and Trittipo, B.L. 1989. Fluid-Loss Control: The Key to Successful Acid Fracturing. *SPE Prod Eng* **4** (3): 215-220; *Trans.,* AIME, 287.

Deysarkar, A.K., Dawson, J.C., Sedillo, L.P., and Knoll-Davis, S. 1984. Crosslinked Acid Gel. *J. Canadian Petroleum Technology* **23** (1): 26-32.

Domingo, X. 1996. Betaines. In *Amphoteric Surfactants*, second edition, ed. E.G. Lomax. 75-190. New York: Marcel Dekker, Inc.

Economides, M.J., Hill, A.D., and Ehlig-Economides, C. 1994. *Petroleum Production Systems*. Upper Saddle River, New Jersey: Prentice Hall, 392-403.

Floriano, M.A. and Caponetti, E. 1999. Micellization in Model Surfactant Systems. *Langmuir* **15** (9): 3143-3151.

Fontana, C., Muruaga, E., Perez, D., Cavazzoli, G., and Krenz, A. 2007. Successful Application of a High Temperature Viscoelastic Surfactant (VES) Fracturing Fluids under Extreme Conditions in Patagonian Wells, San Jorge Basin. Paper SPE 107277 presented at the SPE Europec/EAGE Annual Conference and Exhibition, London, United Kingdom, 11-14 June.

Fu, D. and Chang, F. 2005. Compositions and Methods for Treating a Subterranean Formation. US Patent No. 6,929,070 B2.

Gerhards, R., Jussofie, I., Käseborn, D., Keune, S., and Schulz, R. 1996. Modern Methods for the Analysis of Cocoamidopropyl Betaines. *Tenside, Surfactants, Deterg*. **33** (1): 8-14.

González, J.M., Müller, A.J., Torres, M.F., and Sáez, A.E. 2005. The Role of Shear and Elongation in the Flow of Solutions of Semi-Flexible Polymers through Porous Media. *Acta* **44**: 396-405.

Graham, D.Y. and Sackman, J.W. 1983. Solubility of Calcium Soaps of Long-Chain Fatty Acids in Simulated Intestinal Environment. *Digestive Diseases and Sciences* **28** (8): 733-736.

Hagler, A.T., Huler, E., and Lifson, S. 1974. Energy functions for peptides and proteins. I. Derivation of a Consistent Force Field Including the Hydrogen Bond from Amide Crystals. *J. Am. Chem. Soc.* **96** (17): 5319-5327.

Haile, J.M. 1992. *Molecular Dynamics Simulation*: *Elementary Methods*. New York: John Wiley & Sons, Inc.

Hoefner, M.L., Fogler, H.S., Stenius, P., and Sjöblom, J. 1987. Role of Acid Diffusion in Matrix Acidizing of Carbonates. *J. Pet. Tech.* **39** (2): 203-208.

Hoffmann, H., Rauscher, A., Gradzielski, M., and Schulz, S.F. 1992. Influence of Ionic Surfactants on the Viscoelastic Properties of Zwitterionic Surfactant Solutions. *Langmuir* **8** (9): 2140-2146.

Hoffmann, H., Hofmann, S., and Illner, J.C. 1994. Phase Behavior and Properties of Micellar Solutions of Mixed Zwitterionic and Ionic Surfactants. *Progr. Colloid Polym. Sci.* **97**: 103-109.

Holmberg, K., Jönsson, B., Kronberg, B., and Lindman, B. 2003. *Surfactants and Polymers in Aqueous Solution*, second edition. Chichester, West Sussex, England: John Wiley & Sons, Ltd., 52-75.

Hu, X., Li, Y., Sun, H., Song, X., Li, Q., Cao, X., and Li, Z. 2010. Effect of Divalent Cationic Ions on the Adsorption Behavior of Zwitterionic Surfactant at Silica/Solution Interface. *J. Phys. Chem. B* **114** (27): 8910-8916.

Huang, T. and Crews, J.B. 2008. Do Viscoelastic-Surfactant Diverting Fluids for Acid Treatments Need Internal Breakers? Paper SPE 112484 presented at the SPE International Symposium and Exhibition on Formation Damage Control, Lafayette, Louisiana, 13-15 February.

Huang, T., McElfresh, P.M., and Gabrysch, A.D. 2004. Organic Acid System for High Temperature Acidizing. US Patent No. 6,805,198.

Im, S.H., Jeong, Y.H., and Ryoo, J.J. 2008. Simultaneous Analysis of Anionic, Amphoteric, Nonionic and Cationic Surfactant Mixtures in Shampoo and Hair Conditioner by RP-HPLC/ELSD and LC/MS. *Analytica Chimica Acta* **619** (1): 129-136.

Jorgensen, W.L., Chandrasekhar, J., Madura, J.D., Impey, R.W., and Klein, M.L. 1983. Comparison of Simple Potential Functions for Simulating Liquid Water. *J. Chem. Phys.* **79** (2): 926-935.

Kaibara, K., Iwata, E., Eguchi, Y., Suzuki, M., and Maeda, H. 1997. Dispersion Behavior of Oleic Acid in Aqueous Media: from Micelles to Emulsions. *Colloid Polym Sci*. **275** (8): 777-783.

Kaznessis, Y.N., Kim, S., and Larson, R.G. 2002. Simulations of Zwitterionic and Anionic Phospholipid Monolayers. *Biophys. J*. **82** (4): 1731-1742.

Klein, M.L. and Shinoda, W. 2008. Large-Scale Molecular Dynamics Simulations of Self-Assembling Systems. *Science* **321** (5890): 798-800.

Koenig, H. 1970. Analysis of Amphoteric Surfactants (Die Analyse Amphoterer Tenside). *Fresenius' J. Anal. Chem.* **251** (6): 359-368.

Kondoh, Y. and Takano, S. 1986. Determination of Carboxybetaine Amphoteric Surfactants in Household and Cosmetic Products by High Performance Liquid Chromatography with Prelabeling. *Anal. Sci*. **2** (5): 467-471.

Kristopher, A.K. 2009. Viscoelastic Surfactant-Based Systems in the Niagaran Formation. Paper SPE 125754 presented at the SPE Eastern Regional Meeting, Charleston, West Virginia, 23-25 September.

Lane, J.M.D., Chandross, M., Stevens, M.J., and Grest, G.S. 2008. Water in Nanoconfinement between Hydrophilic Self-Assembled Monolayers. *Langmuir* **24** (10): 5209-5212.

Liu, H., Coston, C., Yassin, M., Uddin, S., and Al-Dhafeeri, F. 2009. A Novel Stimulation Technique for Horizontal Openhole Wells in Carbonate Reservoirs: A Case Study in Kuwait. *SPE Prod & Oper* **24** (1): 43-49.

Lomax, E.G. 1996. Analysis. In *Amphoteric Surfactants*, second edition, ed. E.G. Lomax. 395-412. New York: Marcel Dekker, Inc.

Long, D.A. and Truscott, T.G. 1968. Peptide Kinetics, Part 6. Acid-Catalyzed Hydrolysis of Tetraglycine. *Trans. Faraday Soc.* **64**: 1624-1628.

Lund, K., Fogler, H.S., and McCune, C.C. 1973. Acidization I: The Dissolution of Dolomite in Hydrochloric Acid. *Chem. Eng. Sci*. **28** (3): 691-700.

Lund, K., Fogler, H.S., McCune, C.C., and Ault, J.W. 1975. Acidization II: The Dissolution of Calcite in Hydrochloric Acid. *Chem. Eng. Sci*. **30** (8): 825-835.

Lungwitz, B., Fredd, C., Brady, M., Miller, M., Ali, S., and Hughes, K. 2007. Diversion and Cleanup Studies of Viscoelastic Surfactant-Based Self-Diverting Acid. *SPE Prod & Oper* **22** (1): 121-127.

Lynn, J.D. and Nasr-El-Din, H.A. 2001. A Core-Based Comparison of the Reaction Characteristics of Emulsified and in situ Gelled Acids in Low Permeability, High Temperature, Gas Bearing Carbonates. Paper SPE 65386 presented at the SPE International Symposium on Oilfield Chemistry, Houston, Texas, 13-16 February.

MacKerell, A.D. 1995. Molecular Dynamics Simulation Analysis of a Sodium Dodecyl Sulfate Micelle in Aqueous Solution: Decreased Fluidity of the Micelle Hydrocarbon Interior. *J. Phys. Chem*. **99** (7): 1846-1855.

Maillet, J.B., Lachet, V., and Coveney, P.V. 1999. Large Scale Molecular Dynamics Simulation of Self-assembly Processes in Short and Long Chain Cationic Surfactants. *Phys. Chem. Chem. Phys.* **1** (23): 5277-5290.

Marrink, S.J., Tieleman, D.P., and Mark, A.E. 2000. Molecular Dynamics Simulation of the Kinetics of Spontaneous Micelle Formation. *J. Phys. Chem. B* **104** (51): 12165-12173.

Materials Studio 5.0. 2009. Software Discover/Accelrys, http://accelrys.com/products/materials-studio/. San Diego, California.

McCarthy, S.M., Qu, Q., and Vollmer, D. 2002. The Successful Use of Polymer-Free Diverting Agents for Acid Treatments in the Gulf of Mexico. Paper SPE 73704 presented at the SPE International Symposium and Exhibition on Formation Damage Control, Lafayette, Louisiana, 20-21 February.

Metcalf, S., Lopez, H., Hoff, C., and Woo, G. 2000. Gas Production from Low Permeability Carbonates Enhanced Through Usage of a New Acid Polymer System. Paper SPE 59756 presented at the SPE/CERI Gas Technology Symposium, Calgary, 3-5 April.

Mohamed, S., Nasr-El-Din, H.A., Dossary, K., McClelland, K., and Samuel, M. 2002. Enhancement of Stimulation Treatment of Water Injection Wells Using a New Polymer-Free Diversion System. Paper SPE 78588 presented at the Abu Dhabi International Petroleum Exhibition and Conference, Abu Dhabi, United Arab Emirates, October 13-16.

Mohammed, S.K., Nasr-El-Din, H.A., and Erbil, M.M. 2005. Successful Application of Foamed Viscoelastic Surfactant-Based Acid. Paper SPE 95006 presented at the SPE European Formation Damage Conference, Scheveningen, The Netherlands, 25-27 May.

Mumallah, N.A. 1991. Factors Influencing the Reaction Rate of Hydrochloric Acid and Carbonate Rock. Paper SPE 21036 presented at the SPE International Symposium on Oilfield Chemistry, Anaheim, California, Feb. 20-22.

Muskat, M. 1949. *Physical Principles of Oil Production*. New York: McGraw-Hill Book Co., Inc.

Myers, D., 1988. *Surfactant Science and Technology*, first edition. Hoboken, New Jersey: VCH Publishers, Inc.

Nasr-El-Din, H.A. and Al-Humaidan, A.Y. 2001. Iron Sulfide Scale: Formation, Removal, and Mitigation. Paper SPE 68315 presented at the SPE International Symposium on Oilfield Scale, Aberdeen, 30-31 January.

Nasr-El-Din, H.A., Taylor, K.C., and Al-Hajji, H.H. 2002. Propagation of Cross-Linkers Used in in situ Gelled Acids in Carbonate Reservoirs. Paper SPE 75257 presented at the SPE/DOE Improved Oil Recovery Symposium, Tulsa, 13-17 April.

Nasr-El-Din, H.A., Samuel, E., and Samuel, M. 2003. Application of a New Class of Surfactants in Stimulation Treatments. Paper SPE 84898 presented at the SPE

International Improved Oil Recovery Conference in Asia Pacific, Kuala Lumpur, Malaysia, 20-21 October.

Nasr-El-Din, H.A., Al-Habib, N.S., Al-Mumen, A.A., Jemmali, M., and Samuel, M. 2006a. A New Effective Stimulation Treatment for Long Horizontal Wells Drilled in Carbonate Reservoirs. *SPE Prod &Oper* **21** (3): 330-338.

Nasr-El-Din, H.A., Chesson, J.B., Cawiezel, K.E., and Devine, C.S. 2006b. Lessons Learned and Guidelines for Matrix Acidizing with Viscoelastic Surfactant Diversion in Carbonate Formations. Paper SPE 102468 presented at the SPE Annual Technical Conference and Exhibition, San Antonio, Texas, 24-27 September.

Nasr-El-Din, H.A., Chesson, J.B., Cawiezel, K.E., and Devine, C.S. 2006c. Field Success in Carbonate Acid Diversion, Utilizing Laboratory Data Generated by Parallel Flow Testing. Paper SPE 102828 presented at the SPE Annual Technical Conference & Exhibition, San Antonio, Texas, 24-27 September.

Nasr-El-Din, H.A. and Samuel, M. 2007. Lessons Learned from Using Viscoelastic Surfactants in Well Stimulation. *SPE Prod & Oper* **22** (1): 112-120.

Nasr-El-Din, H.A., Al-Ghamdi, A.H., Al-Qahtani A.A., and Samuel, M.M., 2008. Impact of Acid Additives on the Rheological Properties of a Viscoelastic Surfactant and Their Influence on Field Application. *SPE J.* **13** (1): 35-47.

Nasr-El-Din, H.A., Al-Mohammed, A.M., Al-Aamri, A.D., Al-Fahed, M.A., Chang, F.F. 2009a. Quantitative Analysis of Reaction-Rate Retardation in Surfactant-Based Acids. *SPE Prod & Oper* **24** (1): 107-116.

Nasr-El-Din, H.A., Al-Nakhli, A.R., Al-Driweesh, S.M., Welton, T., Sierra, L., and Van Domelen, M. 2009b. Application of Cationic Surfactant-based Fluids for Acid Diversion. *SPE Prod & Oper* **24** (1): 124-134.

Nosé, S.; Klein, M.L. 1983. Constant Pressure Molecular Dynamics for Molecular Systems. *Mol. Phys.* **50**: 1055-1076.

Nosé, S. 1984a. A Molecular Dynamics Method for Simulations in the Canonical Ensemble. *Mol. Phys.* **52**: 255-268.

Nosé, S. 1984b. A Unified Formulation of the Constant Temperature Molecular Dynamics Methods. *J. Chem. Phys.* **81**: 511-519.

Oei, H.H.Y., Mai, I., and Toro, D.C. 1991. Quantitative Analysis of Anionic or Cationic Surfactants Using a Surfactant Electrode. *J. Soc. Cosmet. Chem.* **42** (5): 309-316.

Pabley, A.S., Ewing, B.C., and Callaway, R.E. 1982. Performance of Crosslinked Hydrochloric Acid in the Rocky Mountain Region. Paper SPE 10877 presented at the SPE Rocky Mountain Regional Meeting, Billings, Montana, 19-21 May.

Parris, N. 1978. Surfactant Analysis by High Performance Liquid Chromatography: I. A Rapid Analysis for Mixtures of Amphoteric Surfactants and Soap. *J. Am. Oil Chem. Soc.* **55** (9): 675-677.

Patruyo, L.G., Müller, A.J., and Sáez, A.E. 2002. Shear and Extensional Rheology of Solutions of Modified Hydroxyethyl Celluloses and Sodium Dodecyl Sulfate. *Polymer* **43**: 6481-6493.

Plantinga, J.M., Donkerbroek, J.J., and Mulder, R.J. 1993. Determination of Betaine and Free Amine in Alkyldimethyl Betaine by Potentiometric Titrations. *J. Am. Oil Chem. Soc.* **70** (1): 97-99.

Pohle, W.D. 1941. Solubility of Calcium Soaps of Gum Rosin, Rosin Acids and Fatty Acids. *J. Amer. Oil Chem. Soc*. **18** (12): 244-245.

Porter, M.R. 1994. *Handbook of Surfactants*, second edition. London: Chapman & Hall.

Qian, Y., Engel, M.H., Macko, S.A., Carpenter, S., and Deming J.W. 1993. Kinetics of Peptide Hydrolysis and Amino Acid Decomposition at High Temperature. *Geochim. Cosmochim. Acta* **57** (14): 3281-3293.

Read, H. 1985. Surfactant Analysis Using HPTLC and the Latroscan. In *Proceedings of the International Symposium on Instrumental High Performance Thin-Layer Chromatography*, third edition, ed. R.E. Kaiser. Institude of Chromatography, Bad Dürkheim, Federal Republic of Germany, 157-171.

Reid, V.W., Longman, G.F., and Heinerth, E. 1967. Determination of Anionic-Active Detergents by Two-Phase Titration. *Tenside* **4**: 292-304.

Reid, V.W., Longman, G.F., and Heinerth, E. 1968. Determination of Anionic Detergents by Two-Phase Titration (II). *Tenside* **5**: 90-96.

Rodríguez-Guadarrama, L.A., Talsania, S.K., Mohanty, K.K., and Rajagopalan, R. 1999. Thermodynamics of Aggregation of Amphiphiles in Solution from Lattice Monte Carlo Simulations. *Langmuir* **15** (2): 437-446.

Rojas, M.R, Müller, A.J., and Sáez, A.E. 2008. Shear Rheology and Porous Media Flow of Wormlike Micelle Solutions Formed by Mixtures of Surfactants of Opposite Charge. *J. Colloid Interface Sci.* **326**, 221-226.

Rosen, M.J., Zhao, F., and Murphy, D.S. 1987. Two-Phase Mixed Indicator Method for the Determination of Zwitterionic Surfactants. *J. Am. Oil Chem. Soc.* **64** (3): 439-441.

Rosen, M.J. 2004. *Surfactants and Interfacial Phenomena*, third edition. Hoboken, New Jersey: John Wiley & Sons, Inc.

Ryjkina, E., Kuhn, H., Rehage, H., Müller, F., and Peggau, J. 2002. Molecular Dynamic Computer Simulations of Phase Behavior of Non-Ionic Surfactants. *Angew. Chem. Int. Ed.* **41** (6): 983-986.

Samuel, M., Card, R.J., Nelson, E.B., Brown, J.E., Vinod, P.S., Temple, H.L., Qu, Q., and Fu, D.K. 1997. Polymer-Free Fluid for Hydraulic Fracturing. Paper SPE 38622 presented at the SPE Annual Conference and Exhibition, San Antonio, Texas, 5-8 October.

Samuel, M. 2001. Methods of Fracturing Subterranean Formations. US Patent No. 6,306,800.

Samuel, M., Marcinew, R., Al-Harbi, M., Samuel, E., Xiao, Z., Ezzat, A.M., Khamees, S.A., Jarrett, C., Ginest, N.H., Bartko, K., Hembling, D., and Nasr-El-Din, H.A. 2003. A New Solids-Free Non-Damaging High Temperature Lost-Circulation Pill: Development and First Field Applications. Paper SPE 81494 presented at the SPE 13th Middle East Oil Show & Conference, Kingdom of Bahrain, 5-8 April.

Samuel, M. and Sandhu, W. 2004. Non-Damaging Self-Diverting Acid Stimulations Revive an Egyptian Oil Field. *World Oil* **225** (2): 88-91.

Saul, D., Tiddy, G.J.T., Wheeler, P.A., and Wills, E. 1974. Phase Structure and Rheological Properties of a Mixed Zwitterionic/Anionic Surfactant System. *J. Chem. Soc. Faraday Trans. I* **70**: 163-170.

Shaughnessy, C.M. and Kunze, K.R. 1981. Understanding Sandstone Acidizing Leads to Improved Field Practices. *J. Pet. Tech.* **33** (7): 1196-1202.

Shelley, J., Watanabe, K., and Klein M.L. 1990. Simulation of a Sodium Dodecylsulfate Micelle in Aqueous Solution. *Int. J. Quantum Chem: Quantum Biol. Sym*. **38** (17): 103-117.

Shelley, J.C. and Shelley, M.Y. 2000. Computer Simulation of Surfactant Solutions. *Curr. Opin. Colloid Interface Sci*. **5** (1-2): 101-110.

Shinoda, W., DeVane, R.H., and Klein, M.L. 2008. Coarse-Grained Molecular Modeling of Non-Ionic Surfactant Self-Assembly. *Soft Matter* **4** (12): 2453-2462.

Srinivas, G., Nielsen, S.O., Moore, P.B., and Klein, M.L. 2006. Molecular Dynamics Simulations of Surfactant Self-Organization at a Solid–Liquid Interface. *J. Am. Chem. Soc*. **128** (3): 848-853.

Stevens, M.J., Hoh, J.H., and Woolf, T.B. 2003. Insights into the Molecular Mechanism of Membrane Fusion from Simulation: Evidence for the Association of Splayed Tails. *Phys. Rev. Lett*. **91** (18): 188102.

Sun, H., Ren, P., and Fried, J.R. 1998. The COMPASS Force Field: Parameterization and Validation for Phosphazenes. *Comput. Theor. Polym. Sci*. **8** (1-2): 229-246.

Tadros, T.F. 2005. *Applied Surfactants*: *Principles and Applications*. Weinheim**,** Germany: Wiley-VCH.

Taylor, K.C. and Nasr-El-Din, H.A. 2002. Coreflood Evaluation of in situ Gelled Acids. Paper SPE 73707 presented at the SPE International Symposium and Exhibition on Formation Damage Control, Lafayette, Louisiana, 20-21 February.

Taylor, K.C. and Nasr-El-Din, H.A. 2003. Laboratory Evaluation of in situ Gelled Acids for Carbonate Reservoirs. *SPE J.* **8** (4): 426-434.

Tegeler, A., Ruess, W., and Gmahl, E. 1995. Determination of Amphoretic Surfactants in Cosmetic Cleansing Products by High-Performance Liquid Chromatography on a Cation-Exchange Column. *J. Chromatogr. A* **715** (1): 195-198.

Tieleman, D.P., van der Spoel, D., and Berendsen, H.J.C. 2000. Molecular Dynamics Simulations of Dodecylphosphocholine Micelles at Three Different Aggregate Sizes: Micellar Structure and Chain Relaxation. *J. Phys. Chem. B*, **104** (27): 6380-6388.

Vytras, K., Kalous, J., and Symerský, J. 1985. Determination of Some Ampholytic and Cationic Surfactants by Potentiometric Titration Based on Ion Pair Formation. *Anal. Chim. Acta* **177**: 219-223.

Wang, Y., Hill, A.D., and Schechter, R.S. 1993. The Optimum Injection Rate for Matrix Acidizing of Carbonate Formations. Paper SPE 26578 presented at the 68th Annual Technical Conference and Exhibition of the Society of Petroleum Engineers, Houston, Texas, 3-6 October.

Watanabe, K., Ferrario, M., and Klein M.L. 1988. Molecular Dynamics Study of a Sodium Octanoate Micelle in Aqueous Solution. *J. Phys. Chem*. **92** (3): 819-821.

Wayne, A.M. 2008. *Geology of Carbonate Reservoirs*: *The Identification, Description, and Characterization of Hydrocarbon Reservoirs in Carbonate Rocks*. Hoboken, New Jersey: John Wiley & Sons, Inc.

Wendoloski, J.J., Kimatian, S.J., Schutt, C.E., and Salemme, F.R. Molecular Dynamics Simulation of a Phospholipid Micelle. *Science* **243** (4891): 636-638.

Williams, B.B., Gidley, J.L., and Schechter, R.S., 1979. *Acidizing Fundamentals.* Monograph Series, SPE, Dallas, Texas **1**: 1-11.

Xu, J., Sun. W., Li, G., and Zhang, G. 2007. Simulation of Micelle of Zwitterionic DSB in NaCl Aqueous Solution. *Chem. Phys. Lett.* **438** (4-6): 326-329.

Yakovlev, D.S. and Boek, E.S. 2007. Molecular Dynamics Simulations of Mixed Cationic/Anionic Wormlike Micelles. *Langmuir* **23** (12): 6588-6597.

Yang, J. 2002. Viscoelastic Wormlike Micelles and Their Applications. *Curr. Opin. Colloid. Interface Sci.* **7** (5-6), 276-281.

Yang, W. and Yang, X. 2010. Molecular Dynamics Study of the Influence of Calcium Ions on Foam Stability. *J. Phys. Chem. B* **114** (31): 10066-10074.

Yeager, V. and Shuchart, C. 1997. In Situ Gels Improve Formation Acidizing. *Oil & Gas J.* **95** (3): 70-72.

Yu, M., Mahmoud, M.A., and Nasr-El-Din, H.A. 2009. Quantitative Analysis of an Amphoteric Surfactant in Acidizing Fluids and Coreflood Effluent. Paper SPE 121715 presented at the SPE International Symposium on Oilfield Chemistry, The Woodlands, Texas, 20-22 April.

Yu, M., Mahmoud, M.A. and Nasr-El-Din, H.A. 2010. Propagation and Retention of Viscoelastic Surfactants Following Matrix Acid Treatments in Carbonate Cores. Paper SPE 128047 presented at the SPE International Symposium on Formation Damage Control, Lafayette, Louisiana, 10-12 February.

Yu, M. Mu, Y., and Nasr-El-Din, H.A. 2011. Impact of Hydrolysis at High Temperatures on the Apparent Viscosity of Carboxybetaine Viscoelastic Surfactant-Based Acid: Experimental and Molecular Dynamics Simulation Studies. Paper SPE 142264 presented at the Production and Operations Symposium, Oklahoma City, Oklahoma, 27-29 March.

Zeiler, C., Alleman, D., and Qu, Q. 2006. Use of Viscoelastic-Surfactant-Based Diverting Agents for Acid Stimulation: Case Histories in GOM. *SPE Prod & Oper* **21** (4): 448-454.

VITA

Name:	Meng Yu
Address:	603 Richardson Building, 3116 TAMU College Station, TX 77843-3116
Email Address:	meng.yu@pe.tamu.edu
Education:	B.S., Chemistry, Sichuan University, 2006 M.S., Chemistry, Texas A&M University, 2008